AFWAL-TR-88-2103

STUDIES OF THE VOLUME AND PLASMA SHEATH PROPERTIES OF RADIO
FREQUENCY DISCHARGES

D. W. ERNIE AND H. J. OSKAM

University of Minnesota
Department of Electrical Engineering
123 Church Street S.E.
Minneapolis, MN 55455

November 1988

Final Report for Period 1 June 1983 - 28 February 1987

Approved for public release; distribution is unlimited
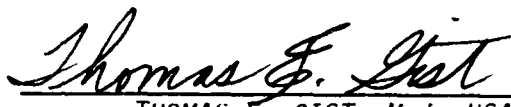
DTIC
ELECTE
MAY 1 8 1989

NOTICE

When Government drawings, specifications, or other data are used for any purpose other than in connection with a definitely Government-related procurement, the United Stated Government incurs no responsibility or any obligation whatsoever. The fact that the Government may have formulated or in any way supplied the said drawings, specifications, or other data, is not to be regarded by implication, or otherwise in any manner construed, as licensing the holder, or any other person or corporation; or as conveying any rights or permission to manufacture, use, or sell any patented invention that may in any way be related thereto.

This report is releasable to the National Technical Information Service (NTIS). At NTIS, it will be available to the general public, including foreign nations.
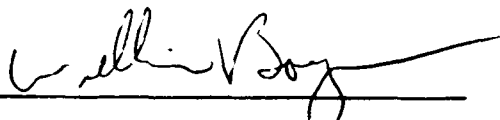
This technical report has been reviewed and is approved for publication.

CHARLES A. DEJOSEPH, JR.
Power Components Branch
Aerospace Power Division
Aero Propulsion and Power Laboratory
FOR THE COMMANDER

THOMAS E. GIST, Maj, USAF
TAM, Advanced Plasma Research Group
Aerospace Power Division
Aero Propulsion and Power Laboratory

WILLIAM U. BORGER
Chief, Aerospace Power Division
Aero Propulsion & Power Laboratory

If your address has changed, if you wish to be removed from our mailing list, or if the addressee is no longer employed by your organization please notify AFWAL/POOC-3, W-PAFB, OH 45433- 6563 to help us maintain a current mailing list.

Copies of this report should not be returned unless is required by security considerations, contractual obligations, or notice on a specific document.

REPORT DOCUMENTATION PAGE

1a. REPORT SECURITY CLASSIFICATION	1b. RESTRICTIVE MARKINGS
UNCLASSIFIED	
2a. SECURITY CLASSIFICATION AUTHORITY	3. DISTRIBUTION/AVAILABILITY OF REPORT
	Approved for public release; distribution
2b. DECLASSIFICATION/DOWNGRADING SCHEDULE	is unlimited
4. PERFORMING ORGANIZATION REPORT NUMBER(S)	5. MONITORING ORGANIZATION REPORT NUMBER(S)
	AFWAL-TR-88-2103

6a. NAME OF PERFORMING ORGANIZATION	6b. OFFICE SYMBOL (If applicable)	7a. NAME OF MONITORING ORGANIZATION
University of Minnesota		Aero Propulsion Laboratory (AFWAL/POOC-3) Air Force Wright Aeronautical Laboratories
6c. ADDRESS (City, State and ZIP Code)		7b. ADDRESS (City, State and ZIP Code)
Dept. of Electrical Engineering 123 Church Street SE Minneapolis, MN 55455		Wright-Patterson Air Force Base, OH 45433-6563

8a. NAME OF FUNDING/SPONSORING ORGANIZATION	8b. OFFICE SYMBOL (If applicable)	9. PROCUREMENT INSTRUMENT IDENTIFICATION NUMBER
Power Components Branch	AFWAL/POOC-3	F33615-83-K-2340

8c. ADDRESS (City, State and ZIP Code)	10. SOURCE OF FUNDING NOS.			
Air Force Wright Aeronautical Laboratories Wright-Patterson AFB, OH 45433-6563	PROGRAM ELEMENT NO.	PROJECT NO.	TASK NO.	WORK UNIT NO.
	61102F	2301	S2	78

11. TITLE (Include Security Classification)
see reverse side

12. PERSONAL AUTHOR(S)
D. W. Ernie and H. J. Oskam

13a. TYPE OF REPORT	13b. TIME COVERED	14. DATE OF REPORT (Yr., Mo., Day)	15. PAGE COUNT
Final	FROM 83-06-01 TO 87-02-28	1988 November	112

16. SUPPLEMENTARY NOTATION

17. COSATI CODES			18. SUBJECT TERMS (Continue on reverse if necessary and identify by block number)
FIELD	GROUP	SUB. GR.	Discharge Modeling, Ion Bombardment in RF Discharges, Electronegative Discharges

19. ABSTRACT (Continue on reverse if necessary and identify by block number)

Radio frequency discharges currently play a major role in the fabrication of microelectronic devices. This manuscript reports on theoretical and experimental studies undertaken in an effort to develop a better understanding of the underlying gas discharge physics occuring in these discharges. An equivalent circuit model was developed for a planar rf reactor based on the physical properties of the plasma sheath. This model shows that the waveforms of the potentials across the plasma sheaths are highly nonlinear and agree with previously reported measurements. These waveforms were subsequently incorporated into a model for the energy distribution of ions bombarding the electrode surfaces in low pressure rf reactors. Numerical calculations based on this model show that the ion bombardment energy distribution is

(continued on reverse side)

20. DISTRIBUTION/AVAILABILITY OF ABSTRACT	21. ABSTRACT SECURITY CLASSIFICATION
UNCLASSIFIED/UNLIMITED ☒ SAME AS RPT. ☐ DTIC USERS ☐	UNCLASSIFIED

22a. NAME OF RESPONSIBLE INDIVIDUAL	22b. TELEPHONE NUMBER (Include Area Code)	22c. OFFICE SYMBOL
Charles A. DeJoseph, Jr.	(513) 255-2923	AFWAL/POOC-3

DD FORM 1473, 83 APR   EDITION OF 1 JAN 73 IS OBSOLETE.

Item 19: Abstract (continued):

bimodal and skewed toward lower impact energies. Experimental measurements were also performed on the ion bombardment energy distribution in a planar rf reactor. The results of these measurements agree with the model predictions at low pressure and give information at higher pressures about the effects of collisions on the distribution, which agree with previous studies.

The importance of negative ions in a discharge through an electronegative gas was investigated by the development of a collisionless plasma sheath model for such a discharge. A sheath criterion was derived and used to determine the effects of negative ions on the sheath properties. The results from this study include an explanation of the confinement of negative ions inside the plasma volume. Finally, a model utilizing a single set of equations was studied and solved, through suitable numerical techniques, for the radial structure of the positive column in dc discharges. The results from this work show the development of both the ambipolar region in the bulk of the positive column and the sheath region near the discharge wall. The importance of the application of this model to discharges at various pressures and the tube radii was studied.

Item 11. Title:

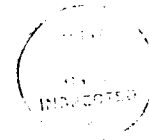Studies of Volume and Plasma Sheath Properties of Radio Frequency Discharges

TABLE OF CONTENTS

SECTION I

INTRODUCTION

Introduction

Radio frequency discharges currently play a major role in the microelectronics industry for the fabrication of integrated circuits. These discharges are typically used for stripping of photoresist, anisotropic etching of semiconductor, oxide, and metal surfaces, and the deposition of organic and inorganic thin films. In all of these applications, it is beneficial to have a good understanding of the physical and chemical processes involved in these discharges and at the surfaces exposed to the discharge. While there is a long history of extensive research on and application of dc discharges, only recently have rf discharges become of significant interest. This report describes theoretical and experimental studies undertaken in an effort to develop a better understanding of some of the underlying gas discharge physics occurring in these discharges.

Section II of this report presents an equivalent circuit model for a planar rf plasma reactor. The physical properties of the plasma sheaths adjacent to the electrodes are incorporated in the model. The sheath capacitances and the conduction currents through the sheaths predicted by the model are time varying and have a highly nonlinear dependence on the potentials across the plasma sheaths. Numerical calculations based on this model show that that the waveforms of the voltage differences across the sheaths are highly nonsinusoidal and agree with reported measurements. The results given this section were reported at the 37th Annual Gaseous Electronics Conference in Boulder, Colorado, October, 1984 and have been published in Physical Review A.

Section III outlines a model for the energy distribution of ions bombarding electrode surfaces in planar rf plasma reactors at low pressures, where collisions in the sheath may be ignored. Given the waveform for the voltage difference across the sheath adjacent to an electrode, the model predicts the ion bombardment energy distribution in the limit where the transit time of the ions across the sheath is much shorter than the period of the applied rf voltage and in the limit where the ion transit time is much longer than the rf period. Numerical calculations utilizing the sheath voltage waveforms from the equivalent circuit model presented in Sec. II show that the ion bombardment energy distribution is bimodal and skewed toward

2

lower ion bombardment energies. The results given in this section were also presented at the 37th Annual Gaseous Electronics Conference in Boulder, Colorado, October, 1984, and are being submitted for publication to the Journal of Vacuum Science and Technology.

In an effort to obtain a reliable experimental data base for comparison with the results from the ion bombardment energy distribution model, an experimental system was designed and constructed to measure the ion bombardment energy distribution at an electrode in a planar rf reactor. The design of and resulting data from this experimental system is reported in Sec. IV. This system was designed so as to fulfill the required assumptions of ion bombardment energy distribution model. During the design and operation of this system, several unanticipated problems arose which were of interest in themselves and are therefore discussed. Section IV also includes results of measurements made with the final functioning design and discusses several conclusions based on these results.

In developing the models presented in Secs. II and III, the plasma sheath model used incorporated the Bohm criterium, which is only applicable to plasmas consisting of a positive ion species, electrons, and neutrals. However, plasmas containing negative ion species, in addition to these other species, are the plasmas of primary interest to the microelectronics industry due to the use of electronegative gases in most plasma assisted processing steps. In an effort to investigate the effects of negative ions on the plasma sheath characteristics, a sheath model was developed for a plasma containing a negative ion species, a positive ion species, electrons, and neutrals. This model is discussed in Sec. V. Under appropriate assumptions, a criterion is derived which must be satisfied in order for the model to be physically realistic. This criterion is then used to calculate the conductivity and capacitance of a plasma sheath in the presence of negative ions. The implications of these results for dc and rf discharges are investigated, including an explanation of the confinement of negative ions inside a plasma volume. This material was presented at the 39th Annual Gaseous Electronics Conference in Monterey, California, October, 1986, and is being submitted for publication to Physical Review A.

Finally, a model is presented in Sec. VI for the radial distribution of ion and electron densities and electric field strength in the positive column of a dc discharge for a plasma consisting of a positive ion species, electrons, and

3

neutrals.. The set of equations involved consists of the particle and momentum conservation equations for the ions and electrons and Poisson's equation. Utilizing this single set of equations and appropriate assumptions, this model has been solved, through suitable numerical techniques. The results from this work show the development of both the ambipolar region in the bulk of the positive column and the sheath region near the discharge wall. The importance of the application of this model to discharges at various pressures and tube radii is discussed. This work was presented at the 39th Annual Gaseous Electronics Conference in Monterey, California, 1986, and is being submitted for publication to Physics of Fluids.

SECTION II

APPLICATION OF THE PHYSICS OF PLASMA SHEATHS TO THE MODELING OF RF PLASMA REACTORS

Application of the physics of plasma sheaths to the modeling of rf plasma reactors

A. Metze,[a] D. W. Ernie, and H. J. Oskam

Department of Electrical Engineering, University of Minnesota, Minneapolis, Minnesota 55455

An equivalent circuit model is presented for a planar rf plasma reactor. The physical properties of the plasma sheath adjacent to the electrodes are incorporated in the model. The sheath capacitances and the conduction currents through the sheaths are time varying and have a highly nonlinear dependence on the potentials across the plasma sheaths. The model shows that the waveforms of the voltage differences across the sheaths are highly nonsinusoidal and agree with reported measurements.

I. INTRODUCTION

The application of rf-excited gaseous discharges in thin-film fabrication technology has become standard during the past decade. The simplest geometry most commonly used is that of two planar electrodes between which the rf voltage is applied.[1] A schematic representation of such a planar rf plasma reactor is shown in Fig. 1. The plasma is separated from each electrode by a plasma sheath. The origin of these plasma sheaths has been discussed by several authors.[2,3]

Positive ions produced in the plasma volume are accelerated across the plasma sheaths and arrive at the electrodes with an energy distribution which is determined by the magnitude and the waveform of the time-dependent potential difference across the sheaths, the gas pressure, etc. This ion bombardment energy distribution determines the degree of anisotropy in thin-film etching, amount of ion impact induced damage to surfaces, etc. Therefore, it is important to obtain a better understanding of the dependence of the ion bombardment energy distribution on parameters such as reactor geometry, frequency of the applied voltage, gas pressure, etc. Suzuki *et al.*[4] and Tsui[5] have reported models relating to the energy distribution of positive ions arriving at the electrodes of a rf plasma reactor. These authors assumed that the electric potential difference across the plasma sheath is simply the superposition of a dc bias and a sinusoidal voltage.

In order to obtain a more accurate model for the ion bombardment energy distribution, it is necessary to develop a model which predicts the waveforms of the voltages across the plasma sheaths in a planar rf plasma reactor. In an effort to determine these waveforms, several authors have used a combination of circuit elements for the representation of the plasma sheaths in equivalent circuit models of a planar plasma reactor. Koenig and Maissel[6] used a static capacitor in parallel with a diode. The capacitor represented the sheath capacitance, while the diode approximated the effect of electrons reaching the electrodes. Horwitz[7] added a parallel resistor to the previous model, while other authors have used a simple parallel combination consisting of a resistor and capacitor of fixed values.[8,9] The latter model is sometimes further simplified by a purely linear resistive network for excitation frequencies below a few megahertz and by a purely linear capacitive network for higher frequencies.[9,10]

The purpose of the present paper is to demonstrate that an equivalent circuit model of a plasma reactor can be developed using known physical properties of plasma sheaths. The main feature of the proposed model is the inclusion of the nonlinear dependence of the sheath properties on the voltage across the sheath. The purpose of the model is to evaluate the effects of the nonlinear sheath properties on the resulting voltage waveforms and the dc voltage biases across the plasma sheaths. The resulting sheath voltage waveforms can then be used to more accurately predict the ion bombardment energy distribution at the surface of the electrodes in a planar rf plasma reactor.

II. MODEL OF THE PLASMA SHEATH IN A PLANAR rf GASEOUS DISCHARGE

The schematic representation of a planar plasma sheath used in the following discussion is shown in Fig. 2. During the discussion of the sheath properties the Bohm[11] criterium will be used. This criterion implies that, for a surface biased strongly negative with respect to a plasma, the ions are accelerated across a pre-sheath by the applied electric field such that they enter the plasma sheath with a velocity perpendicular to the sheath boundary and with a magnitude equal to or greater than $(kT_e/M)^{1/2}$. Here, k is Boltzmann's constant, M is the ion mass, and T_e is the electron temperature.

Several assumptions will be made in order to simplify the present discussion. Refinements of the model can be in-
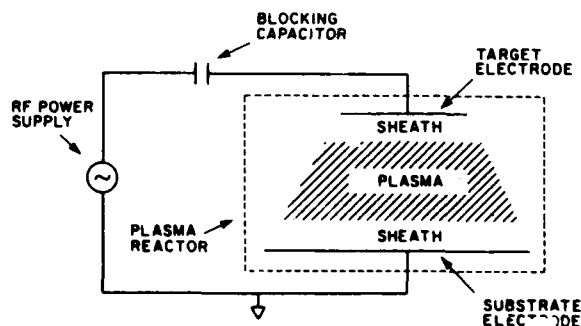

FIG. 1. Schematic representation of a planar rf reactor.

[a] Present address: Honeywell Systems and Research Center, 3660 Technology Drive, Minneapolis, MN 55418.
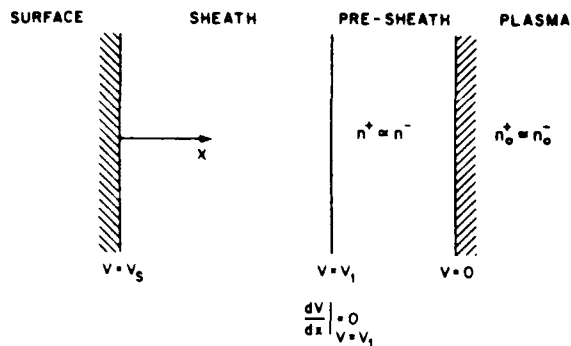
FIG. 2. Schematic representation of a planar plasma sheath.

cluded in future discussions. The assumptions used for the present model are the following:

(1) The charged particles are electrons and one type of positive ions. The presence of more than one type of positive ion will only slightly modify the model presented. In many applications of plasma processing of materials electronegative gases are used. Plasmas produced in these gases will contain negative ions. The presence of negative ions is excluded in the present model since an accurate incorporation of these ions complicates the model of the plasma sheath. However, as long as the negative ion density inside the plasma sheath is small compared to that of the positive ion density, the present model is a good approximation.

(2) The electrons and ions have Maxwellian velocity distributions inside the plasma with temperatures of T_e and T_i, respectively.

(3) The electron temperature T_e is constant in time, while the ion temperature T_i is equal to the constant neutral gas temperature T_g. The assumption of constant T_e limits the model to a minimum frequency of the applied power source. The numerical calculations presented in this paper for a planar plasma reactor are for a plasma produced in argon. For these conditions, the energy modulation of the majority of the electrons is small for frequencies larger than approximately 50 kHz and gas pressures smaller than approximately 1 Torr.[12]

(4) The electron and ion densities inside the plasma volume are constant in time. The validity of this assumption depends on the rate of loss of the charged particles from the plasma volume as well as on the mechanism by which the plasma is maintained. The charged particle density modulation due to loss by ambipolar diffusion in a plasma reactor is small for frequencies larger than approximately 50 kHz and pressures larger than approximately 0.1 Torr.[13] The periodic charged particle current across the plasma sheaths towards the electrodes is governed by the properties of the plasma sheath. The model shows that this number loss of charged particles is small compared to the charge particle density inside the plasma, since only a relatively small fraction of the plasma electrons and ions is able to reach the electrodes.

The modulation in the rate of production of charged particles depends on the maintenance mechanism of the discharge plasma. For instance, if the plasma electrons (ions) are mainly produced by secondary electrons emitted due to ion bombardment of the electrodes, the rate of charged parti-

cle production inside the plasma can be considerably modulated. This is caused by the energy and flux modulation of these electrons due to the time-dependence voltage difference across the plasma sheath. The possible effect of this phenomenon is not included in the present model.

(5) The influence of collisions between charged particles and neutral particles inside the plasma sheath on the charged particle motion can be neglected (collisionless sheath). For instance, this is a good assumption for the charged particle densities (sheath dimensions) and gas pressures (charged particle mean free paths) used for anisotropic etching of films in a planar rf plasma reactor.

(6) The transit time τ, of ions through the plasma sheath is not larger than $1/f$, where f is the frequency of the applied voltage. If this condition is satisfied, then the thickness of the plasma sheath will, at each time, correspond to the steady-state thickness related to the instantaneous voltage $V_s(t)$ across the sheath. Calculations for argon ions and plasma densities of 10^{10} cm^{-3} show that τ, is smaller than 0.5×10^{-6} s. Therefore, this assumption appears to be valid for frequencies up to approximately 1 MHz.

(7) The flux of electrons collected by the electrodes depends only on the instantaneous voltage across the plasma sheath and not on the frequency of the voltage waveform. Numerical calculations by the authors indicate that this assumption is valid for frequencies up to a few megahertz.[14]

(8) The Bohm sheath criterium can be used in the form that the speed with which the ions enter the plasma sheath is equal to $(kT_e/M)^{1/2}$ and is valid for the range of voltages across the plasma sheaths of interest.[15]

(9) The electric field is zero at the boundary between the pre-sheath and the plasma sheath.[16]

(10) The electrons have a Boltzmann density distribution in the pre-sheath and the plasma sheath.[17]

The two quantities related to the plasma sheath which have to be included in the equivalent circuit model of a planar rf plasma reactor presented in the next section are the capacitance C_s of the plasma sheath and the conduction current I through the sheath. An expression for C_s as a function of sheath potential $(V_s - V_1)$ can be derived by noting that the displacement current I_d for the sheath capacitance is given by[18]

$$I_d = \frac{dQ}{dt} = \frac{dQ}{dV_s}\frac{dV_s}{dt} \equiv C_s\frac{dV_s}{dt}, \tag{1}$$

where Q is the surface charge on the electrode. For a planar electrode, the sheath capacitance C_s is thus given by

$$C_s \equiv \frac{dQ}{dV_s} = -\epsilon_0 \int \frac{\partial \mathbf{E}_A}{\partial V_s}\cdot d\mathbf{A} = -\epsilon_0 A\frac{\partial E_A}{\partial V_s}, \tag{2}$$

where ϵ_0 is the permittivity of free space and it is assumed that the electric field at the electrode surface $\mathbf{E}_A$ is normal to and uniform over the electrode surface with area A.

Using the mentioned assumptions, it can be shown that

$$E_A = -\left(\frac{2kT_e n_1}{\epsilon_0}\right)^{1/2}$$

$$\times\left[\exp\left(\frac{e(V_s - V_1)}{kT_e}\right) + \left(\frac{V_s}{V_1}\right)^{1/2} - 2\right]^{1/2}$$

7

for $-\infty < V_s(t) < V_1$ (3a)

$E_A = 0$ for $V_1 < V_s(t) < 0$.   (3b)

Here,

$$V_1 = -(kT_e/2e) \qquad (4)$$

$$n_1 = n_0 \exp(eV_1/kT_e), \qquad (5)$$

where n_0 is the density of electrons and ions inside the plasma. Equations (2) and (3) show that $C_s(V_s)$ is time varying and has a strong nonlinear dependence on $V_s(t)$.

The assumptions made imply that the conduction current $I(V_s)$ through the plasma sheath is given by the static plasma probe current-voltage characteristic (Langmuir probe curve) derived by including the Bohm criterium, i.e.,

$$I(V_s) = AJ_c \exp(eV_s/kT_e) + AJ_i \quad \text{for} \quad V_s(t) < 0. \qquad (6)$$

Here, A is the area of the electrode and the saturated charged particle current densities are

$$J_c = -en_0\bar{v}_e/4 = -en_0(kT_e/2\pi m)^{1/2} \qquad (7)$$

and

$$J_i = 0.605 n_0 e(kT_e/M)^{1/2}, \qquad (8)$$

where m and M are the electron and ion mass, respectively, and $\bar{v}_e$ is the average electron speed inside the plasma.

The expressions given in this section for the capacitance $C_s(V_s)$ of the plasma sheath and the conduction current $I(V_s)$ through the plasma sheath will be used in the equivalent circuit model for a planar rf discharge presented in the following section.

III. EQUIVALENT CIRCUIT MODEL FOR A PLANAR rf PLASMA REACTOR

A schematic of the equivalent electric circuit model used in the present discussion is shown in Fig. 3. Here, V_{rf} is the voltage of the applied rf signal from a matched rf power supply; V_T and V_p are the potentials of the target electrode and the plasma, respectively, and $V_{SS} = V_p$ and $V_{ST} = V_T - V_p$ are the voltages across the substrate-plasma sheath and the target-plasma sheath, respectively. The blocking capacitor is represented by C_B; C_{ST} and I_T represent the capacitance of and conduction current through the
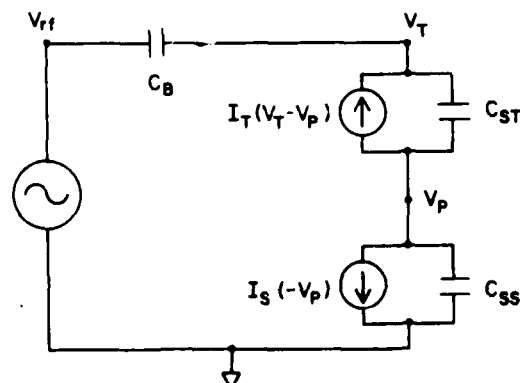

FIG. 3. Equivalent electric circuit model of a plasma reactor.

sheath adjacent to the target electrode, respectively, while C_{SS} and I_S represent the corresponding values for the sheath adjacent to the substrate electrode. The expressions for C_{ST} and C_{SS} are given by Eqs. (2) and (3), while the expressions for I_T and I_S are given by Eqs. (6), (7), and (8).

The electrical resistance of the plasma has been neglected in this circuit model. This resistance is small with respect to the sheath resistance for the plasma electron densities and voltage frequency range considered in the present discussion. However, inclusion of the plasma resistance does not introduce any complications for the circuit model.

The purpose of the model is to derive the time dependence of V_p, V_T, the total current at the node denoted by V_T, and the conduction currents through the plasma sheaths in this circuit. From these results, quantities such as the sheath potentials as a function of time and the resulting dc self biases can also be calculated.

From this equivalent circuit model and from conservation of current at the nodes denoted by V_T and V_p, it follows that

$$C_{ST}\frac{d}{dt}(V_p - V_T) + C_B\frac{d}{dt}(V_{rf} - V_T) + I_T = 0, \qquad (9a)$$

$$C_{SS}\frac{d}{dt}V_p + C_{ST}\frac{d}{dt}(V_p - V_T) + I_T + I_S = 0. \qquad (9b)$$

If Eqs. (2) and (3) for $C_S(V_S)$ and Eq. (6) for $I(V_S)$ are used in the current continuity Eqs. (9), the set of continuity equations can be solved numerically for $V_p(t)$ and $V_T(t)$. In addition, by then using these results, the current in the circuit at the node denoted by V_T and the conduction currents I_S and I_I in the plasma sheaths can be calculated.

IV. NUMERICAL RESULTS AND DISCUSSION

Numerical simulations were performed based on the equivalent circuit model for the following assumed conditions:

$M = 40$ amu (argon discharge),

$n_0 = 10^{10}$ particles/cm^3 (charged particle density in plasma),

$T_i = 500$ K (ion temperature),

$T_e = 23\,200$ K (electron temperature),

$A_T = 100\,\pi$ cm^2 (area of target electrode),

$V_{rf} = 1000 \sin \omega t$ (applied rf voltage).

These conditions imply that

$J_i = 214\,\mu$A/cm^2 (saturated ion current),

$J_e = -38$ mA/cm^2 (saturated electron current),

$V_F = -10.35$ V (floating potential).

The floating potential is the voltage difference across the plasma sheath and pre-sheath for which the total conduction current through the sheath is zero. Its value is given by

$$V_F = -(kT_e/e)\ln(-J_e/J_i), \qquad (10)$$

which follows directly from Eq. (6).

Figure 4 shows the calculated waveforms for the voltage V_T across the plasma reactor and the plasma potential V_p. The calculations relate to a frequency $f = 100$ kHz, a blocking capacitance $C_B = 150$ pF, and an electrode area ratio $A_T/A_s = 1.0$, where A_T is the area of the target electrode

3083   J. Appl. Phys., Vol. 60, No. 9, 1 November 1986
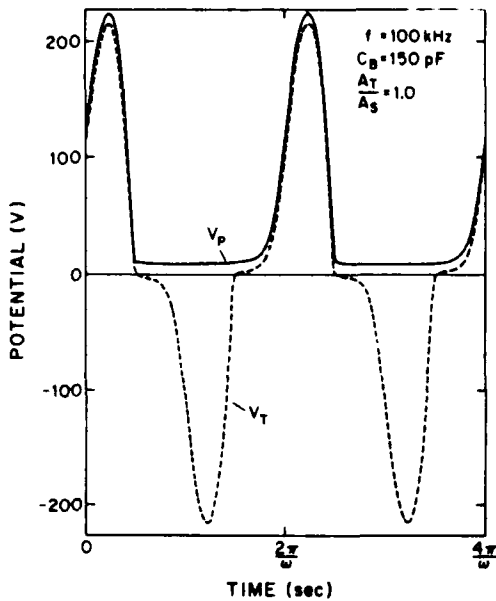
Metze, Ernie, and Oskam   3083

8

FIG. 4. Calculated waveforms of the voltage V_T across the plasma reactor and the plasma potential V_p for equal areas of the target and substrate electrodes.

and A_s is the area of the substrate electrode. The sheath voltage waveforms $V_{SS} = -V_p$ and $V_{ST} = V_T - V_p$ are shown in Fig. 5. These calculated waveforms show that both electrodes always have a negative potential with respect to the plasma. These results are in very good agreement with measurements by Bruce.[19] Figure 6 shows an expanded view of the waveforms of the sheath voltages close to the floating
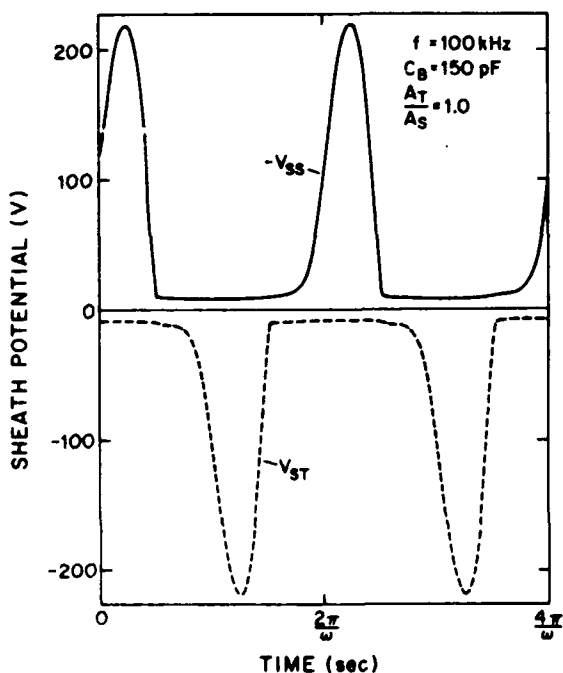

FIG. 5. Calculated waveform of the potential V_{ST} across the plasma sheath adjacent to the target electrode and that of the potential V_{SS} across the substrate electrode sheath for $A_T/A_S = 1$.
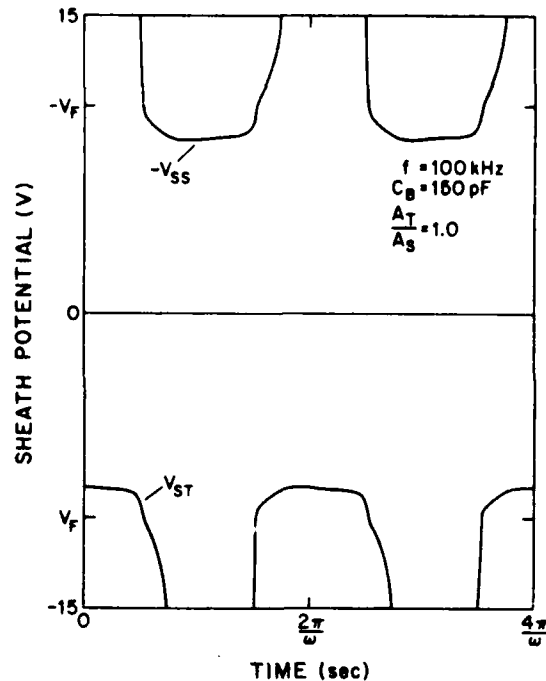

FIG. 6. Calculated sheath voltage waveforms V_{ST} and V_{SS} close to the floating potential V_F for $A_T/A_S = 1$.

potential V_F where it is seen that the smallest magnitude of the time dependent sheath potential is only slightly smaller than $|V_F|$. The nonsinusoidal nature of the sheath voltage waveforms V_{SS} and V_{ST} (and, hence, of V_p and V_T) is due to the highly nonlinear properties of the sheath capacitances C_{SS} and C_{ST} and the conduction currents I_S and I_T through the plasma sheaths. At this frequency, these waveform shapes are predominantly determined by the large difference in magnitude between the saturated ion current and the larger saturated electron current and by the exponential increase of the electron current through the plasma sheath with decreasing values of $|V_S|$. Since no net dc current component can flow in the circuit, the magnitude of the sheath potentials need only be slightly smaller than $|V_F|$ for part of the rf cycle, during which time sufficient net electron current flows in order to balance the net ion current which flows during the remainder of the rf cycle.

The waveform of the conduction current I_T through the sheath adjacent to the target electrode is shown in Fig. 7. This current becomes independent of the sheath voltage V_{ST} (and thus time) for large negative sheath voltages (saturated ion current only), while the contribution of the electron current only becomes important for values of V_{ST} close to the floating potential V_F (compare with Figs. 5 and 6). For this symmetrical condition ($A_T = A_S$) the waveform of I_S is identical with that of I_T, but is shifted by π/ω s, as can be expected. The waveform of the total current, I_{total}, through the discharge is shown in Fig. 8. This waveform is again nonsinusoidal as can be expected from the nonlinear properties of the plasma sheaths. It should also be noted that the time averages of the currents I_T, I_S, and I_{total} are equal to zero, as is required, since no net dc current component can flow in the circuit.
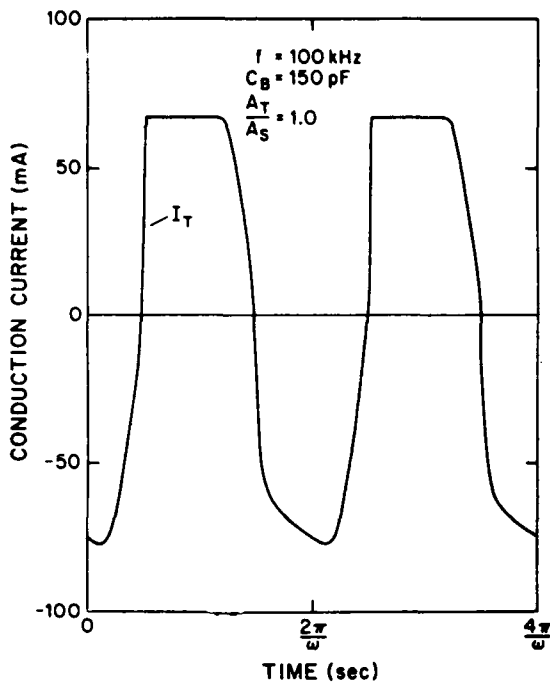
9

FIG. 7. Calculated waveform of the conduction current I_T through the plasma sheath adjacent to the target electrode for $A_T/A_S = 1$.

FIG. 9. Calculated waveform of the potential V_{ST} across the plasma sheath adjacent to the target electrode and that of the potential V_{SS} across the substrate electrode sheath for $A_T/A_S = 0.2$.

The next sequence of figures gives the various waveforms for an experimental condition in which the area of the substate electrode is five times the area of the target electrode ($A_T = 100\pi$ cm^2 and $A_S = 500\pi$ cm^2). The value of the blocking capacitor was slightly changed in these calculations in order to keep the voltage amplitude across the reactor, V_T, approximately the same as in the previous calculations for the symmetrical condition ($A_T/A_S = 1$). Figure 9 shows
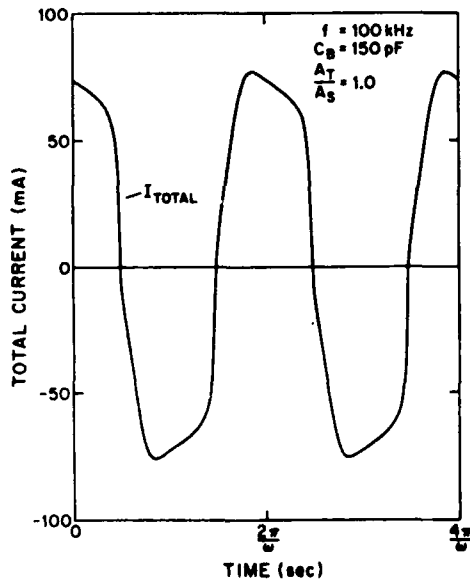
the waveforms of the sheath potentials V_{ST} and V_{SS}, while Fig. 10 shows an expanded view of these waveforms close to the floating potential V_F. The maximum value of $|V_{ST}|$ is about twice the amplitude of the voltage, V_T, across the plasma reactor, while the value of V_{SS} remains close to the value of V_F. The latter effect is shown in more detail in Fig. 11.

FIG. 8. Calculated waveform of the total current I_{total} through the plasma reactor for $A_T/A_S = 1$.

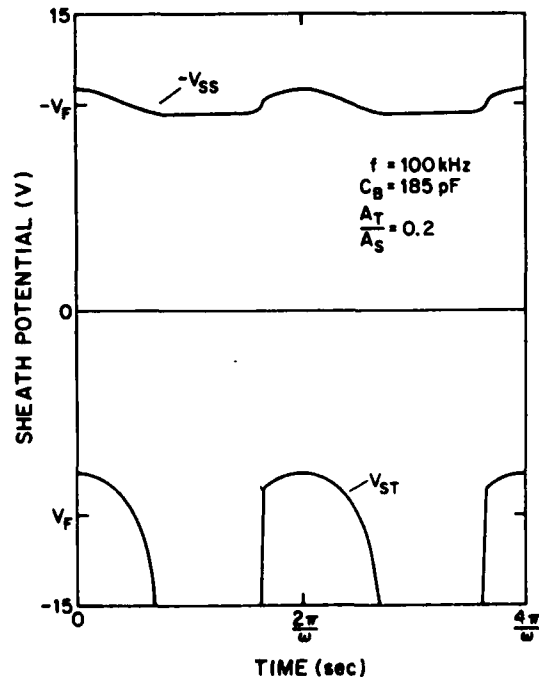**FIG. 10.** Calculated sheath voltage waveforms V_{ST} and V_{SS} close to the floating potential V_F for $A_T/A_S = 0.2$.
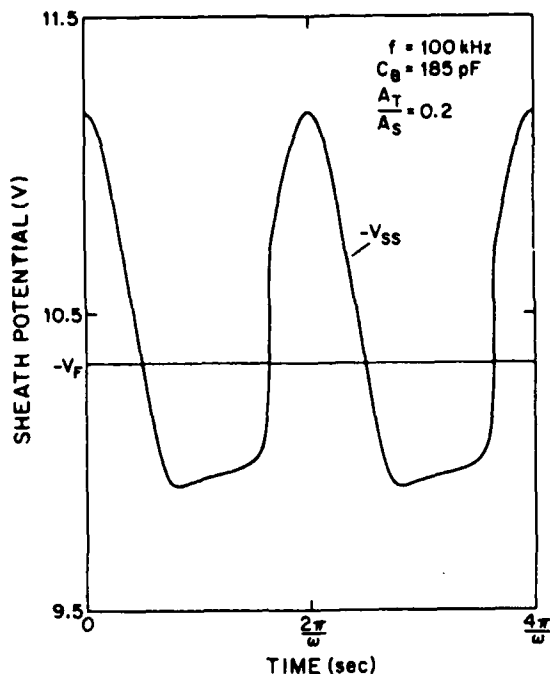
10

FIG. 11. Calculated sheath voltage waveform V_{ss} very close to the floating potential V_F for $A_T/A_S = 0.2$.

FIG. 13. Calculated waveform of the conduction current I_S through the plasma sheath adjacent to the substrate electrode for $A_T/A_S = 0.2$.

The waveforms of the conduction currents, I_T and I_S, through the two plasma sheaths are shown in Figs. 12 and 13, respectively. The waveform of I_T is analogous to that for the symmetrical configuration. However, the electron current contributes significantly to I_S during all times, since the saturated ion current at the substrate electrode is 336 mA, while at the target electrode this current is only 67 mA. The

reason that the amplitude of V_{ST} is much larger than that of V_{ss} is the difference in electron and saturated ion currents at the two electrodes due to the difference in A_T and A_S. The variation in V_{ss} required in order to adjust I_S for the variation in I_T becomes smaller than the variation in V_{ST} as the ratio A_T/A_S becomes smaller. The waveform of the total current through the plasma reactor is shown in Fig. 14.

V. CONCLUSIONS

The model presented is based on the inclusion of the physical properties of plasma sheaths in an equivalent circuit representation of a planar rf-excited gaseous discharge. The
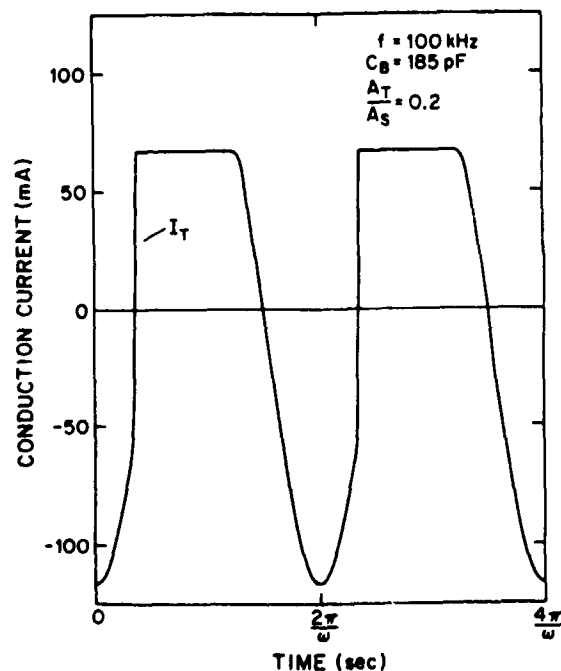

FIG. 12. Calculated waveform of the conduction current I_T through the plasma sheath adjacent to the target electrode for $A_T/A_S = 0.2$.
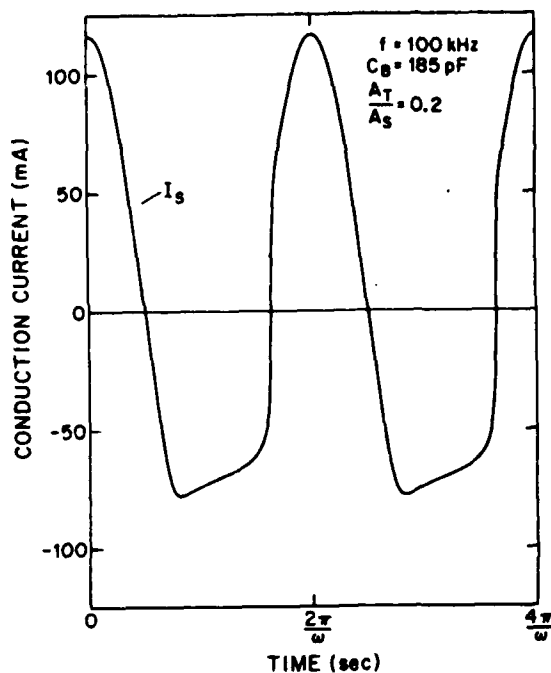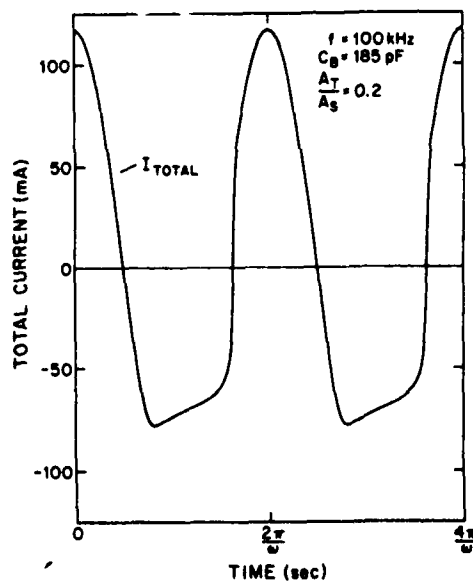

FIG. 14. Calculated waveform of the total current I_{total} through the plasma reactor for $A_T/A_S = 0.2$.

3086   J. Appl. Phys., Vol. 60, No. 9, 1 November 1986

Metze, Ernie, and Oskam   3086

11

proposed model is valid under the assumptions made in Sec. II. The model shows that the waveforms of the voltage differences across the plasma sheaths are highly nonsinusoidal. These waveforms are in agreement with studies reported by Bruce.[19] The resulting current waveforms in the circuit are also highly nonsinusoidal. The waveforms of the voltage, V_r, across the reactor and of the total current, I_{total}, through the reactor have important implications when determining the power applied to the reactor. This model also shows that the relative amplitudes of the voltage waveforms across the target and substrate plasma sheaths depend on the area ratio of the electrodes, with the largest amplitude waveform across the sheath adjacent to the smallest area electrode.

The effect of the calculated nonsinusoidal waveform of the plasma sheath voltage on the energy distribution of the positive ions arriving at the electrodes has been investigated and will be reported in a separate paper. An extension of the model to include the presence of negative ions inside the plasma sheath is currently in progress.

ACKNOWLEDGMENTS

[1]The results described in this paper are also relevant for plasma reactors of different geometries as long as the thickness of the plasma sheaths is small compared to the electrode dimensions. Calculations show that for the electron (ion) number densities typical in low-pressure plasma reactors, the thickness of the plasma sheath is of the order of 1 mm. The model calculations presented here can also be extended to take into account the effect of reactor walls, etc., on the electrical characteristics of the reactor by adding circuit elements to the equivalent electric circuit model discussed in Sec. III.

[2]A. Garscadden and H. G. Emeleus, Proc. Phys. Soc. 79, 535 (1962); A. Garscadden and P. Bletzinger, Rev. Sci. Instrum. 35, 912 (1964).

[3]H. S. Butler and G. S. Kino, Phys. Fluids 67, 1346 (1963).

[4]Keizo Suzuki, Ken Ninomiya, Shigeru Nishimatsu, and Sadayuki Okudaira, J. Vac. Sci. Technol. B 3, 1025 (1985).

[5]R. T. C. Tsui, Phys. Rev. 168, 107 (1968).

[6]H. R. Koenig and L. I. Maissel, IBM J. Res. Dev. 14, 168 (1970).

[7]Chris M. Horwitz, J. Vac. Sci. Technol. A 1, 60 (1983).

[8]A. J. van Roosemalen, W. G. W. van den Hoek, and H. Kalter, J. Appl. Phys. 58, 653 (1985).

[9]C. B. Zarowin, J. Electrochem. Soc. 130, 1144 (1983).

[10]K. Köhler, D. E. Horne, and J. W. Coburn, J. Appl. Phys. 58, 3350 (1985).

[11]D. Bohm, in *The Characteristics of Electrical Discharges in Magnetic Fields*, edited by A. Guthrie and R. K. Wakerling (McGraw-Hill, New York, 1949), Chap. 3.

[12]This assumption is valid for electron energy modulation due to elastic interactions of electrons with atoms. [H. J. Oskam, Philips Res. Repts. 13, 335 (1958)]. The energy modulation due to mutual charged particle interactions can be neglected for the assumed charge particle number densities of about 10^{10} cm^{-3}. Inelastic interactions between electrons and atoms involve only the small fraction of electrons in the high-energy tail of the electron energy distribution.

[13]The time constant τ_D related to charged particle loss by ambipolar diffusion is, for an active plasma, given by $\tau_D = (L/\pi)^2(T_g/T_e)(D_+)^{-1}$, where L is the distance between the electrodes, D_+ is the diffusion coefficient of the ions, and T_g and T_e are the electron and gas temperatures, respectively.

[14]D. W. Ernie and H. J. Oskam, Final Technical Report, IBM, 1985.

[15]An extension of the Bohm sheath criterium to a surface biased slightly negative with respect to a plasma showed that this assumption is valid to within 5% for the smallest sheath voltage encountered in the present model (R. W. Carlson, Ph. D. thesis, University of Minnesota 1966).

[16]The ion current density is determined by the plasma density n_0 at the interface between the plasma and the pre-sheath, the electron temperature, and the ion velocity, which is given by Bohm's criterium. The electron current density is determined by the plasma density n_0, the electron temperature, and the voltage across the sheath. Therefore, for a fixed potential between the plasma and the electrode, a nonzero value of the electric field at the sheath edge will only result in a slightly thinner plasma sheath and, thus, in a smaller transit time of the positive ions across the sheath.

[17]The fraction of electrons able to reach the electrodes for the sheath voltages encountered in the model is very small. The influence of this electron loss on the Boltzmann density distribution of the electrons in the sheath is very small (R. W. Carlson, Ph.D. thesis, University of Minnesota 1966).

[18]The potential difference between the electrode and the plasma is V_S. Therefore, the potential across the plasma sheath is $(V_S - V_1)$, where V_1 is the potential across the pre-sheath in Bohm's model (Fig. 2). In the present model it is assumed that T_e is independent of time. Therefore, V_1 can be omitted in Eqs. (1) and (2).

[19]R. H. Bruce, J. Appl. Phys. 52, 7064 (1981).

3087   J. Appl. Phys., Vol. 60, No. 9, 1 November 1986

Metze, Ernie, and Oskam   3087

12

SECTION III

THE ENERGY DISTRIBUTION OF IONS BOMBARDING ELECTRODE SURFACES IN RF PLASMA REACTORS

The Energy Distribution of Ions Bombarding Electrode Surfaces in RF Plasma Reactors

A. Metze,[a] D. W. Ernie, and H. J. Oskam
Department of Electrical Engineering
University of Minnesota
Minneapolis, MN 55455

ABSTRACT

A model is presented for the energy distribution of ions bombarding electrode surfaces in planar rf plasma reactors at low pressures, where collisions in the sheath may be ignored. Given the waveform for the voltage difference across the sheath adjacent to an electrode, the model predicts the ion bombardment energy distribution in the limit $t_r \ll 1/f$ and $t_r \gg 1/f$, where t_r is the transit time of the ions across the sheath and f is the frequency of the applied rf voltage. Utilizing sheath voltage waveforms from a previously published equivalent circuit model of a rf reactor[1], the model shows that the ion bombardment energy distribution is bimodal and skewed toward lower ion bombardment energies. The model also demonstrates one of the mechanisms responsible for narrowing of the ion bombardment energy distribution with increasing rf frequency. These results are compared with experimental measurements.

I. INTRODUCTION

Radio frequency gas discharges currently play a major role in the microelectronics industry for the fabrication of integrated circuits. These discharges are typically used for stripping of photoresist, anisotropic etching of semiconductor, oxide, and metal surfaces, and the deposition of organic and inorganic thin films. In a rf discharge, positive ions produced in the plasma volume are accelerated across the plasma sheath and may arrive at the electrodes with significant bombardment energy. Because the sheath

---

[a]Present address: Honeywell Systems and Research Center, 3660 Technology Drive, Minneapolis, MN 55418.

[1]A. Metze, D. W. Ernie, and H. J. Oskam, J. Appl. Phys. **60**, 3081 (1986).

structure (e.g., sheath thickness, sheath voltage, etc.) in an rf discharge is a periodic function of time, the resulting time averaged bombardment energy is not constant, but has a distribution of bombardment energies. In all the above mentioned applications , the ion bombardment energy distribution with which ions bombard the surfaces being processed is a critical factor in determining the resulting device quality and properties. For example, the ion bombardment energy distribution determines the degree of anisotropy in thin film etching, the amount of ion impact induced surface damage to semiconductor and oxide surfaces, the erosion rate of photoresist, and the degree of cross linking in polymer film deposition.[2,3] Therefore, it is important to obtain a better understanding of the dependence of the ion bombardment energy distribution on discharge parameters such as reactor geometry, frequency of the applied rf voltage, gas pressure, gas composition, etc.

The ion bombardment energy distribution in rf plasma reactors has been investigated experimentally by several authors. Vasile and Smolinsky studied the ion bombardment energy distribution at the wall of a 13.6 Mhz rf discharge in a mixture of argon and vinyltrimethylsilane at a few hundred milliTorr utilizing a retarding grid energy analyzer followed by a quadrupole mass spectrometer.[4] A similar arrangement was used by Thompson et al. to measure the ion bombardment energy distribution at an electrode of a 13.6 MHz discharge in SF_6, CF_3Cl, and CF_3Br for pressures of 0.2-1.0 Torr.[5] In both cases, the measured ion bombardment energy distribution consisted of a single peak at a bombardment energy and with an energy spread determined by the discharge pressure and power. Measurements of the ion bombardment energy distribution at the electrodes of a planar rf reactor have been studied by Coburn and colleagues for frequencies of 100 KHz-13.6 MHz in Ar at pressures of 20-50 mTorr using an electrostatic energy

[2]D. L. Flamm, V. M. Donnelly, and D. E. Ibbotson, in *VLSI Electronics*, edited by N. G. Einspruch and D. M. Brown (Academic, Orlando, 1984), Vol. 8, Chap. 8, p. 189.

[3]Russ. A. Morgan, Plasma Etching in Semiconductor Fabrication, Plasma Technology, 1 (Elsevier, New York, 1985).

[4]M. J. Vasile and G. Smolinsky, Int. J. Mass Spectrum. Ion Phys. 12, 133 (1973).

[5]B. E. Thompson, K. D. Allen, A. D. Richards, and H. H. Sawin, J. Appl. Phys. 59, 1890 (1986).

analyzer followed by a quadrupole mass spectrometer.[6-8] Results from these studies, in which collision effects were minimized by a judicious choice of the analyzed ion species, showed that the shape of the ion bombardment energy distributions is a function of the rf frequency, the ion mass, and the gas pressure. The shape was bimodal for low gas pressure, low rf frequency, and low mass ions, but became a single peak at higher pressure, frequency, and ion mass. Similar results have recently been reported by Briand et al. in Ar, CF_4, and SF_6 rf discharges [9]

Theoretical work has also been performed in an effort to calculate the ion bombardment energy distribution in a planar rf reactor. Tsui modeled the ion bombardment energy distribution in a rf reactor, calculating a bimodal distribution shape, with the distribution skewed toward higher energies.[10] Okamoto and Tamagawa subsequently calculated the energy spread of the ion bombardment energy distribution at the electrode of an rf reactor as a function of rf frequency in the limit where the transit time of the ions through the sheath, t_r, is large with respect to the period of the applied rf voltage, $1/f$, where f is the frequency of the applied voltage.[11] Their results indicated that the ion bombardment energy distribution is single peaked. Recently, Suzuki et al. have have considered the limit where $t_r << 1/f$.[12] They calculated the minimum and maximum bombardment energy and the spread of the energy distribution. While all of the above authors ignored the effect of collisions in the sheath, Monte Carlo techniques have recently been used by Kushner[13] and Thompson[14] et al. to investigate the ion bombardment energy distribution at the electrode of a planar rf plasma reactor in the presence of collisions. The Monte Carlo simulations show the

---

[6]J. W. Coburn and E. Kay, J. Appl. Phys. **43**, 4965 (1972).

[7]K. Köhler, J. W. Coburn, D. E. Horne, and E. Kay, J. Appl. Phys. **57**, 59 (1985).

[8]K. Köhler, D. E. Horne, and J. W. Coburn, J. Appl. Phys. **58**, 3350 (1985).

[9]P. Briand, G. Turban, and B. Grollean, Mat. Res. Soc. Symp. Proc. **68**, 109 (1986).

[10]R.T.C. Tsui, Phys. Rev. **168**, 107 (1968).

[11]Y. Okamoto and H. Tamagawa, J. Phys. Soc. Japan **29**, 187 (1970).

[12]K. Suzuki, K. Ninomiya, S. Nishimatsu, and S. Okudaira, J. Vac. Sci. Technol. **B3**, 1025 (1985).

[13]M. J. Kushner, J. Appl. Phys. **58**, 4024 (1985).

[14]B. E. Thompson, H. H. Sawin, and D. A. Fisher, (private communications).

dependence of the shape of the distribution on discharge parameters such as rf frequency, ion mass, pressure, etc. The results display both single peak and bimodal ion bombardment energy distributions, depending on the discharge conditions. All of the above studies were performed assuming that the electric potential difference across the plasma sheath is the superposition of a dc bias voltage and a sinusoidal rf voltage, or a version of this shape clipped to the floating potential of the sheath.

This paper presents calculations of the ion bombardment energy distribution at the electrode of a planar rf plasma reactor. A theoretical model is developed in the next section for the ion bombardment energy distribution at a surface exposed to the plasma. The model assumes a collisionless plasma sheath. The application of this model in the limits $t_r \ll 1/f$ and $t_r \gg 1/f$ will be discussed. Then, utilizing sheath voltage waveforms predicted by an equivalent circuit model for a planar rf plasma reactor,[1] calculations will be presented for the ion bombardment energy distribution at the electrode for both limiting cases. The effect of the various discharge parameters on the ion bombardment energy distribution will be discussed and the results compared with experiments. The resulting ion bombardment energy distribution has important consequences for the fabrication of microelectronic devices.

II. MODEL OF THE ION BOMBARDMENT ENERGY DISTRIBUTION

A. Plasma Sheath Model

The model for a planar plasma sheath in a rf discharge used in this paper is similar to the plasma sheath model presented previously.[1] A schematic representation of the plasma sheath is shown in Fig. 1. In order to arrive at a tractable, yet physically realistic solution, the following assumptions will be made. For a detailed discussion of the applicability of these assumptions refer to Ref. 1.

(1) The plasma consists of a singly charged positive ion species, electrons, and neutrals.

(2) The ions and electrons have a Maxwellian energy distribution with temperatures T_i and T_e, respectively.
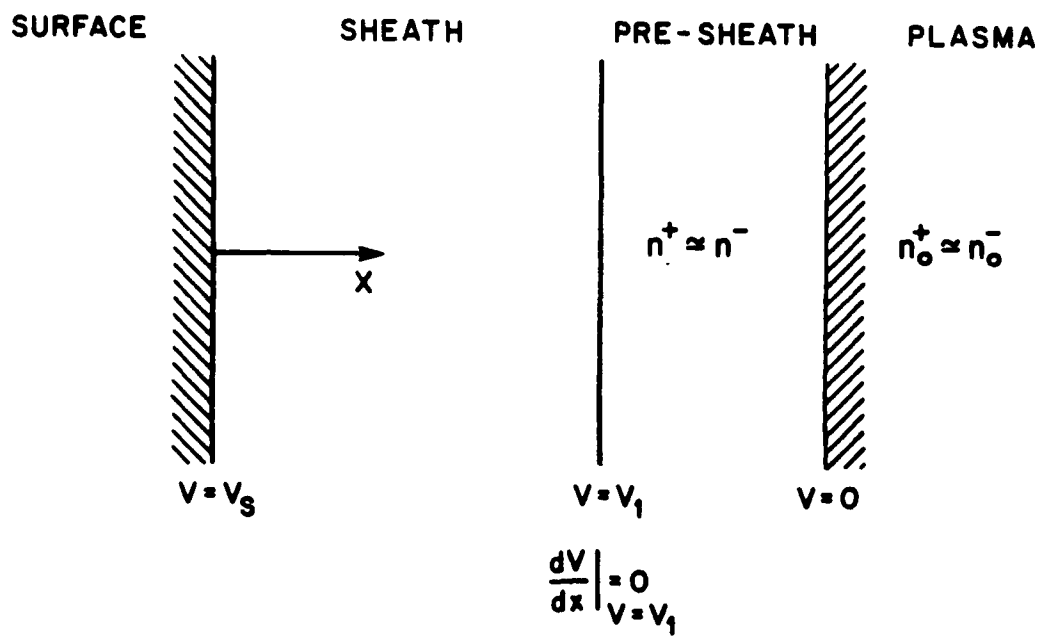
17

Fig. 1 Schematic representation of a planar plasma sheath.

(3) The ion and electron temperatures T_i and T_e are independent of time and spatial coordinates, with T_i being equal to the neutral gas temperature.

(4) The ion and electron densities inside the plasma volume, n_o^+ and n_o^-, respectively, are constant in time.

(5) The plasma sheath is collisionless.

(6) The ions enter the sheath from the pre-sheath with a speed equal to $(kT_e/M)^{1/2}$, as required by the Bohm sheath criterium.[15] Here, k is Boltzman's constant and M is the ion mass

(7) The electric field $\xi(x)$ is zero at the boundary between the pre-sheath and the plasma sheath.

(8) The electrons have a Boltzman density distribution in the pre-sheath.

(9) The influence of the electrons in the sheath can be neglected. The validity of this assumption depends on the voltage across the plasma sheath and the sheath properties of interest. For a surface biased negatively with respect to the plasma so that $V_S \ll V_1$, where $V_1 = - kT_e/2e$ and V_S is the voltage across the plasma sheath, only a small fraction of the electrons penetrate a significant distance into the sheath. Thus the electrons have little effect on the electric field in the majority of the sheath region. As a consequence, the electrons have little effect on the motion of the ions through the plasma sheath. Since this is the parameter of interest, as discussed below, the influence of electrons in the sheath can be ignored for situations where $V_S \ll V_1$. Indeed, this is always the case for an electrode surface in a planar rf reactor, as demonstrated by the sheath voltage waveforms calculated in Ref. 1.

(10) The rate at which ions enter the sheath from the pre-sheath is constant. This assumption is valid in the limit $t_r \ll 1/f$. For this limit, although the sheath thickness d will be a function of time, d will change slowly relative to the response time of the ions. For the limit $t_r \gg 1/f$, this assumption is also valid, since the sheath thickness d will then be a constant determined by the time averaged sheath voltage V_{dc} (i.e., the dc self bias), since the response time of the ions will be slow relative to changes in the sheath voltage. Calculations for the discharge parameters used in the

---

[15]D. Bohm, in *The Characteristics of Electrical Discharges in Magnetic Fields*, edited by A Guthrie and R. K. Wakerling (McGraw-Hill, New York, 1949), Chap. 3.

following discussion show that this assumption is valid for frequencies less than approximately 1 MHz and greater than approximately 10MHz.

Using the above assumptions, Poisson's equation in the sheath region is

$$\frac{d\xi^2}{dV(x)} = \frac{-2en_1}{\varepsilon_0} \left(\frac{-2eV_1}{M}\right)^{1/2} \left[\frac{-2eV(x)}{M}\right]^{-1/2}. \tag{1}$$

where the density of ions and electrons at the boundary between the pre-sheath and the sheath is

$$n_1 = n_0 \exp(eV_1/kT_e). \tag{2}$$

Under assumption (7), Eq. (1) can be integrated to yield

$$\xi[V(x)] = -2\left(\frac{-en_1}{\varepsilon_0}V_1\right)^{1/2} \left[\left(\frac{V(x)}{V_1}\right)^{1/2} - 1\right]^{1/2}. \tag{3}$$

Likewise, since $\xi(x) = -dV(x)/dx$, Eq. (3) can be integrated to yield

$$d - x = \frac{2}{3}\left(\frac{\varepsilon_0}{en_1}\right)^{1/2}(-V_1)^{1/2} \left[\left(\frac{V(x)}{V_1}\right)^{1/2} - 1\right]^{1/2} \left[\left(\frac{V(x)}{V_1}\right)^{1/2} + 2\right], \tag{4}$$

where the sheath thickness d is given by

$$d = \frac{2}{3}\left(\frac{\varepsilon_0}{en_1}\right)^{1/2}(-V_1)^{1/2} \left[\left(\frac{V_S}{V_1}\right)^{1/2} - 1\right]^{1/2} \left[\left(\frac{V_S}{V_1}\right)^{1/2} + 2\right]. \tag{5}$$

Using Eqs. (3), (4), and (5), it can be shown that

$$\xi(x) = -2\left(\frac{-en_1}{\varepsilon_0}V_1\right)^{1/2} \left\{\left[\frac{b}{2a} + \left(1 + \frac{b^2}{4a^2}\right)^{1/2}\right]^{1/3} + \left[\frac{b}{2a} - \left(1 + \frac{b^2}{4a^2}\right)^{1/2}\right]^{1/3}\right\}, \tag{6a}$$

where

$$a = \frac{2}{3}\left(\frac{\varepsilon_0}{en_1}\right)^{1/2}(-V_1)^{1/2} \tag{6b}$$

and

$$b = d - x. \tag{6c}$$

The above results for Eqs. (3)-(6) are equivalent to the Child-Langmuir sheath model, where $V_1 = -kT_e/2e$, as required by the Bohm criterium. The

20

above expressions give d and $\xi(x)$ as a function of the voltage V_S across the sheath.

B. Ion Bombardment Energy Distribution For $t_r \ll 1/f$

For a planar rf plasma reactor, the sheath voltage is a function of time, $V_S(t)$. If the transit time of the ions across the sheath is short with respect to the period of the applied rf voltage, i.e., $t_r \ll 1/f$, the sheath parameters d and $\xi(x)$ will be given by Eqs. (5) and (6), with $V_S = V_S(t)$. Therefore, d and $\xi(x)$ are also functions of time, i.e., d(t) and x(x,t). As a consequence, the resulting ion bombardment energy for an ion E(t) will be a function of time and will be determined by the time at which the ion enters the sheath region.

Consider the following equation of motion for an ion which enters the sheath at time $t = t_i$,

$$M \frac{d^2}{dt^2} x(t) = e\, \xi(x,t) \; , \tag{7a}$$

with initial conditions

$$x(t=t_i) = d(t=t_i) \tag{7b}$$

and

$$\frac{d}{dt} x(t) \Big|_{t=t_i} = -\left(\frac{-2eV_1}{M}\right)^{1/2} . \tag{7c}$$

Equation (7) can be solved for the velocity of the ion $dx(t)/dt$ at any time $t \geq t_i$ and for the transit time of the ion across the sheath, $t_r(t_i)$, which is now a function of the time when the ion entered the sheath. The resulting bombardment energy E(t) of the ion is then given by

$$E[t_i + t_r(t_i)] = \frac{M}{2}\left[\frac{d}{dt} x(t)\right]^2 \Big|_{t=t_i+t_r(t_i)} . \tag{8a}$$

However, since the sheath voltage is periodic, all the sheath parameters and the resulting ion bombardment energy will be periodic. Therefore,

$$E[t_i + t_r(t_i)] = E(\phi) \; , \tag{8b}$$

21

where ϕ is the phase angle of the sheath voltage at the time t_i and where $0 \leq \phi < 2\pi$.

If $P_E(E)dE$ is the probability that an ion will strike the surface with a bombardment energy in the interval dE and $P_\phi(\phi)d\phi$ is the probability that an ion is injected into the sheath with a phase angle in the interval $d\phi$, then

$$P_E(E) = P_\phi(\phi) \left| \frac{d\phi}{dE} \right| .$$

As a result of assumption (10), $P_\phi(\phi) = 1/2\pi$. Therefore, the ion bombardment energy distribution $P_E(E)$ is given by

$$P_E(E) = \frac{1}{2\pi} \left| \frac{d\phi}{dE} \right| , \qquad (9)$$

where $|d\phi/dE|$ is determined from Eq. (8).
It is worth noting that

$$\lim_{t_r f \to 0} E(\phi) \to - eV_S(\phi) ,$$

where $V_S(\phi)$ is the sheath voltage at phase angle ϕ. Therefore, Eq. (9) simplifies for $t_r f \to 0$ to

$$P_E(E) = \frac{1}{2\pi e} \left| \frac{d\phi}{dV_S} \right| . \qquad (10)$$

C. Ion Bombardment Energy Distribution For $t_r \gg 1/f$

If $t_r \gg 1/f$, the ions will not be able to respond to the instantaneous sheath voltage, but only to the average value V_{dc}. In this situation, the sheath thickness d is constant and can be assumed to be given by Eq. (5), with $V_S = V_{dc}$. Likewise, the electric field in the sheath can be assumed to have a constant shape, but a time dependent magnitude, as given by

$$\xi(x,t) = \xi_{dc}(x) \frac{V_S(t)}{V_{dc}}, \qquad (11)$$

where $\xi_{dc}(x)$ is given by Eq. (6) with $V_S=V_{dc}$. For this case, Eq. (7), (8), and (9) can again be solved utilizing the constant sheath thickness assumption and Eq. (11), yielding the ion bombardment energy distribution $P_E(E)$.

III. NUMERICAL RESULTS AND DISCUSSION

Numerical calculations were performed based on the above ion bombardment energy distribution model for the discharge conditions assumed in Ref. 1, i.e.,

M = 40 amu (argon discharge),
n_o = 10^{10} particles/cm^3 (charged particle density in the plasma),
T_i = 500 °K (ion temperature),
T_e = 23,200 °K (electron temperature).

For these discharge parameters, calculations show that 0.1 μs < t_r < 0.5 μs.

The sheath voltage waveforms for the target electrode presented in Ref. 1 were used for $V_S(t)$ in these calculations. These waveforms are reproduced in Figs. 2 and 3 for future reference. Fig. 2 is for a planar rf reactor with an electrode area ratio $A_T/A_S=1.0$, while Fig. 3 is for $A_T/A_S=0.2$, where A_T is the area of the target electrode and A_S is the area of the substrate electrode. These sheath voltage waveforms were derived for f=100 KHz and can therefore be directly used in the ion bombardment energy distribution model for the limiting case $t_r \ll 1/f$. Calculations were performed at f=100 KHz using these waveforms. In addition, in order to investigate the effect of frequency on the ion bombardment energy distribution, calculations were also performed at f=13.6 MHz, where the limiting situation $t_r \gg 1/f$ applies. For this situation, the same sheath voltage waveforms from Figs. 2 and 3 were again used, even though these waveforms probably do not accurately reflect the actual sheath voltage waveforms at this frequency. However, as shown below, these calculations are useful for demonstrating the effect of frequency on the resulting ion bombardment energy distribution, independent of the effect of frequency on other sheath properties, such as the sheath voltage waveform.

In order to more accurately compare the results presented below with experimental measurements of the ion bombardment energy distribution, it

23

Fig. 2. Calculated waveform of the potential V_{ST} across the plasma sheath adjacent to the target electrode (and that of the potential V_{SS} across the substrate electrode) for $A_T/A_S=1$, from Ref. 1.
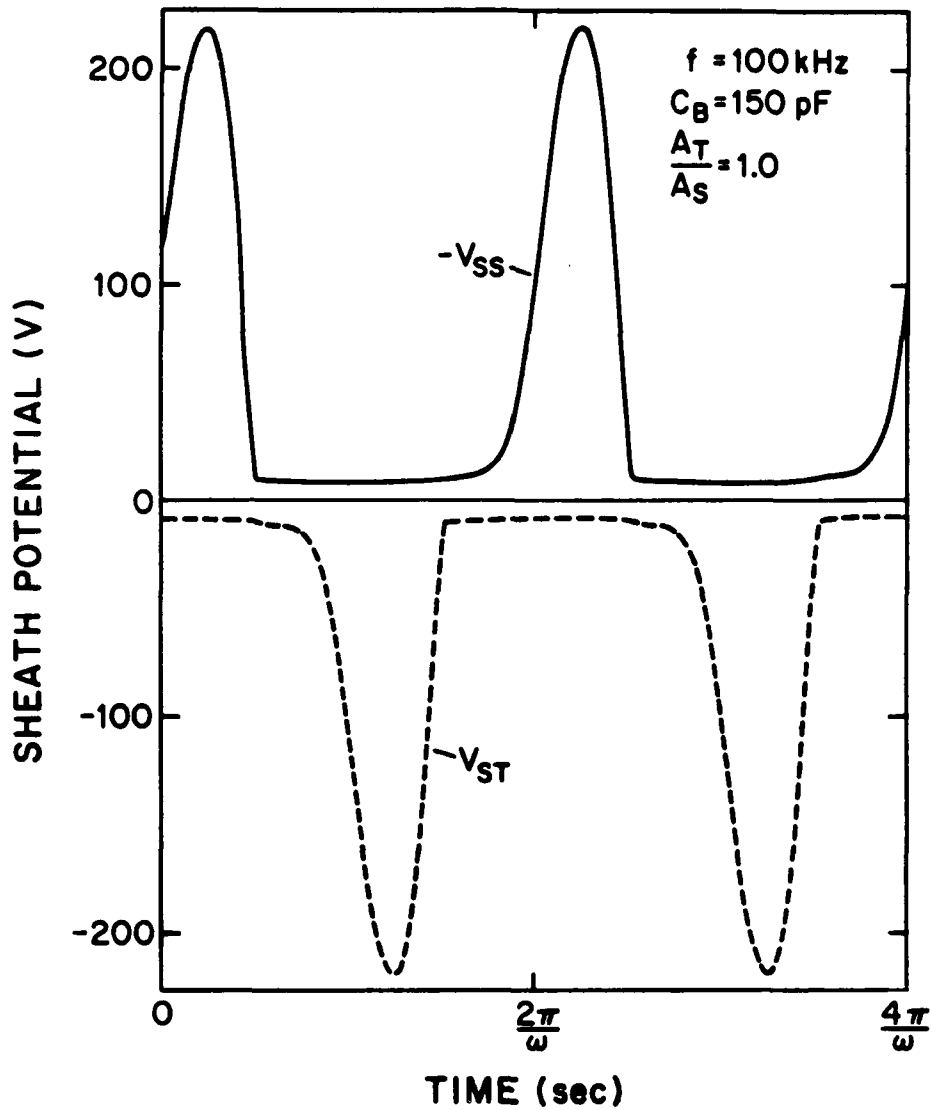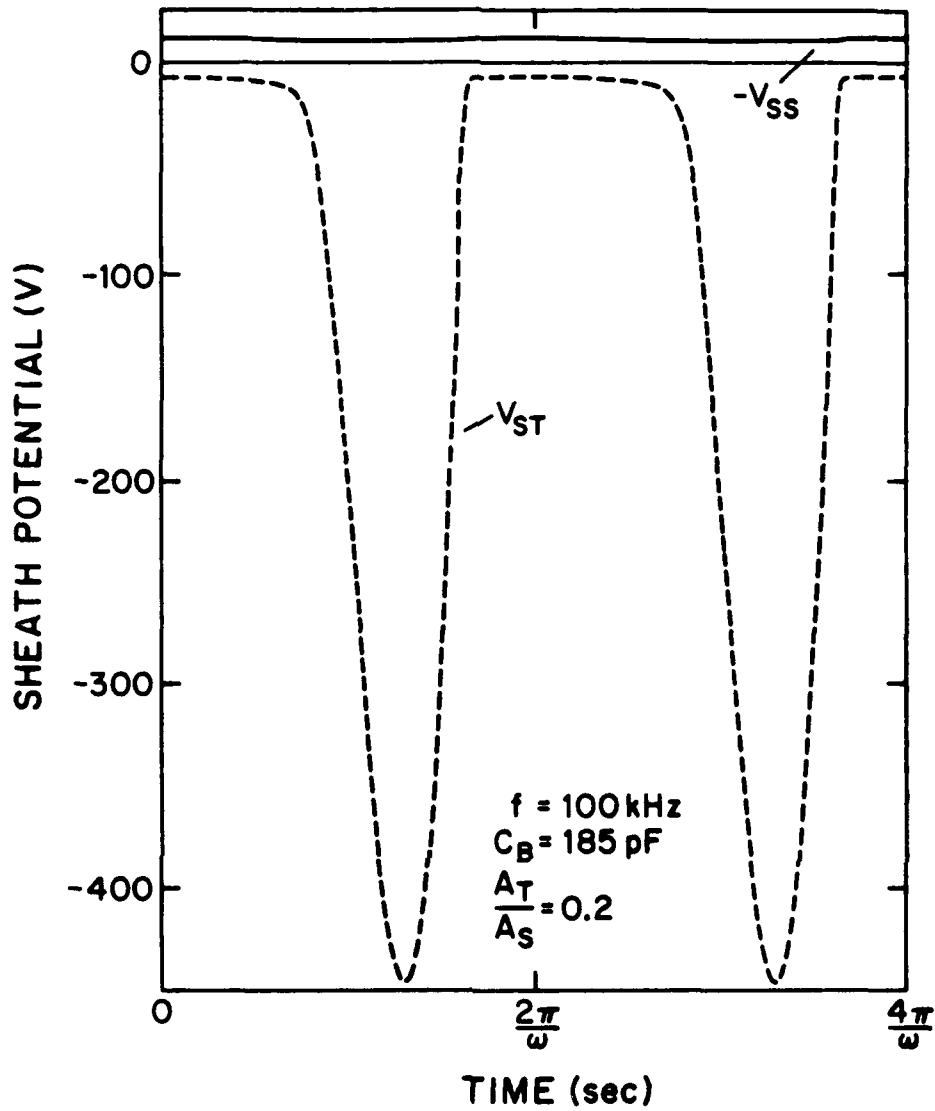
Fig. 3. Calculated waveform of the potential V_{ST} across the plasma sheath adjacent to the target electrode (and that of the potential V_{SS} across the substrate electrode) for A_T/A_S=0.2, from Ref. 1.

25

was desirable to fold in the effect of the finite energy resolution of an experimental energy analysis system. If it is assumed that , to first order, the energy analyzer has a square transmission window of width ΔE, the quantity measured by the experimental system will be the ion bombardment energy distribution $P_E(E)\Delta E$. In the following discussion, results are presented for $P_E(E)\Delta E$ with $\Delta E=0.5$ eV.

Figures 4 and 5 show the calculations of the ion bombardment energy distribution for two different electrode area ratios utilizing the target sheath voltage waveforms from Figs. 2 and 3, respectively, for f=100 KHz and 1 MHz. As can be seen from these results, the ion bombardment energy distributions are bimodal and skewed toward lower energies. The bimodal characteristic of the distributions can be qualitatively explained by considering Eq. (10) for the limit $t_r f \rightarrow 0$. In this limit, $P_E(E)\Delta E$ is inversely related to the derivative with respect to phase angle (or time) of the sheath voltage waveform . Thus, the resulting ion bombardment energy distribution has a lower value for those energy ranges which correspond to locations on the sheath voltage waveform where the waveform is a rapidly changing function of phase angle (or time). In addition, the skewing of the distributions is due to the nonsinusoidal shape of the sheath voltage waveforms which results in the ions being accelerated for a large fraction of each rf cycle by a small sheath potential and only for a small fraction of each rf cycle by a large sheath potential. Thus, a larger number of ions impact the target electrode with low bombardment energy than with high bombardment energy.

Figs. 4 and 5 also show that the energy spread of the distribution narrows with increasing frequency. This is to be expected, since at low excitation frequencies (e.g., at 100 KHz) the ions traverse the sheath in a fraction of the rf period. Consequently, the ions bombard the the sheath with an energy $-eV_S(t_i)$, where $V_S(t_i)$ is the sheath voltage at the instant when the ions enter the sheath. Therefore, the resulting energy spread in the distribution function is essentially determined by the peak to peak amplitude of the sheath voltage waveform. If, however, the ion transit time is long with respect to the rf period (e.g., at 13.6 MHz), then the ions are effectively accelerated across the sheath by the time average of the sheath voltage waveform. In this case, a smaller percentage of the energy gained by the ions in the sheath can be attributed to the rf component of the sheath
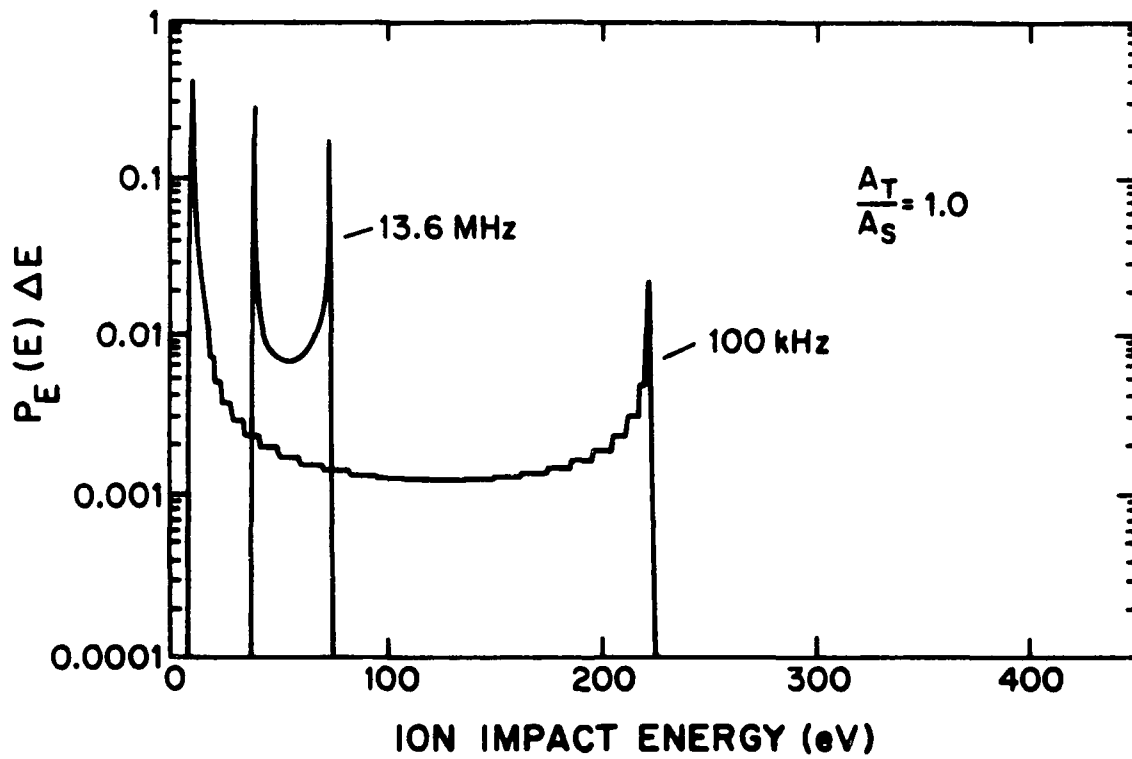
26

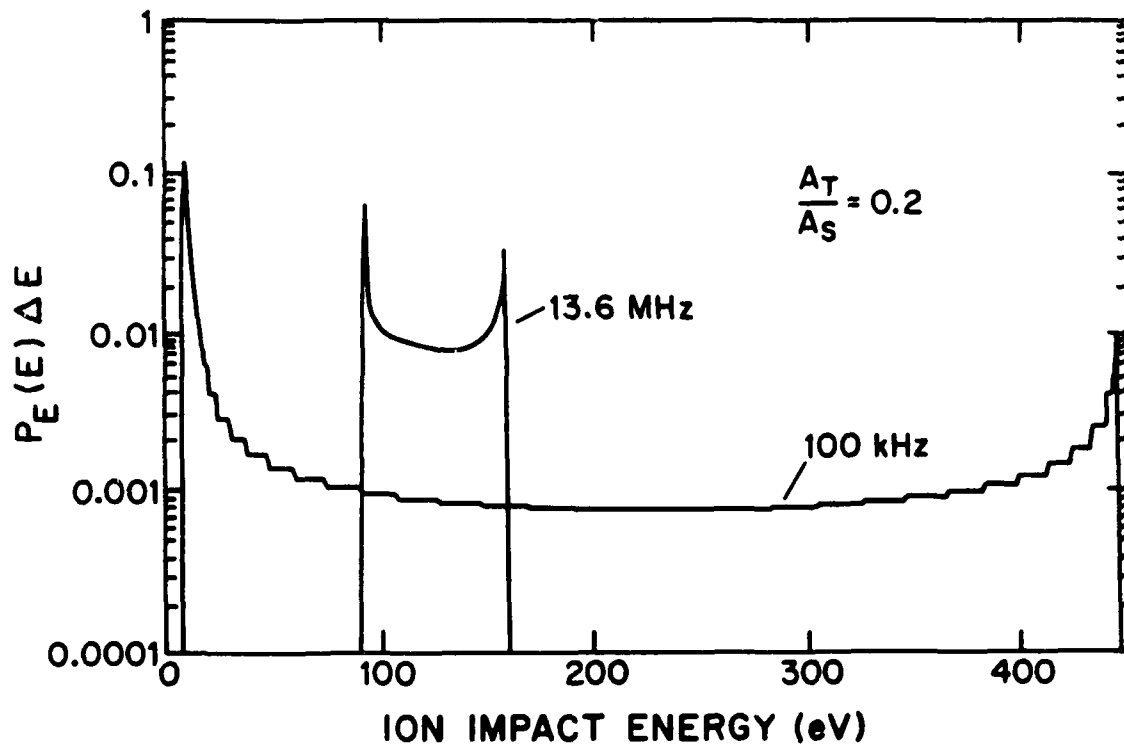Fig. 4. Calculated ion bombardment energy distribution for $A_T/A_S=1$.

Fig. 5. Calculated ion bombardment energy distribution for $A_T/A_S = 0.2$.

voltage. As a result, the energy spread of the ion bombardment energy distribution decreases with increasing frequency.

The results of these calculations can be compared with the experimental measurements of Coburn and Kay.[6] In their studies, the energy distribution of the ion surface flux at an electrode was determined for low pressures and for minority ion species which did not undergo significant resonance charge transfer collisions. Thus, the experimental conditions closely approximated the collisionless sheath assumption used in deriving our model. The shape of the energy distributions shown in Figs 4 and 5 agree well with the experimental results. In both cases, the distributions are bimodal and skewed toward lower energy. In addition, the experimental studies showed the distribution narrowing with increasing ion mass, for a fixed rf frequency. This narrowing is similar to the narrowing of the spread in the distribution predicted by our model. This similarity results from the fact that both effects are due a change in the ratio of the ion transit time to the rf period. This ratio may be increased by either increasing the ion mass, which causes an increase in the ion transit time, or by increasing the rf frequency, which decreases the rf period.

Finally, a comparison between Figs. 4 and 5 shows that the ion bombardment energy achieves higher values in Fig. 5 than in Fig. 4. This occurs since the area of the target electrode is smaller than the area of the substrate electrode for the data given in Fig. 5, while the areas are equal in for Fig. 4. Since the sheath voltage waveforms in Figs. 2 and 3 were both for the same peak to peak rf voltage applied across the reactor electrodes, the target sheath voltage waveform had a larger peak to peak magnitude for the case of unequal area electrodes. Thus, the ion bombardment energies are higher in Fig. 5, where the target electrode is smaller than the substrate electrode.

IV. CONCLUSIONS

A model has been presented for the ion bombardment energy distribution at an electrode of a planar rf plasma reactor. The model is valid under the conditions given in Sec. II, where it was assumed that the sheath adjacent to the electrode is collisionless and that the electron temperature and the charged particle density in the plasma are independent of time. Given the

sheath voltage waveforms, the model predicts the ion bombardment energy distribution in the limit $t_r \ll 1/f$ and $t_r \gg 1/f$, where t_r is the transit time of the ions across the sheath and f is the frequency of the applied rf voltage. Numerical calculations were performed at f=100 KHz and 13.6 MHz using this model with the sheath voltage waveforms given in Ref. 1 for the target electrode. Although these sheath voltage waveforms are strictly valid only for the calculations at f=100 KHz, where $t_r \ll 1/f$, they were also used for the calculations at f=13.6 MHz, where $t_r \gg 1/f$, in order to determine the effect of frequency on the ion bombardment energy distribution independent of the effect of frequency on other sheath properties.

The resulting numerical calculations show that the ion bombardment energy distribution is bimodal and skewed toward lower energy. In addition, the energy spread of the distribution narrows with increasing frequency. Finally, the increase in ion bombardment energy with decreasing target electrode to substrate electrode area ratio is demonstrated. A qualitative explanation of these effects has been given. These results compare favorably with previous experimental studies.[6]

As indicated, the above results were derived under the assumption of a collisionless sheath and are, therefore, valid only at low pressures and/or for ion species which do not undergo significant resonance charge transfer collisions. It is anticipated that the incorporation of the effects of collisions will be to smear out the resulting ion bombardment energy distribution and displace the high energy peak in the distribution toward lower bombardment energy. This result would be consistent with previous experimental studies were collisions in the sheath were an important factor.[5,9] An extension of the model to include the effect of collisions is currently in progress.

A further constraint on the validity of these results is imposed by the assumptions of a constant electron temperature and charged particle density in the plasma. As discussed in Ref. 1, the energy modulation of the majority of the electrons is small for frequencies larger than approximately 50 KHz and gas pressures smaller than approximately 1 Torr, for the case of argon discharges discussed in this paper. Even for other gases (e.g., CF_4, SiH_4, etc.), this assumption is probably still valid in the low pressure regime required by the collisionless sheath assumption. The validity of the assumption of a constant charged particle density in the plasma volume

depends on the loss rate of the charged particles from the plasma and the production rate of the particles in the plasma. In particular, the modulation in the production rate (and, therefore, of the density) of the charged particles depends on the maintenance mechanism of the discharge, as discussed in Ref. 1. The production mechanism of primary importance is, however, a function of the discharge parameters such as frequency of the applied rf voltage, gas pressure, gas mixture, etc. The possible effect of this production rate modulation is not included in the present model.

ACKNOWLEDGMENTS

SECTION IV

AN EXPERIMENTAL STUDY OF ION BOMBARDMENT ENERGY DISTRIBUTIONS IN RF DISCHARGES

An Experimental Study of Ion Bombardment Energy Distributions in RF Discharges

M. F. Toups, D. W. Ernie, and H. J. Oskam
Department of Electrical Engineering
University of Minnesota
Minneapolis, MN 55455

I. INTRODUCTION

The energy with which ions in a plasma strike a surface exposed to the plasma is the subject of much current interest. This is especially true for radio frequency, i.e., rf, driven plasmas which are used by the microelectronics industry in the fabrication of integrated circuits. Two such examples of the use of rf plasmas are plasma etching and plasma deposition. In both plasma etching and plasma deposition, the energy with which ions strike the substrate surface can be very critical in determining the properties and quality of the process. For example, the ion bombardment energy distribution is known to effect the amount of surface damage and the degree of anisotropy during rf plasma etching[1].

Measurements of the ion bombardment energy distribution of ions incident on an electrode in a rf plasma reactor have been reported previously by other researchers. Coburn and coworkers developed an ion energy analysis system which combined a 90° deflection electrostatic hemispherical bandpass energy analyzer with a quadrupole mass analyzer. This system was initially described in a study[2] of ion bombardment energy distributions in dc discharges used for dc sputter deposition. This system was subsequently modified to measure the ion bombardment energy distributions that occur in rf diode sputter deposition[3]. In this publication, these ion bombardment energy distributions were then utilized to determine the maximum ion bombardment energy for several different discharge situations. However, only a single set of ion bombardment energy

---

[1]D. L. Flamm, V. M. Donnelly, and D. E. Ibbotson, in *VLSI Electronics*, edited by N. G. Einspruch and D. M. Brown (Academic, Orlando, 1984), Vol. 8, Chap. 8, p. 189.

[2]J. W. Coburn, Rev. Sci. Instrumen. **41**, 1219 (1970).

[3]J. W. Coburn and E. Kay, J. Appl. Phys. **43**, 4965 (1972).

distribution curves for H_3^+, H_2O^+, and Eu^+ from a discharge in argon driven with 100 Watts of 13.56 MHz rf power were presented in this paper. Two similar studies[4, 5] by these investigators included ion bombardment energy distributions for: Ar_2^+ in a 50 mTorr, 13.56 MHz argon discharge; ArH^+ in a 20 mTorr, 13.56 MHz argon discharge; and ArH^+ in a 100 kHz, 50 mTorr argon discharge.

Vasile[6] utilized a system consisting of a retarding grid energy analyzer in conjunction with a quadrupole mass spectrometer to measure the ion bombardment energy distributions of F_2^+ and F^+ ions in a rf discharge for a mixture of helium and fluorine. RF discharges in chlorine were studied by Donnelly, Flamm, and Bruce[7] using a retarding grid energy analyzer with a quadrupole mass spectrometer. Thompson, Allen, Richards, and Sawin[8] studied the ion bombardment energy distributions in discharges of gases containing various fluorine and chlorine compounds. They also used a retarding grid energy analyzer, but with a plate as a detector. Thus, their ion energy distribution results were not mass resolved.

Other studies have measured the ion bombardment energy distribution incident on the wall in contact with the plasma rather than an electrode. A study was performed by Vasile and Smolinsky[9] using a reactant gas mixture of argon and vinyltrimethylsilane. Measurements have also been made of the ion bombardment energy distributions in a rf driven Thonemann ion source. A paper by Erő[10] contains a high resolution ion bombardment energy distribution obtained by using an electrostatic deflection energy analyzer.

The study described here was undertaken as part of an effort to provide a database on rf discharges for use in the modeling of rf reactors. The need for accurate data on rf discharges which arose during the development of a model for rf discharges by Metze, Ernie, and Oskam[11]

[4]K. Köhler, J. W. Coburn, D. E. Horne, E. Kay, and J. H. Keller, J. Appl. Phys. **57**, 59 (1985).

[5]K. Köhler, D. E. Horne, and J. W. Coburn, J. Appl. Phys. **58**, 3350 (1985).

[6]M. J. Vasile, J. Appl. Phys. **51**, 2503 (1980).

[7]V. M. Donnelly and D. L. Flamm, J. Appl. Phys. **58**, 2135 (1985).

[8]B. E. Thompson, K. D. Allen, A. D. Richards, and H. H. Sawin, J. Appl. Phys. **59**, 1890 (1986).

[9]M. J. Vasile and G. Smolinsky, Int. J. Mass Spectrom. Ion Phys. **12**, 133 (1973).

[10]J. Erő, Nuclear Instrm. **3**, 303 (1958).

[11]A. Metze, D. W. Ernie, and H. J. Oskam, J. Appl. Phys. **60**, 3081 (1986).

demonstrated the necessity for this experimental work. This model has been used to predict the ion bombardment energy distributions at the electrodes of a capacitively coupled rf discharge[12]. Since only limited experimental data for the ion bombardment energy distribution in rf discharges was available, these experiments were undertaken to increase the range of pressures and frequencies over which the ion bombardment energy distributions have been measured so that a more realistic comparison can be made with the model predictions. Since it is desirable to first understand the physics of the rf plasma, noble gases were used in these experiments in order to simplify complications due to chemical reactions in the plasma. It is hoped that the refinement of present models of a rf plasma using the results of these experiments will ultimately lead to a better understanding of more complicated plasma systems, such as those currently used in the plasma processing environment.

II. EXPERIMENTAL APPARATUS

A. General Configuration

The vacuum system used in these experiments is shown schematically in Fig. 1. This vacuum system consisted of two separate chambers. The first chamber is the reactor chamber in which the desired rf discharge was maintained. The second chamber is the analysis chamber which housed a retarding grid energy analyzer and a quadrupole mass spectrometer. The two chambers were separated by a wall containing a 100 μm diameter sampling orifice which allowed for sampling of the particles that were incident on this wall of the reactor chamber followed by subsequent analysis of these sampled particles in the analysis chamber.

---

[12]A. Metze, D. W. Ernie, and H. J. Oskam, 37th Gaseous Electronics Conference, Bull. Amer. Phys. Soc. **30**, 145 (1985).
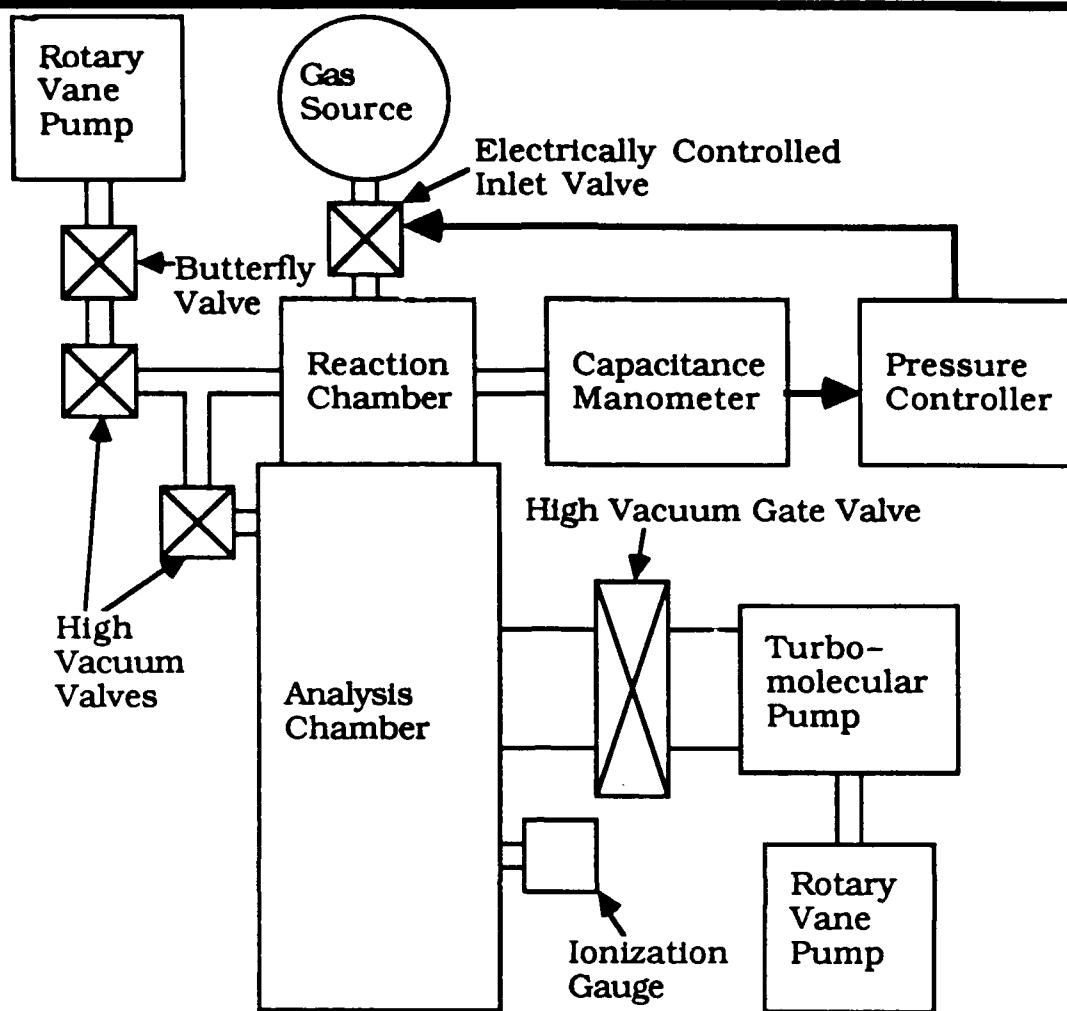
FIG. 1. Block diagram of the vacuum system.

A high vacuum valve interconnected the reactor chamber and the analysis chamber and wss used for evacuating the reactor by the analysis chamber's vacuum pumps when the system wss not in use. During data acquisition, this valve was closed and the plasma reactor chamber was maintained at a constant pressure by an electronic feedback control system which used a capacitance manometer as input and controled an electrically controlled inlet valve which was connected to the gas source. A two stage rotary vane pump was also connected to the reactor chamber through a second high vacuum valve and a butterfly valve. The system was normally operated in a quasi-static mode with these two valves closed. In the quasi-static mode, the only loss of gas from the reactor was through the sampling

orifice. In order to compensate for this loss, a equal amount of reactant gas was introduced into the plasma reactor through the electrically controlled inlet valve. By this means, the pressure in the reactor was held at a constant value. In this mode of operation, the mechanical pump was simply used to rough down the reactor chamber before interconnecting it with the analysis chamber for further evacuation. In addition, however, the butterfly valve allowed the system to also be used as a flowing system where the pressure was again maintained at a constant value, but the gas loss was than determined by both the loss due to the orifice and the loss through the butterfly valve. In this mode, the mechanical pump had an active role and the flow rate was determined by the butterfly valve setting. In either mode, the pressure control system made it possible to maintain any desired constant pressure from 10 mTorr to 10 Torr.

The analysis chamber housed the energy analyzer, a quadrupole mass spectrometer, and an ion multiplier detector. This chamber was evacuated by a turbomolecular pump which was backed by a two-stage rotary vane pump. When the reactor chamber was evacuated, the analysis chamber achieved a pressure of 10^{-8} Torr. At all pressures of the reactor chamber used in the experiments, the pressure of the analysis chamber was always below 10^{-5} Torr. It was necessary to maintain this low pressure in the analysis chamber so that the sampled particles from the reactor undergo no additional collisions in the analysis chamber. The pressure in this chamber was monitored by an ionization gauge.

The energy analyzers used were of the retarding grid type. A retarding grid energy analyzer utilizes a metal mesh or grid which is attached to a variable voltage source. A beam of charged particles with a certain kinetic energy directed towards the grid can only reach and pass through the grid if the kinetic energy of the particles is greater than the product of the charge on the particle times the electric potential of the grid measured with respect to the electric potential at the location where the particles originated. A properly designed retarding grid energy analyzer allows all the particles with a kinetic energy to charge ratio greater than the retarding voltage to pass through the grid and be detected by the detection system. Thus, it should be noted that a retarding grid energy analyzer yields an integral of the ion energy probability density function and not the function itself. However, the ion energy probability density function may be found by

taking the derivative of the measured result with respect to the ion energy. Actually, for many uses, one is more interested in the number of ions having an impact energy greater (or less) than a certain energy. This is the parameter that was directly measured by a retarding grid energy analyzer.

The quadrupole mass analysis system consisted of a quadrupole mass filter and an electrostatic lense array to help focus the incoming ion beam into the quadrupole. There was also an electron impact ionization assembly within the lense array. This allowed mass analysis of the neutral content of the beam extracted through the orifice from the plasma. The ion multiplier detector was run in a pulse counting mode in order to achieve high sensitivity. The resulting mass analysis system had enough sensitivity to allow for a mass analysis of residual background gases when the entire system was evacuated to 10^{-8} Torr. Besides the vacuum system, there were support electronics for maintaining and biasing the plasma and for the quadrupole mass spectrometer and its ion multiplier detector system. Further support equipment was also provided for the energy analysis system. A computer controlled data acquisition system was used to coordinate the operation of the quadrupole and energy analysis systems.

B. Initial Design of Reactor and Energy Analyzer

Two different reactor chamber designs were used. The first reactor was of the cylindrical discharge tube type and is diagrammed in Fig. 2. The discharge tube was constructed of 2.5 cm diameter Pyrex tubing. The sampling orifice was located in a narrow metal band which replaced a small section of the Pyrex tubing. A 100 μm diameter orifice was machined in the band at a location where the band was 20 μm thick. This combination of metal thickness and orifice size was chosen in order to minimize collisions with the sides of the orifice and to ensure that the flow through the orifice was in a molecular regime. The discharge tube contained three additional electrodes, any given pair of which could be chosen as the anode and cathode. These electrodes were initially short sections of hollow stainless steel tubing. However, other electrode shapes for the cathode were tried in order to alleviate problems with noise in the discharge, as discused below.

39

To Gas Inlet Valve

Tc Capacitance Monameter

Cylindrical Electrode with 100 μm Orifice

To High Vacuum Valve

Cylindrical Electrodes

Pyrex Window
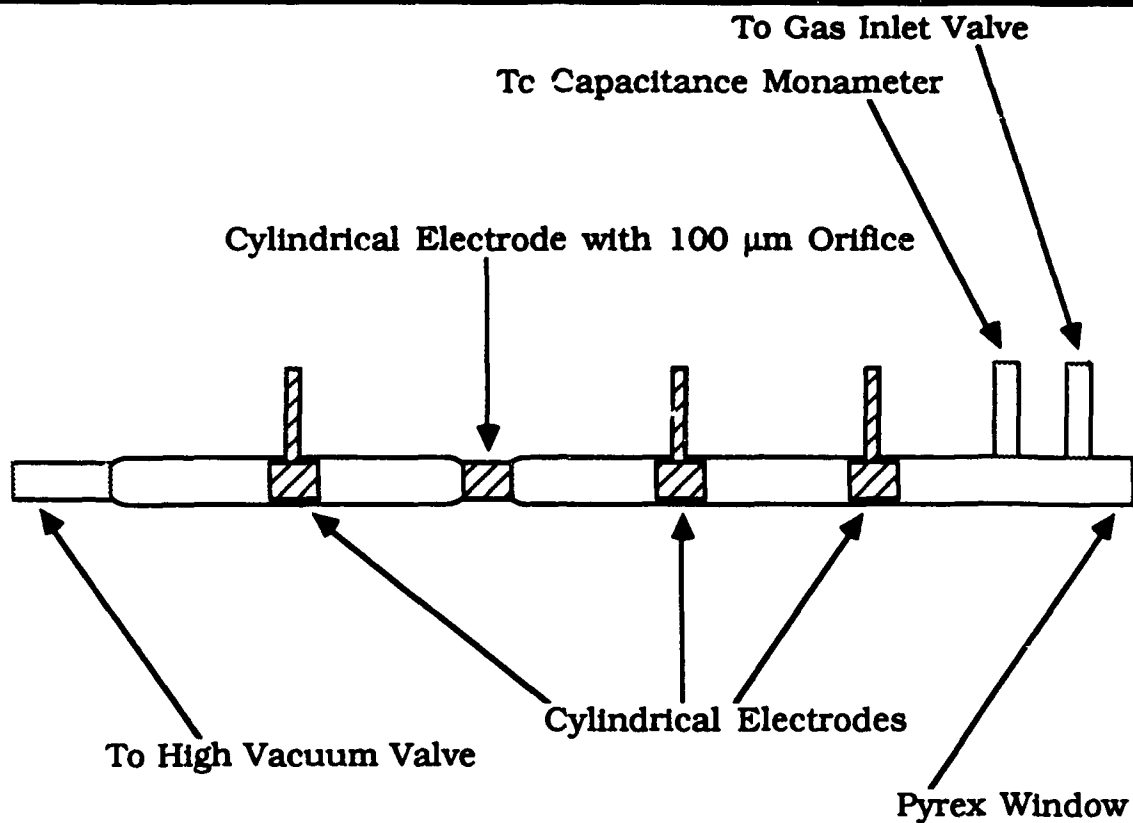
FIG. 2. Design of the cylindrical reactor.

In the experiments which utilized the cylindrical reactor shown in Fig. 2, the reactor was biased as shown in Fig. 3. The dc current in the discharge tube was set by supply V_0. The dc potential of the anode with respect to ground was determined by supply V_B. As a result, V_B could effectively be used to apply a dc bias potential to the sampling electrode with respect to the potential of the plasma at the location of the sampling electrode. This was done by first allowing the sampling electrode to float and measuring the voltage on the sampling electrode with respect to ground, yielding the sum of the electric potential of the plasma at the location of the sampling electrode and the floating potential of the wall with respect to the plasma. This voltage could be adjusted by adjusting V_B. Then, when the sampling electrode was subsequently grounded, a voltage equal to the floating potential minus the previously measured voltage was effectively applied between the plasma and the sampling electrode.

40

Supply V_{rf} provided an additional small rf potential to the discharge region without significantly disturbing the dc conditions of the tube. It should be noted that even though the anode and cathode of the discharge tube were at different dc potentials, they (and the entire plasma in the discharge tube) were at the same rf potential. This biasing arrangement allowed for a known rf potential superimposed with an adjustable dc potential to be applied between the plasma and the sampling electrode. This biasing arrangement corresponded to the conditions across a single sheath used in developing the ion bombardment energy distribution model previously mentioned, i.e., Refs. 11 and 12. It was hoped that this setup could yield information on the effect of a time varying sheath potential on the energy distribution of ions traversing the sheath.
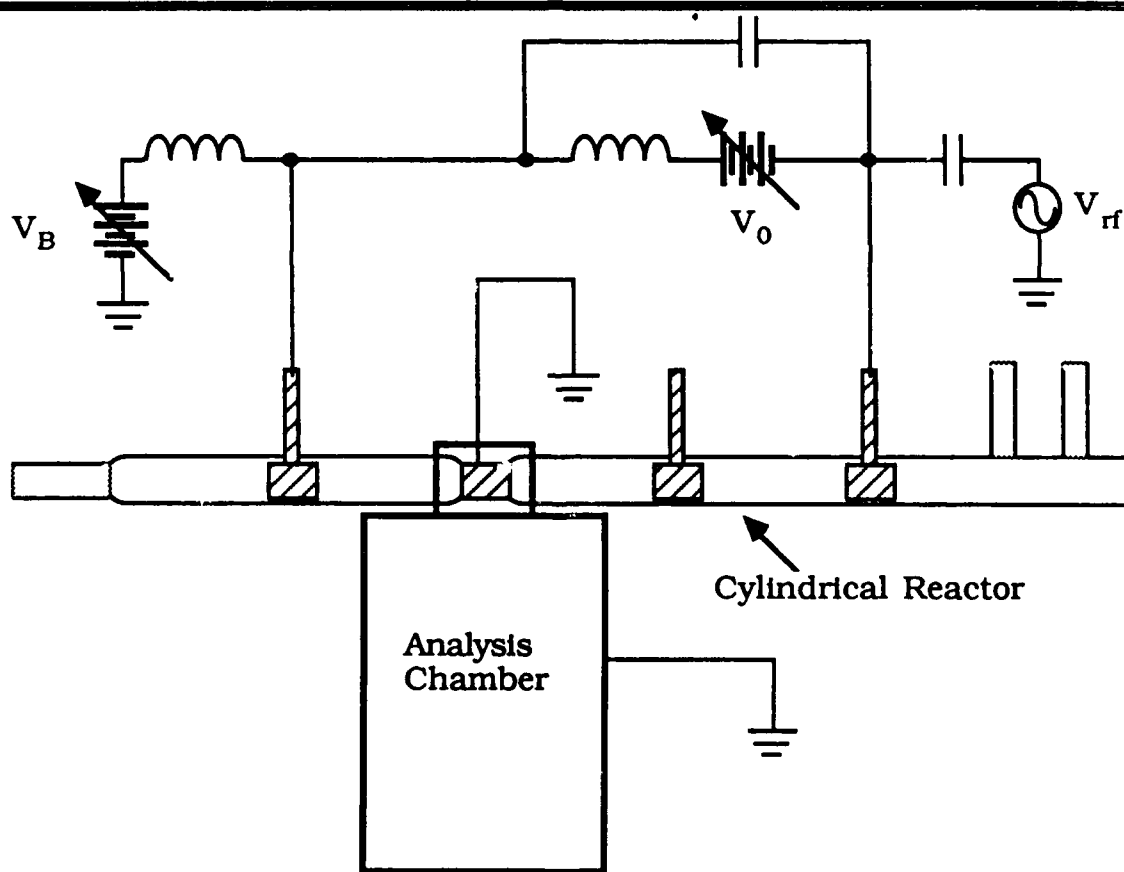

FIG. 3. Biasing scheme used with the cylindrical reactor.

The initial experimental setup utilized the cylindrical discharge tube described above and a three grid planar retarding grid energy analyzer. The energy analyzer was located at the entrance to the focusing lenses of the quadrupole mass spectrometer. This setup failed to yield acceptable results for several reasons. First, the electrostatic lenses of the quadrupole are themselves energy selective. A small variation in the bias potential of the electrostatic lenses produced large changes in the resulting ion energy distribution measurement. An attempt to correct this problem was made by removing the electrostatic lenses from the quadrupole and mounting the energy analyzer directly on the quadrupole itself. However, this failed to yield the desired improvement because the quadrupole itself is also energy selective. However, an additional and far worse problem was the criticality of the alignment of the quadrupole and the orifice, with small changes in the alignment of the quadrupole relative to the orifice resulting in large deviations in the measured ion energy distribution. It was realized that if the incoming ion beam is not perfectly perpendicular to the energy analyzer, the varying potential on the second grid would cause the beam to be deflected by varying amounts depending upon the potential applied to this grid and the velocity of the individual ions. This, in turn, caused the beam to be misaligned by varying amounts when entering the quadrupole and, hence, the amount of the beam actually detected had an additional functional dependence on of the potential applied to the retarding grid. In fact, it was possible to align the system so that the amount of signal detected increased over a region where the retarding potential for positive ions was also increasing. This is clearly an invalid result, since an increase in the retarding potential can only result in a decrease in the number of positive ions passing through the energy analyzer. This increase in signal was not due to an increase in the number of positive ions transmitted through the energy analyzer, but due to the ion beam being swept into alignment with the quadrupole by the energy analyzer so that the transmission losses of the quadrupole were reduced. Because of these problems it was decided that, although the quadrupole could be used to determine which ionic species were present, it could not be used in conjunction with a retarding grid energy analyzer to yield unambiguous ion bombardment energy distributions. Subsequent experiments were performed using a plate (or mesh) behind the energy analyzer as the detector. While this scheme did not allow for the

42

measurement of mass analyzed ion bombardment energy distributions, it did yield reliable results. Furthermore, by choosing the correct discharge conditions, the sampled ion beam could be made to consist of predominantly one ion species, as confirmed by mass spectrometer analysis.

This resulting setup still failed to yield the desired results due to oscillations in the dc discharge. It was found that when there was no applied rf potential and the sampling electrode was allowed to float, the voltage of the sampling electrode tended to oscillate. This oscillation generally had an amplitude of about ten volts and was strongly affected by the current through the tube and the gas pressure within the tube. Since previous studies[13] had indicated that the noise in dc discharges may be a strong function of anode size and decreases for increasing anode area, attempts were made to eliminate these oscillations by increasing the area of the anode and by using a planar anode surface. While these new design features did decrease the oscillations slightly, this decrease was not sufficient to allow the measurements to be performed at the required pressures. Because of this oscillation problem, the cylindrical discharge tube design was abandoned and the planar reactor described in the next section was constructed.

C. Final Design of Reactor and Energy Analyzer

The second reactor chamber was a parallel plate reactor as shown in Fig. 4. The reactor chamber consisted of a 10 cm Pyrex bell jar mounted on a 15 cm adapter plate in the center of which was a 100 μm diameter orifice which connected the reactor chamber to the analysis chamber. The adapter flange served as one electrode for the discharge. The second electrode was a 9 cm metal plate which ccould be placed a variable distance from the lower electrode. This reactor realistically represented the geometry for which the equivalent circuit model of an rf discharge given in Ref. 11 was derived.

[13]A. Garscadden, in *Gaseous Electronics*, edited by M. N. Hirsh and H. J. Oskam (Academic, New York, 1978), Vol. 1, Chap. 2.2, p. 65.
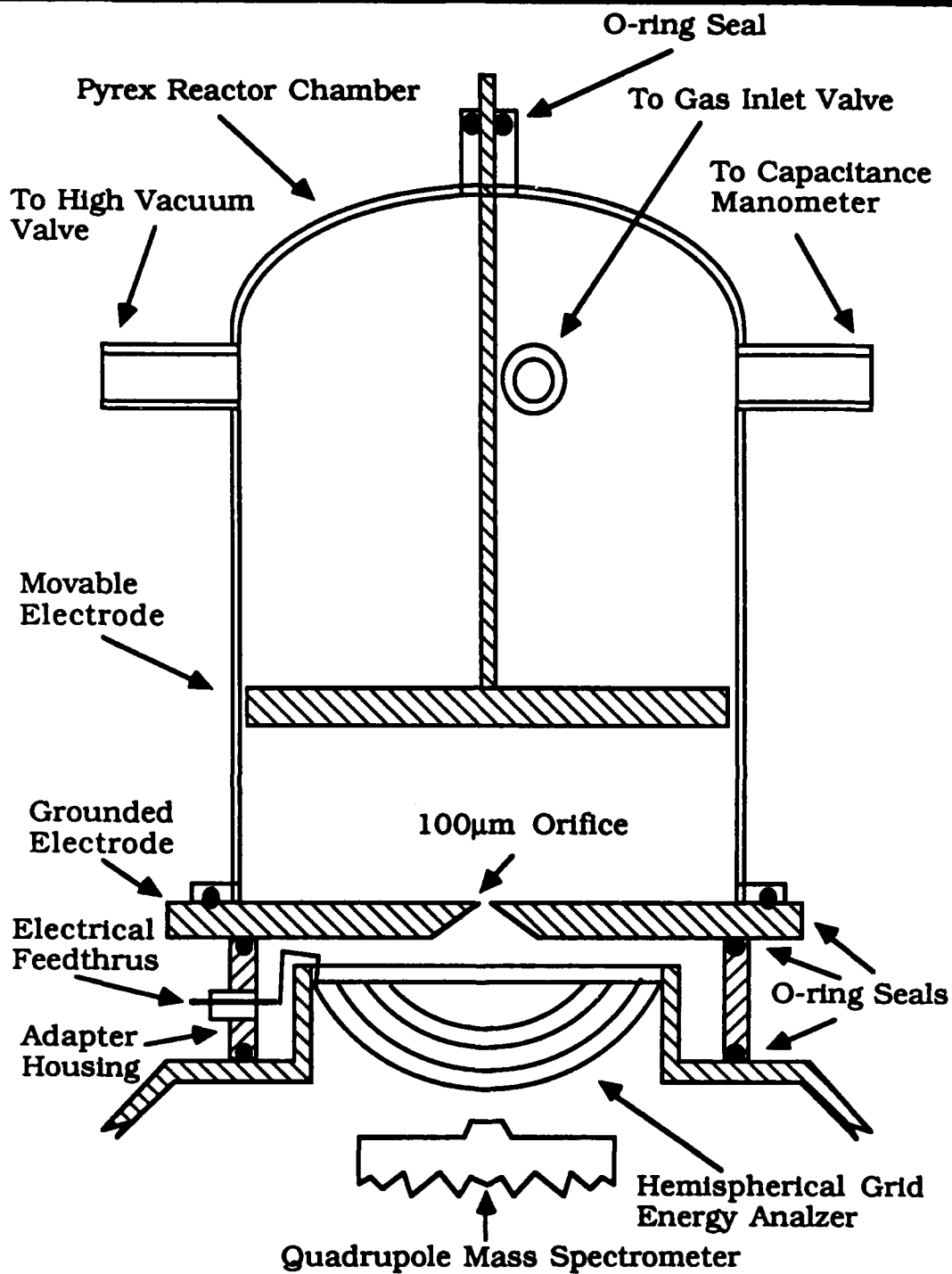
FIG. 4. Design of the parallel plate reactor and the hemispherical energy analyzer

In the series of experiments described in section III which utilized the planar reactor shown in Fig. 4, the planar reactor was driven by a

variable frequency rf power supply. The method of applying the rf power to the parallel plate reactor is shown in Fig. 5. It consisted of the power supply and a matching network which was connected through a blocking capacitor, C_B, to the driven electrode. Different matching networks were used, depending upon the frequency of operation desired. One successful method was to use a transformer wound on a ferrite core and designed for the desired frequency of operation. The use of the blocking capacitor was most useful at higher frequencies, since it then allows the time-averaged (dc) current through the reactor to be measured by grounding the blocking inductor shown in Fig. 5 through a dc ammeter. In the same manner, the average dc potential at the driven electrode can be determined by connecting the blocking inductor to a dc voltmeter. A variation of this method was used at lower frequencies, where the blocking capacitor C_B, the blocking inductor, and the ammeter and voltmeter were omitted.

FIG. 5. Biasing network used with the parallel plate reactor.
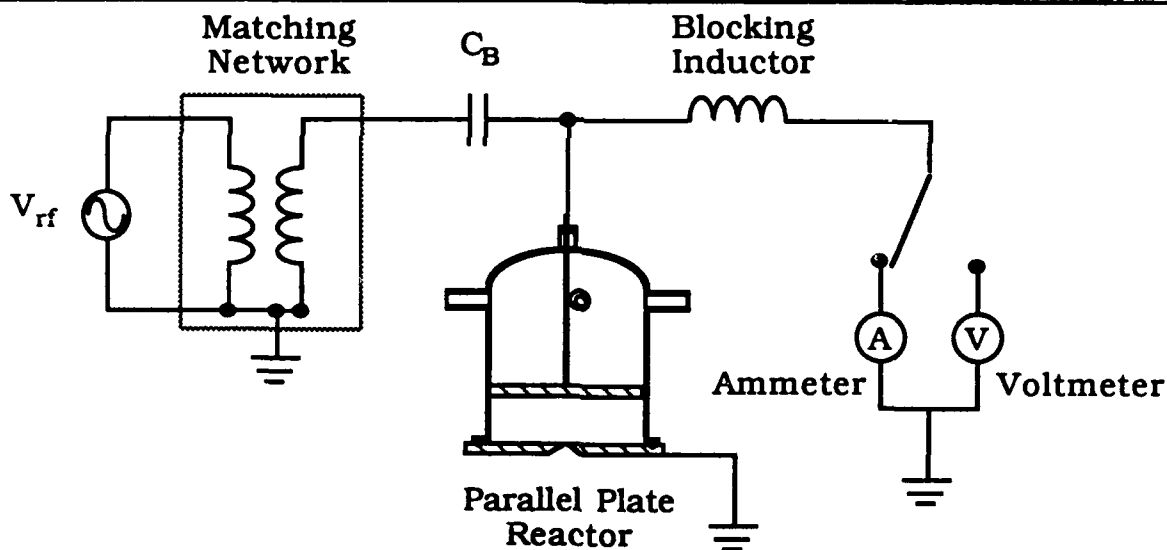
In order to increase the resolution of the energy analyzer and to alleviate the alignment problems previously mentioned, the energy analyzer also underwent a major design revision. This final version of energy analyzer utilized three hemispherical grids with a fourth hemispherical plate (or grid) being used as a detector. Since the grids were hemispherical and the

orifice was located at the center of curvature of the grids, the retarding electric field is parallel to the ion's velocity. This will help prevent any loss of resolution by limiting the deflection of the ions from their original path. Since the detector was also hemispherical, the detection of the ions no longer depends critically on the alignment of the orifice and the detector. Initially the detector was a grid. This grid was subsequently replaced by a plate in order improve the signal sensitivity by collecting all of the ion beam rather than just the fraction that was collected by the partially transparent grid. As expected, no major changes in the shape of the measured ion energy distribution function were found when changing from the grid detector to the plate detector. However, as expected, this resulted in a large increase in the detected ion current.

Considering the grids shown in Fig. 4 to be numbered according to their order from the orifice, the first grid, the orifice, and the vacuum housing were all at ground potential so that the ion trajectories were undisturbed until the ions passed through the first grid. The second grid's voltage was controlled by the data acquisition system and was varied to exclude all ions with a kinetic energy to charge ratio less than a desired value. The third grid was placed at a fixed potential of -5 Volts in order to block electrons which had also been sampled through the orifice and to repel any secondary electrons emitted from the detector back onto the detector. The signal from the detector plate was interfaced to the data acquisition system.

The operation of the planar plasma reactor and the hemispherical retarding grid energy analyzer was verified experimentally. This was done by measuring the energy distribution of positive ions from a dc discharge where the upper electrode was used as the anode and the lower electrode containing the sampling orifice was used as the cathode. The results found in these measurements were consistent with the results reported previously by Davis and Vanderslice[14]. Subsequently, experiments were performed using rf voltages across the reactor. The results of these experiments will be described in the following sections. The results and behavior of the experimental setup under all these conditions indicate that the system performed as desired.

---

[14]W. D. Davis and T. A. Vanderslice, Phys. Rev. 131, 219 (1963).

III. EXPERIMENTAL METHOD AND RESULTS

Using the final version of the experimental setup described in Section II, various experiments were performed in which a single experimental parameter was varied while the other parameters were held constant. The independent parameters considered in these experiments were: the pressure of the reactant gas in the reactor, the type of reactant gas (or reactant gas mixture), the area ratio of the electrode surfaces, the electrode spacing, the magnitude of the voltage across the reactor, and the frequency of the voltage across the reactor. Results on the study of the ion bombardment energy distribution using this experimental setup are presented below, grouped according to the discharge parameter varied.

A. Effect of Varying Pressure

Data was obtained with a 13.6 MHz, 200 V peak-to-peak voltage across the reactor for different values of gas pressure with neon as the reactant gas. Figure 6a shows the ion current collected as a function of the retarding grid voltage. The ion bombardment energy distribution is shown in Fig. 6b and is the derivative of the data shown in Fig. 6a. As shown in Fig. 6b, for a pressure of 25 and 50 mTorr, the energy distribution of the neon ions is basically a single narrow peak at an energy of 50 eV. The distribution drops off rapidly from its peak value for energies greater than 50 eV. However, the distribution drops off more slowly and in a manner that appears exponential for energies less than 50 eV. However, at a pressure of 100 mTorr, the low energy side of the peak drops off much slower, so that the distribution decreases almost linearly with decreasing energy. The high energy side of the peak remains relatively unchanged. At 200 mTorr, the distribution takes on an almost symmetric shape with the peak in the distribution now shifted to the center of the distribution. At 400 and 800 mTorr, the peak shifts towards even lower energies. In addition, the maximum detected ion bombardment energy also decreases as the pressure increases for these curves.
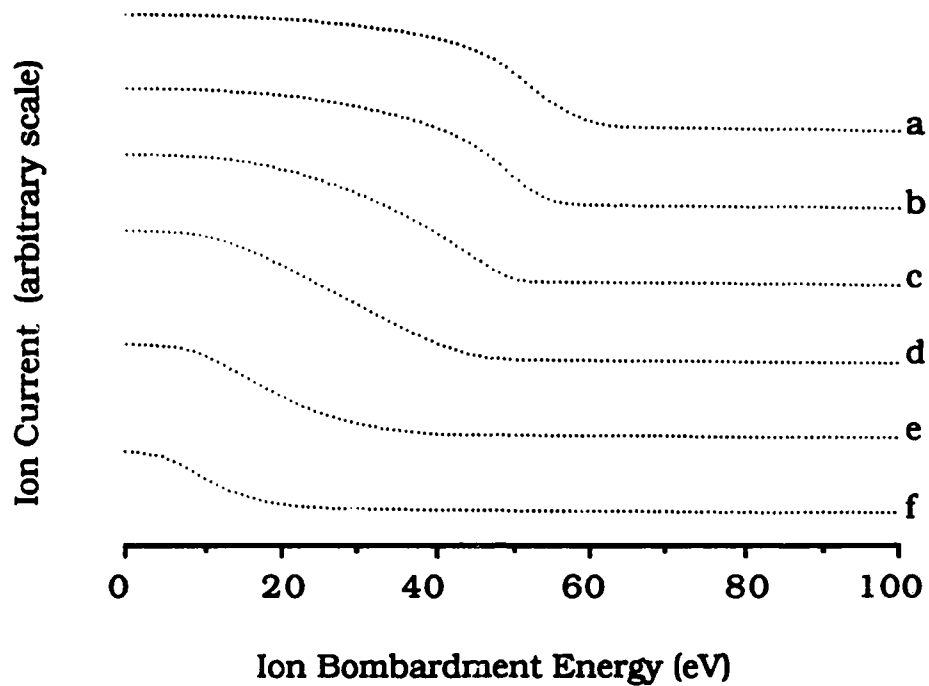
47

FIG. 6a. The ion current detected as a function of ion bombardment energy. The data was obtained with a 13.6 MHz 200 V peak-to-peak sine wave applied to the upper electrode. The pressure of neon in the reactor was: (a) 25 mTorr; (b) 50 mTorr; (c): 100 mTorr; (d) 200 mTorr; (e) 400 mTorr; (f) 800 mTorr.
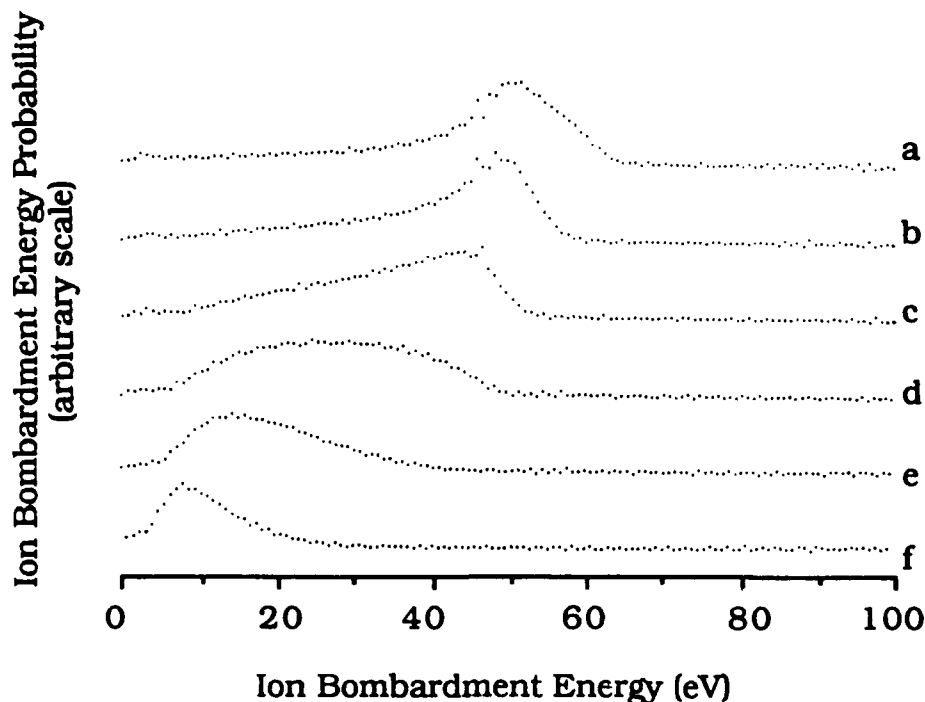
FIG. 6b. The ion bombardment energy distribution calculated from the data shown in Fig. 6a. The data was obtained using a 13.6 MHz 200 V peak-to-peak sine wave applied to the upper electrode. The pressure of neon in the reactor was: (a) 25 mTorr; (b) 50 mTorr; (c): 100 mTorr; (d) 200 mTorr; (e) 400 mTorr; (f) 800 mTorr.

The changes in the ion bombardment energy distribution as a result of the changes in the pressure of neon in the reactor chamber are consistent with what is expected. At pressures below 50 mTorr, the ions that traverse the sheath do so without a significant number of these ions experiencing a collision. This is expected since the mean free path of a neon ion in neon is approximately 1 cm at a pressure of 25 mTorr, while the sheath has a dimension on the order of 1 mm. As the pressure increases, the mean free path of the ion decreases and at 200 mTorr the mean free path is approximately 1 mm. Therefore, at 200 mTorr, it expected that only about half of the ions traverse the sheath without experiencing a collision. Since in neon, the predominant collision mechanism is symmetric resonant charge transfer,[15] the ions that undergo collision will transfer almost all of their

---

[15]B. Chapman, *Glow Discharge Processes* (Wiley, New York, 1980), p.39.

kinetic energy to the neutral neon atoms. Thus the energy with which an ion bombards the surface will be the energy that the ion gains from the electric field in the sheath after its last collision before reaching the surface. Since at 200 mTorr, most ions undergo a single collision, the peak in the energy distribution is shifted to half of the energy of the peak at 25 mTorr. At 400 mTorr, the mean free path for an ions is 0.5 mm and most ions undergo a collision a fourth of the sheath distance from the surface and the energy of the peak in the distribution is shifted to a fourth of the 25 mTorr value. Similarly, at 800 mTorr, the mean free path is 0.25 mm and most ions undergo a collision an eighth of the sheath distance and the energy of the peak is roughly an eighth of the 25 mTorr value. This analysis is only approximate since it is known that the variation of the potential in the sheath is not linear and thus the collision distances used above are only rough estimates. In addition, the sheath dimension is actually a function of the pressure. However, this simple analysis does show that the measured effect of pressure on the ion bombardment energy distribution is consistent with known data about the mean free path of neon ions in neon.

One further interesting observation is that the total ion current collected does not depend upon the pressure from 25 mTorr to 200 mTorr for these measurements at 13.6 MHz with the voltage across the reactor held constant at 200 V peak-peak. This would imply that the density of ions and electrons is independent of the gas pressure in this range and is only dependent on the reactor voltage.

B. Effect of Varying Frequency

Observations on the effects of varying frequency were performed in neon at pressures from 50 to a 500 mTorr. While this work was only qualitative in nature, one observation of relevance is that as the frequency is lowered, the voltage required across the reactor to maintain a discharge increases dramatically. For example, below a few MHz, the peak-to-peak voltage required to sustain the discharge increases to several hundred Volts, while at 13.6 MHz a discharge may be maintained with a peak-to-peak voltage of less than 50 Volts. These observations show that the sustaining mechanisms of the plasma are influenced by the frequency at which the plasma is driven. At lower frequencies (below a few hundred kHz), when an

electrode is at a negative potential with respect to the other electrode, it will act in a manner which is similar to a cathode in a dc discharge. Therefore, the production of ion-electron pairs near the electrode will be the result of electron impact ionization due to secondary electrons which are emitted by ion bombardment of the electrode and which are accelerated back into the plasma. It should be noted that this mechanism is also present at higher frequencies (above a few MHz). In addition, at lower frequencies, the electron temperature and possibly the electron density will be time varying and modulated by the driving rf voltage. At higher frequencies, the situation is different. At these frequencies, the electron temperature in the plasma will be time independent and the high-energy electrons in the tail of the electron energy distribution will contribute significantly to the production of ion-electron pairs[16]. This contribution is less important at the lower frequencies since the electrons do not reach equilibrium.

C. Effect of Varying Voltage

The data in Fig. 7 was obtained from a rf discharge in neon at a frequency of 13.6 MHz and at a pressure of 50 mTorr. Figure 7a shows the measured ion current and Fig. 7b shows the resulting ion bombardment energy distribution. The voltage across the reactor was a sine wave with a peak-to-peak amplitude which was varied from 40 V to 500 V. Several trends are indicated by the data shown in Fig. 7b. First, the width of the peak in the ion bombardment energy distribution appears uneffected by changes in the magnitude of the voltage across the reactor. This peak width is approximately 15 eV. However, the energy of the peak increases as the voltage across the reactor increases. Finally, the positive ion current detected also increases as the voltage across the reactor increases.

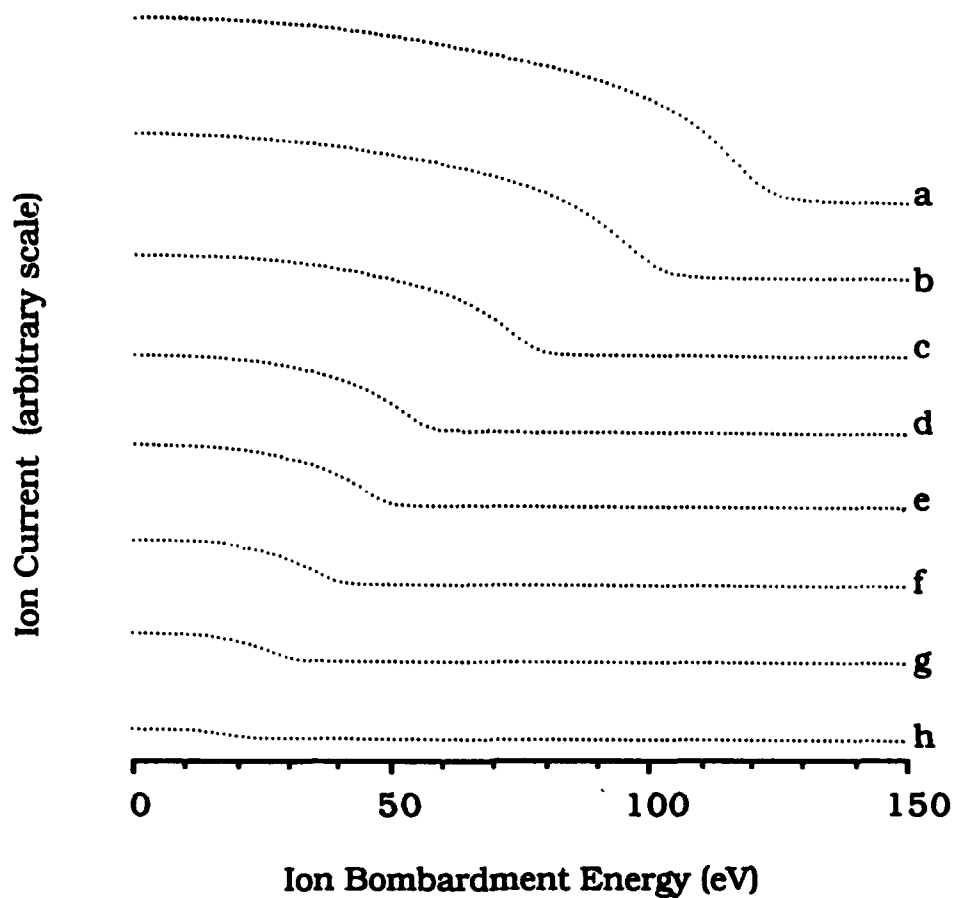[16]M. Gill, Vacuum **34**, 357 (1984).

FIG. 7a. The ion current detected as a function of ion bombardment energy. The pressure of neon in the reactor was 50 mTorr. A 13.6 MHz sine wave was applied to the upper electrode with a peak-to-peak voltage of: (a) 500 V; (b) 400 V; (c) 300 V; (d) 200 V; (e) 160 V; (f) 120 V; (g) 80 V; (h) 40 V.
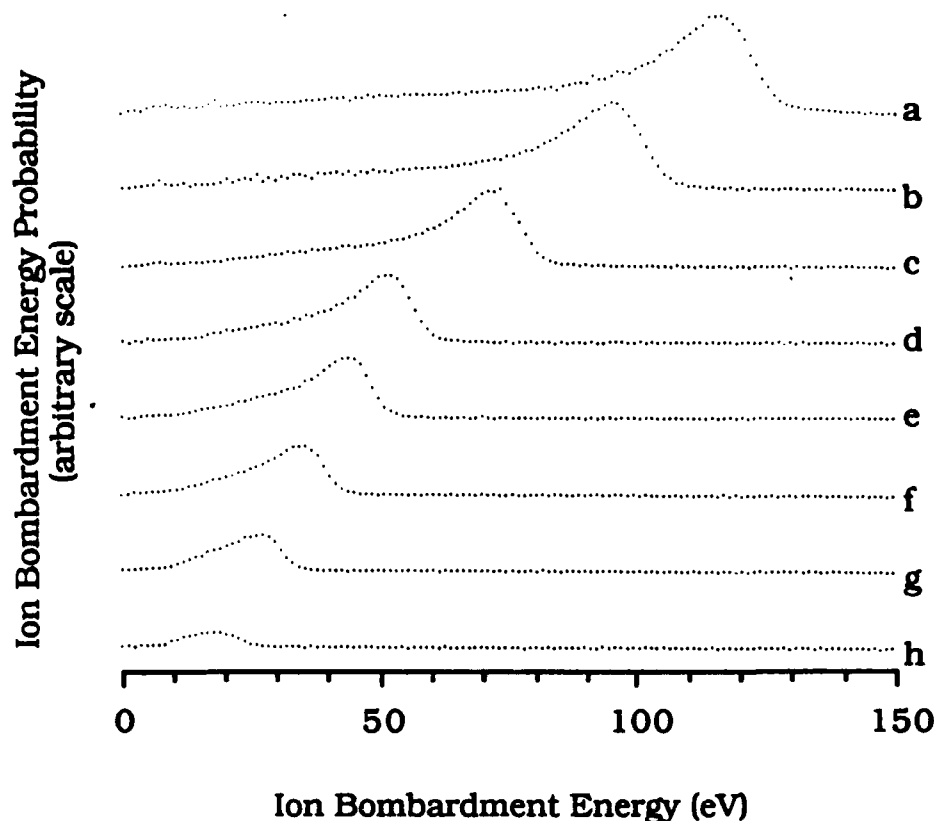
FIG. 7b. The ion bombardment energy distribution as calculated from the data presented in Fig. 7a. The pressure of neon in the reactor was 50 mTorr. A 13.6 MHz sine wave was applied to the upper electrode with a peak-to-peak voltage of: (a) 500 V; (b) 400 V; (c) 300 V; (d) 200 V; (e) 160 V; (f) 120 V; (g) 80 V; (h) 40 V.

In Fig. 8, the peak in the ion bombardment energy for the distributions given in Fig. 7b are graphed as a function of the peak-to-peak voltage across the reactor. This graph shows that the peak ion bombardment energy E_{peak} is a linear function of the peak-to-peak voltage V_{p-p} across the reactor. Using the model presented in Refs.11 and 12, one can predict the dependence of the peak in the ion bombardment energy on the peak-to-peak voltage across the reactor. For a planar rf reactor with approximately equal area electrodes, the voltage across the sheath at an electrode can be approximated by the floating potential during half the rf cycle. During the other half of the rf cycle, the voltage may be approximated by the floating

potential plus the positive half of the applied sine wave. Since, at frequencies in the MHz range, the ions take several rf cycles to traverse the sheath, the ions which do not undergo collisions bombard the surface with an energy corresponding to the average voltage across the sheath times the charge on the ion. Collisions would have the effect of broadening the ion bombardment energy distribution around this predicted peak value. Under the simplifying assumptions given, the time averaged voltage across the sheath is the floating potential V_f plus the peak-to-peak voltage divided by 2π. Thus, the peak ion bombardment energy should be given by $E_{peak}/q = V_f + 0.159\,V_{p-p}$, where q is the the charge of the bombarding positive ion. However, as indicated by a least squares fit, the data presented in Fig. 8 is linear with a slope of 0.21 rather than 0.159. One possible explanation for this discrepancy is the assumption that the ions have an average energy equal to the average voltage across the sheath times the charge on the ion. This assumption is partially based on the idea that the ions enter the sheath with an equal probability for all possible phase angles of the applied potential. This is not completely accurate, since the sheath will change its thickness for changes in the electric potential across the sheath. Therefore, it is more probable that ions will enter the sheath during that portion of the rf cycle where the voltage across the sheath and, hence, the sheath thickness is largest. This would lead to a larger value for the peak ion bombardment energy, as is observed. The intercept of the data presented in Fig. 8 predicts a floating potential of 9.3 volts which is consistent with the predictions of the model presented in Ref. 11.
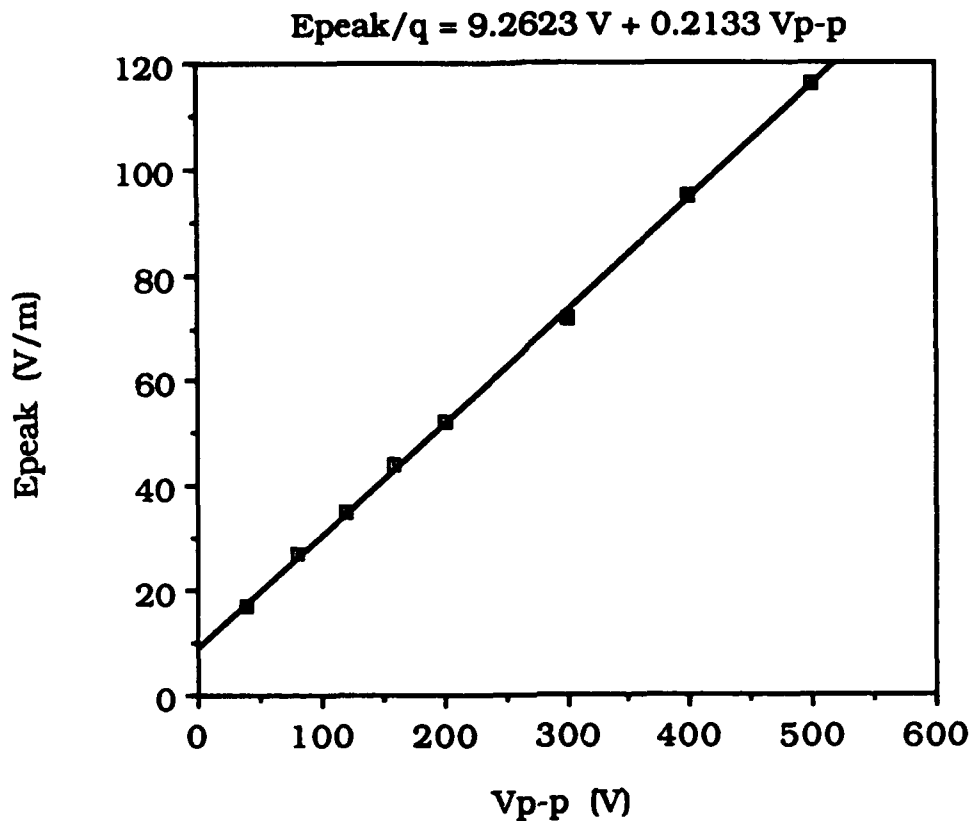
Epeak/q = 9.2623 V + 0.2133 Vp-p

FIG. 8. Dependence of the peak in the ion bombardment energy of the data presented in Fig. 7b on the peak-to-peak voltage across the reactor.

D. Effects of Changing the Electrode Spacing and Area Ratio

The measurements show very little effect of the electrode spacing on the discharge characteristics or the resulting ion bombardment energy distribution at 13.6 MHz and spacings between 6 cm and 15 cm. Results at 13.6 MHz also show little effect of the area ratio on the shape of the ion bombardment energy distribution. However, the time-averaged dc potential of the driven electrode is more negative when the area of the driven electrode is reduced. In addition, the magnitude of the time averaged dc current through the reactor when the upper electrode is dc grounded

through the blocking inductor also increases as the area of the driven electrode is reduced.

IV. IMPLICATIONS OF EXPERIMENTAL RESULTS FOR MODELING RF DISCHARGES

From the data that has been collected, one observation is apparent. The effect of collisions in the sheath region must be considered in modeling the ion bombardment energy distribution of the positive ions. At pressures of 100 mTorr and above in neon, the effect of collisions on the measured ion bombardment energy distribution is quite dramatic. In a weakly ionized plasma, the predominant collisions will be between ions and neutrals. Of the different ion–neutral collision mechanisms, the most probable is symmetrical resonant charge transfer for helium and neon ions moving in their parent gas.[17]

A further limiting factor in the application of the model presented in Refs. 11 and 12 to these experiments is that the model does not include the mechanisms which sustain the plasma. Because these mechanisms are not included, the model cannot predict the voltages necessary to initiate or maintain a rf discharge. These mechanisms may be important in determining the ion bombardment energy distribution. The importance of the sustaining mechanisms is shown by the changes in the voltage necessary to maintain a rf discharge at different frequencies.

Furthermore, most of the data presented, was collected at higher frequencies where the assumptions used in the derivation of the model presented in Refs. 11 and 12 are no longer strictly valid. These assumptions also limit the lower limit of the frequencies for which the model is valid. However, using the measurements that have been performed, it is possible to qualitatively predict the behavior of the ion bombardment energy distribution at pressures below 100 mTorr using the model. Furthermore, the measurements at higher pressures can be qualitatively predicted by modifying the ion bombardment energy distributions predicted by the model to include the effect of ion-neutral collisions in the sheath.

---

[17]see Ref. 15.

The experiments that have been performed have yielded information which can be used to improve the model. These experiments have confirmed that the model yields reasonable results for the ion bombardment energy distributions in a rf neon discharge. The experiments also show areas in which the model needs to be improved.

ACKNOWLEDGEMENTS

SECTION V

A COLLISIONLESS PLASMA SHEATH MODEL FOR A PLASMA CONTAINING NEGATIVE IONS

A Collisionless Plasma Sheath Model for a Plasma Containing Negative Ions

M. F. Toups, D. W. Ernie, and H. J. Oskam
Department of Electrical Engineering
University of Minnesota
Minneapolis, MN 55455

ABSTRACT

A sheath model is derived for a plasma containing negative ions which is in contact with a surface. The plasma is assumed to consist of a singly charged positive ion species, a singly charged negative ion species, electrons, and neutrals. The model is derived assuming that the entire potential difference between the surface and the bulk of the plasma occurs across a sheath region. The thickness of the sheath region is assumed to be small with respect to the mean free paths of the particles involved, so that in the sheath region collisions and particle production may be ignored. It is shown that a criterion exists which must be satisfied in order for the model to be physically realistic. This criterion is then utilized, under appropriate assumptions about the velocity distribution functions of positive ions, negative ions, and electrons entering the sheath, to derive expressions for the conductivity and capacitance of a plasma sheath. Numerical results for these expressions are presented for cases which are representative of a typical plasma containing negative ions. Implications of the model for rf and dc discharges are discussed including an explanation of the confinement of negative ions inside a plasma volume.

I. INTRODUCTION

The study of the properties of plasmas and plasma sheaths has a long history. In order to model the complete plasma phenomena, the plasma has historically been divided into two regions. The first region is the plasma region, where the effect of any space charge on the electric potential may be neglected. The second is a sheath region, where the effect of ion and electron generation may be neglected. Much of the basis for the modern

60

theory of a plasma can be found in a paper by Tonks and Langmuir.[1] Their paper was mainly concerned with the case where the mean free path of the positive ions was large with respect to the dimensions of the container, so that it could be assumed that the positive ions undergo no collisions from the time they are created until the time they recombine at the surface. It was also assumed that the positive ions are created with zero initial velocity. Using these two assumptions, Tonks and Langmuir were able to derive an expression for the spatially dependent velocity distribution and density of the positive ions as a function of the electric potential and the rate of production of the positive ions. By then further assuming that the electrons have a Maxwellian velocity distribution throughout the plasma, they derived an equation (to subsequently be referred to as Tonks and Langmuir's plasma-sheath equation) for the potential at any point in the plasma.

Tonks and Langmuir were able to approximate the solution to their plasma-sheath equation in the plasma region by means of a series expansion under the assumption that the effect of the space charge on the electric potential could be neglected. Their paper also included some work for cases in which collisions and space charge effects could no longer be neglected.

The plasma sheath region was modelled by Bohm.[2] He assumed that at the plasma sheath edge, the velocity distribution of the positive ions is monoenergetic and that the positive ions undergo no collisions within the sheath region. This assumption can be valid in the plasma-sheath, even for plasmas where collisions involving the positive ions in the bulk of the plasma cannot be ignored. This is an idea which was in part expressed earlier by Tonks and Langmuir.[3] The assumption that the positive ions undergo no collisions is valid if the sheath is smaller than the mean free path of the positive ions. Bohm also ignored any changes in the potential within the plasma region. Bohm then derived a criterion which the positive ions must satisfy in order for the model to be physically realistic. Bohm's criterion was that in a plasma consisting of a singly charged positive ion species,

---

[1]L. Tonks and I. Langmuir, Phys. Rev. **34**, 876 (1929).

[2]David Bohm, in *The Characteristics of Electrical Discharges in Magnetic Fields*, edited by A. Gutherie, and R. K. Wakerling (McGraw-Hill, New York, 1949) chapter 3.

[3]see Ref. 1, page 902, "...., but there is a wide range of pressures for which the ion may drift in the plasma yet fall freely through the greater part of a thin sheath." Also, see page 901-906 of Ref. 1 for a solution in the sheath region.

electrons, and neutrals, monoenergetic positive ions must enter the sheath from the plasma with a kinetic energy greater than or equal to half the electron thermal energy.

Harrison and Thompson[4] attempted to generalize the criterion given by Bohm to the case of a distribution of velocities for the positive ions. However, as pointed out by Hall,[5] Harrison and Thompson's generalization is not valid for an arbitrary distribution as was claimed. Hall[6] also published some further important comments on the misuse of the Bohm criterion with regard to the concept of plasma stability and plasma oscillations.

The concept of the plasma and sheath regions was revisited by Caruso and Cavaliere.[7] Their contribution was to show that the sheath region and plasma region solutions are a special form of asymptotic solutions of Tonks and Langmuir's plasma-sheath equation. Self[8] solved Tonks and Langmuir's plasma-sheath equation numerically without neglecting the space charge effects or dividing the equation into sheath and plasma regions. Self's method of solution eliminates the problems which arise when one attempts to match an asymptotic plasma solution to an asymptotic sheath solution. However, since Tonks and Langmuir's plasma sheath equation assumes that the positive ions undergo no collisions after creation (i.e., a collisionless plasma as well as a collisionless sheath), Self's solution is limited in its application to actual dc discharges.

All of these previous studies involved plasma systems consisting of at most three particles: a single positive ion species, electrons, and neutrals. However, plasmas containing negative ion species are of current interest due to the use of electronegative gases in plasma processes used by the microelectronics industry. Negative ions are also of current interest in ion sources used for negative ion beam production. In this paper, a four particle plasma which consists of a single positive ion species, a single negative ion species, electrons, and neutrals will be considered. The interaction of the plasma with a surface which is in contact with the plasma, leading to the

[4]E. R. Harrison and W. B. Thompson, Proc. Phys. Soc.London, **74**, 145 (1959).

[5]L. S. Hall, Proc. Phys. Soc. London, **80**, 309 (1962).

[6]L. S. Hall, Phys. Fluids, **4**, 388 (1961).

[7]A. Caruso and A. Cavalier, Nuovo Cimento, **26**, 5221 (1962).

[8]S. A. Self, Phys. Fluids, **6**, 1762 (1963).

formation of a sheath region, will be modelled. An overview of the model will be presented in the beginning of the next section. Subsequently, the assumptions which are made in deriving the model and the derivation of the model will be presented. Finally, the applicability of the model's assumptions to actual discharges and the implications of the model for rf and dc discharges will be discussed.

It will be shown that even for the situation where the density of negative ions in the bulk of the plasma is much larger than the density of electrons in the bulk of the plasma, a space charge sheath develops between the plasma and a surface in contact with the plasma. As a consequence of this sheath, the surface still floats at a significant negative potential with respect to the plasma. Therefore, the negative ions are essentially trapped in the plasma by the floating potential at the surface and, in most instances, their density in the bulk of the plasma increases until volume losses equal volume production.

II. SHEATH MODEL AND THE SHEATH CRITERION

A surface in contact with a plasma results in a disturbance of the plasma. The surface acts as a recombination center for the positive ions, negative ions, and electrons. This results in a flux of positive ions, negative ions, and electrons to the surface and a flux of neutral particles from the surface back into the plasma. In steady state, the loss of charged particles at the surface must be balanced by the production of ions and electrons within the body of the plasma and any net flux of charged particles or electric current collected at the surface must be balanced by an electric current passing through an external circuit back into the body of the plasma via another electrode surface. It is well known that in the case where there are no negative ions, if the net current collected at the surface is zero, then the surface will float at a negative electric potential with respect to the bulk of the plasma. This potential is required to reduce the value of the electron current collected at the surface to the value of the positive ion current collected and is due to the differences in the masses and average energies of these particles. It is also expected that most of the potential difference between the plasma and the surface will be confined to a small region, the

sheath, due to the property that a plasma tends to shield itself from electric fields so as to remain field free.
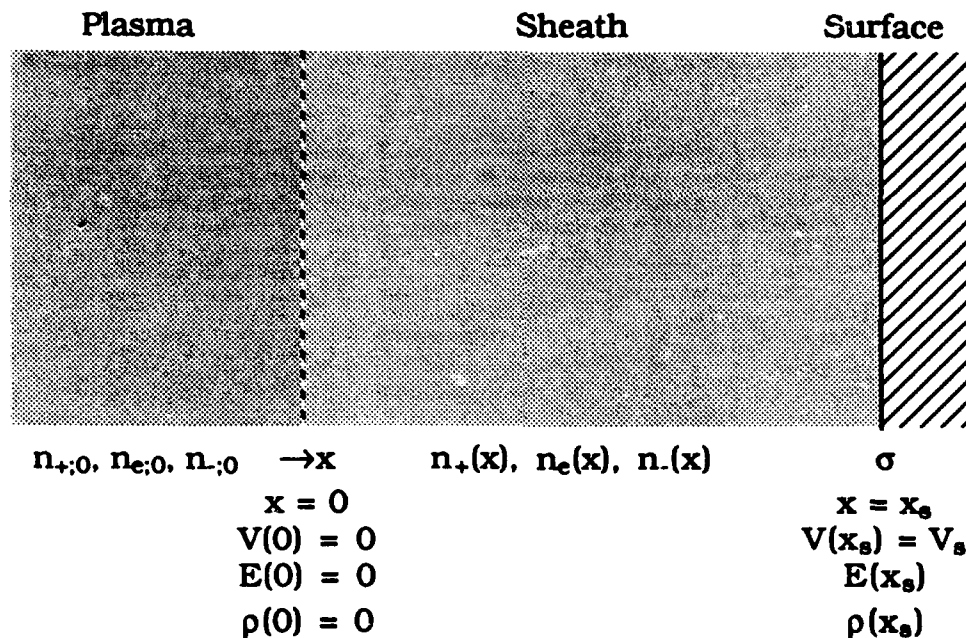

FIG. 1. Diagram of the sheath model presented in section II.

The picture of the plasma which will be used in this model is shown in Fig. 1. In this model, there is an arbitrary distinction between the plasma and sheath regions. The plasma region supplies charged particles to balance the charged particles which are lost to the surface. The plasma region is shielded from the potential of the surface by the sheath region and is a relatively neutral, field-free, and equipotential region. However, in the sheath region, the charge density, the electric field, and electric potential undergo large changes. At the surface, charged particles are neutralized by transferring their charge to the surface. The surface will in general have a surface charge residing on it.

A. Assumptions

In deriving this model, the following assumptions will be made. These assumptions are similar to the assumptions used by Bohm[2], with additional

assumptions regarding the negative ions. The applicability and validity of these assumptions will be discussed in section V.

(1) The plasma consists of only four types of particles: one species of singly charged positive ions, one species of singly charged negative ions, electrons, and neutrals.

(2) The surface is planar and both the plasma and surface are infinite in extent, so that the problem may be treated as one-dimensional.

(3) All of the voltage difference between the surface and the plasma is contained in the sheath region. The rest of the plasma is considered to be field free and neutral.

(4) The surface is assumed to be at a negative potential with respect to the plasma.

(5) The electrons are in thermodynamic equilibrium with themselves and may be characterized by an electron temperature T_e which is spatially independent. Also, it is assumed that negative ions are in thermodynamic equilibrium with themselves and may be characterized by a negative ion temperature T_-. It is not required that the electrons and negative ions be in equilibrium with each other.

(6) The electron and negative ion densities in the sheath are given by a Boltzmann density distribution.

(7) The positive ions undergo no collisions while traversing the sheath.

(8) The positive ions enter the sheath region with a monoenergetic drift velocity. This implies that at the plasma sheath edge, the ions have a drift energy much greater than their thermal energy.

(9) Any charged particle which strikes the surface is neutralized at the surface. No charged particles are reflected or emitted by the surface.

B. Derivation of the Sheath Criterion

The electric field $E(x)$ at any point x in the sheath is given by Guass' law

$$\frac{dE(x)}{dx} = \frac{\rho(x)}{\varepsilon_0},$$

(1)

65

where $\rho(x)$ is the charge density and ε_0 is the permittivity of free space. In general, the charge density will contain a term for each ionized species. For the case being considered in this paper, the charge density is given by

$$\rho(x) = e\ [n_+(x) - n_e(x) - n_-(x)]\ , \tag{2}$$

where e is the magnitude of the charge carried by an electron and $n_+(x)$, $n_e(x)$, and $n_-(x)$ are the number densities of singly charged positive ions, electrons, and singly charged negative ions respectively. The electric field is related to the electric potential $V(x)$ by

$$E(x) = \frac{-\ dV(x)}{dx}\ . \tag{3}$$

Multiplying Eqs . (1) and (3) together yields

$$E(x)\ \frac{d\,E(x)}{dx} = \frac{-\ \rho(x)}{\varepsilon_0}\ \frac{dV(x)}{dx}\ . \tag{4}$$

This equation can then be integrated once with respect to x giving

$$\int_0^x E(x)\ \frac{d\,E(x)}{dx}\ dx = -\ \int_0^x \frac{\rho(x)}{\varepsilon_0}\ \frac{dV(x)}{dx}\ dx\ . \tag{5}$$

The left side is easily integrated to yield

$$\frac{1}{2}\ \{E^2(x) - E^2(0)\} = -\ \int_0^x \frac{\rho(x)}{\varepsilon_0}\ \frac{dV(x)}{dx}\ dx\ . \tag{6}$$

Assumption (3) states that the electric field in the plasma is insignificant compared to its value in the sheath, therefore we assume

$$E(0) = 0\ . \tag{7}$$

Since the electric potential due to a distribution of free charges in a collisionless region must be a monotonic function of x, it is possible to express the charge density in Eq. (6) as a function of V rather than x yielding

66

$$E^2(x) = \frac{-2}{\varepsilon_0} \int_0^{V(x)} \rho(V)\, dV \ . \tag{8}$$

The expression for the electric field $E(x)$ in the sheath is easily found by noting that the electric field s directed toward the surface throughout the sheath region when the surface is at a negative electric potential with respect to the plasma. Thus,

$$E(x) = \sqrt{E^2(x)} \ . \tag{9}$$

Finally, since the square of the electric field must always be positive as noted by Bohm[2], the condition

$$\frac{-2}{\varepsilon_0} \int_0^{V(x)} \rho(V)\, dV \geq 0 \tag{10}$$

must be satisfied for any negative value of the potential in the sheath. It is this condition which will be referred to as the sheath criterion.

C. Calculation of the Particle Densities

Using assumptions (4) and (5), the densities for the negative particles in the sheath region relative to their values at the sheath edge are given by Boltzmann density distributions. Defining voltage equivalents V_e and V_- for the temperatures T_e and T_- of the electrons and negative ions respectively by

$$V_e = \frac{k\,T_e}{e} \tag{11}$$

and

$$V_- = \frac{k\,T_-}{e} \ . \tag{12}$$

where k is Boltzmann's constant. The Boltzmann density distributions may be written as

$$n_e(x) = n_{e;0} \, \exp\!\left(\frac{V(x)}{V_e}\right) , \qquad (13)$$

and

$$n_-(x) = n_{-;0} \, \exp\!\left(\frac{V(x)}{V_-}\right) . \qquad (14)$$

Here $n_{e;0}$ and $n_{-;0}$ are respectively the densities of the electrons and negative ions at the plasma sheath edge, i.e., $x = 0$. By assumptions (3), (5), and (6), these are also the values of these densities throughout the plasma region.

The density of the accelerated particles (i.e., positive ions) is calculated by noting that assumptions (7) and (8) require the flux of the positive ions to be a constant value throughout the sheath. Therefore,

$$n_+(x) \, \nu_+(x) = n_{+;0} \, \nu_{+;0} . \qquad (15)$$

where $\nu_+(x)$ and $\nu_{+;0}$ are the velocities of the positive ions at a point x in the sheath and at the plasma sheath edge (i.e., $x = 0$) respectively and where $n_{+;0}$ is the positive ion density at the sheath edge.

Since the positive ions undergo no collisions, Conservation of Energy can be used to relate the velocity of the particle to the potential at any given point in the sheath, yielding

$$\frac{m_+ \, \nu_+^2(x)}{2 \, e} + e \, V(x) = \frac{m_+ \, \nu_{+;0}^2}{2} + e \, V(0) , \qquad (16)$$

where m_+ is the mass of the positive ion. Without loss of generality, the potential at the sheath edge can be set equal to zero as indicated in Fig. 1, yielding

$$\nu_+(x) = \sqrt{\nu_{+;0}^2 - \frac{2 \, e \, V(x)}{m_+}} . \qquad (17)$$

Substituting this expression into Eq. (15) results in the following expression relating the positive ion density at any given point in the sheath to the electric potential at that point:

$$n_+(x) = \frac{n_{+;0}\, v_{+;0}}{\sqrt{v_{+;0}^2 - \frac{2\,e\,V(x)}{m_+}}}. \qquad (18)$$

By defining the voltage equivalent V_+ of the injection velocity as

$$V_+ = \frac{m_+\, v_{+;0}^2}{2\,e}, \qquad (19)$$

Eq. (18) may be rewritten as

$$n_+(x) = \frac{n_{+;0}}{\sqrt{1 - \frac{V(x)}{V_+}}}. \qquad (20)$$

Using Eqs. (2), (13), (14) and (20), the total net charge density at any location in the sheath is given by

$$\rho(x) = e \left\{ \frac{n_{+;0}}{\sqrt{1 - \frac{V(x)}{V_+}}} - n_{e;0}\, \exp\!\left(\frac{V(x)}{V_e}\right) - n_{-;0}\, \exp\!\left(\frac{V(x)}{V_-}\right) \right\}. \qquad (21)$$

D. Evaluating the Sheath Criterion

It is convenient to introduce the quantity α_0 as the ratio of the negative ion density to the positive ion density at the sheath edge, i.e.,

$$\alpha_0 = \frac{n_{-;0}}{n_{+;0}}. \qquad (22)$$

Since assumption (3) requires charge neutrality at the sheath edge,

$$n_{+;0} - n_{e;0} - n_{-;0} = 0. \qquad (23)$$

Therefore, the densities of the negative particles at the plasma sheath edge may be written in terms of α_0 and the positive ion density at the plasma sheath edge,

$$n_{e;0} = n_{+;0}\,(1 - \alpha_0) \qquad (24)$$

69

and

$$n_{-;0} = n_{+;0} \, \alpha_0 . \tag{25}$$

Consequently, Eq. (21) may be re-expressed in terms of α_0 and the positive ion density at the sheath edge yielding

$$\rho(x) = e \, n_{+;0} \left\{ \frac{1}{\sqrt{1 - \frac{V(x)}{V_+}}} - (1 - \alpha_0) \exp\left(\frac{V(x)}{V_e}\right) - \alpha_0 \exp\left(\frac{V(x)}{V_-}\right) \right\} . \tag{26}$$

Substituting this expression into Eq. (8) and performing the integration results in the following expression for the square of the electric field at any point in the sheath:

$$E^2(x) = \frac{2 \, e \, n_{+;0}}{\varepsilon_0} \left\{ 2 \, V_+ \left[\sqrt{1 - \frac{V(x)}{V_+}} - 1 \right] + (1 - \alpha_0) \, V_e \left[\exp\left(\frac{V(x)}{V_e}\right) - 1 \right] \right.$$
$$\left. + \alpha_0 \, V_- \left[\exp\left(\frac{V(x)}{V_-}\right) - 1 \right] \right\} . \tag{27}$$

In order to satisfy the sheath criterion of Eq. (10), the ion injection velocity is required to be such that the above expression is always non-negative for any negative value of the potential. This requires that the term enclosed in braces in Eq. (26) be positive for any negative value of the potential, i.e.,

$$2 \, V_+ \left[\sqrt{1 - \frac{V(x)}{V_+}} - 1 \right] + (1 - \alpha_0) \, V_e \left[\exp\left(\frac{V(x)}{V_e}\right) - 1 \right]$$
$$+ \alpha_0 \, V_- \left[\exp\left(\frac{V(x)}{V_-}\right) - 1 \right] \geq 0 . \tag{28}$$

Solving inequality (28) for the square root yields

$$\sqrt{1 - \frac{V(x)}{V_+}} \geq \frac{1}{2 \, V_+} \left\{ (1 - \alpha_0) \, V_e \left[1 - \exp\left(\frac{V(x)}{V_e}\right) \right] + \alpha_0 \, V_- \left[1 - \exp\left(\frac{V(x)}{V_-}\right) \right] \right\}$$
$$+ 1 . \tag{29}$$

Since both sides of Eq. (29) are positive for all negative values of the potential, one can multiply the inequality by the voltage equivalent of the injection velocity and then square both sides. Collecting the terms which involve the voltage equivalent of the injection velocity results in the inequality

$$V_+ \{ - V(x) - F[V(x)] \} \geq \frac{1}{4} F^2[V(x)] , \tag{30}$$

where

$$F[V(x)] = (1 - \alpha_0) V_e \left[1 - \exp\left(\frac{V(x)}{V_e}\right)\right] + \alpha_0 V_- \left[1 - \exp\left(\frac{V(x)}{V_-}\right)\right]. \tag{31}$$

The term which multiplies the voltage equivalent of the injection velocity on the left hand side of Eq. (30) is shown in Appendix A to be non-negative for all negative values of the potential. Therefore, the voltage equivalent of the injection velocity for any negative value of the potential must satisfy

$$V_+ \geq \frac{F^2[V(x)]}{4 \{ - V(x) - F[V(x)] \}} . \tag{32}$$

The minimum value of the injection velocity $V_{+;min}$ required by Eq. (31) is equal to the maximum value of the right hand side of Eq. (31) over all negative values for the potential.

Finally, it can be shown that for the case of no negative ion species (i.e., $\alpha_0=0$), the method used by Bohm[2] in deriving his classical sheath criterion utilizing a Taylor's series expansion is equivalent to requiring that the Eq. (32) hold at the sheath edge. In particular, since Eq. (32) must be true for any negative value of the potential, it must be true at the sheath edge (i.e., $x = 0$) where the electric potential vanishes. In this limit, as shown in Appendix B, the inequality reduces to

$$V_+ \geq \frac{1}{(1-\alpha_0) \dfrac{2}{V_e} + \alpha_0 \dfrac{2}{V_-}} . \tag{33}$$

This is a necessary condition for Eq. (10) to be satisfied. In addition for the case where $\alpha_0=0$, as shown in Appendix C, Eq. (33) is also a sufficient condition for the sheath criterion of Eq. (10) to hold. Then the maximum

71

value of the right hand side of Eq. (32) does occur at the plasma sheath edge and has the value $V_{+;min}=V_e/2$ when $\alpha_0=0$, which is the result obtained by Bohm. However, in the case of negative ion species, the maximum value of the right hand side of Eq. (32) does not occur at the plasma sheath edge where the potential vanishes and Eq. (33), while necessary, is not sufficient to guarantee that the sheath criterion given by Eq. (10) is indeed satisfied.

III. SHEATH CHARACTERISTICS

A. Current Characteristic and the Floating Potential

Based on the sheath model presented in the previous sections, it is possible to derive the conduction current density through the sheath as a function of the potential across the sheath. The conduction current density due to the positive ions j_+ is independent of the voltage across the sheath, and is given by

$$j_+ = e\, n_{+;0}\, v_{+;0} = e\, n_{+;0}\, \sqrt{\frac{2\, e\, V_+}{m_+}}. \tag{34}$$

Using assumptions (4), (5), (6), and (9), the electron and negative ion conduction currents, $j_e(V_s)$ and $j_-(V_s)$ respectively, are a function of the voltage across the sheath V_s and are given by

$$j_e(V_s) = -\, e\, n_{e;0}\sqrt{\frac{e\, V_e}{2\, \pi\, m_e}}\, \exp\!\left(\frac{V_s}{V_e}\right)$$

$$= -\, e\, n_{+;0}\, (1 - \alpha_0)\sqrt{\frac{e\, V_e}{2\, \pi\, m_e}}\, \exp\!\left(\frac{V_s}{V_e}\right) \tag{35}$$

and

$$j_-(V_s) = -\, e\, n_{-;0}\sqrt{\frac{e\, V_-}{2\, \pi\, m_-}}\, \exp\!\left(\frac{V_s}{V_-}\right)$$

$$= -\, e\, n_{+;0}\, \alpha_0\sqrt{\frac{e\, V_-}{2\, \pi\, m_-}}\, \exp\!\left(\frac{V_s}{V_-}\right). \tag{36}$$

72

where m_e and m_- are the electron and negative ion masses respectively. The total conduction current density $j_c(V_s)$ is the sum of the contributions from each type of particle yielding the conduction current characteristic

$$j_c(V_s) = e\, n_{+;0}\left\{\sqrt{\frac{2\, e\, V_+}{m_+}} - (1 - \alpha_0)\sqrt{\frac{e\, V_e}{2\, \pi\, m_e}}\, \exp\!\left(\frac{V_s}{V_e}\right)\right.$$

$$\left. - \alpha_0\sqrt{\frac{e\, V_-}{2\, \pi\, m_-}}\, \exp\!\left(\frac{V_s}{V_-}\right)\right\}.\tag{37}$$

The floating potential V_f is then the voltage for which the net conduction current collected at the surface is zero, i.e.,

$$j_c(V_f) = 0\,.\tag{38}$$

B. Capacitance Characteristic

It is also possible to calculate the capacitance of the sheath. As a consequence of Gauss' law, the surface charge density σ residing on the surface bounding the plasma is

$$\sigma = -\,\varepsilon_0\, E(V_s)\,.\tag{39}$$

If the voltage across the sheath is time dependent then the charge residing on the surface will be time dependent, resulting in a displacement current j_d, given by

$$j_d = \frac{d\sigma}{dt} = -\,\varepsilon_0\frac{dE(V_s)}{dt} = -\,\varepsilon_0\frac{dE(V_s)}{dV_s}\frac{dV_s}{dt}\,.\tag{40}$$

From this equation, a capacitance per unit area c_s due to the plasma sheath may be defined as

$$c_s = -\,\varepsilon_0\frac{dE(V_s)}{dV_s}\,.\tag{41}$$

The capacitance may be evaluated by noting that the electric field at the surface is given by

73

$$E(V_s) = \sqrt{\frac{-2}{\varepsilon_0} \int_0^{V_s} \rho(V)\, dV} \ . \tag{42}$$

Then, the resulting derivative of the electric field at the surface with respect to the voltage across the sheath is

$$\frac{dE(V_s)}{dV_s} = \frac{\dfrac{-\rho(V_s)}{\varepsilon_0}}{\sqrt{\dfrac{-2}{\varepsilon_0} \int_0^{V_s} \rho(V)\, dV}} \ . \tag{43}$$

Consequently, using Eqs. (41) through (43), the capacitance per unit area can be written as

$$c_s = \frac{\rho(V_s)}{E(V_s)} \ . \tag{44}$$

IV. NUMERICAL EXAMPLES OF SHEATH CHARACTERISTICS

In order to perform numerical calculations of the sheath characteristics, the following values for certain parameters of the plasma system were assumed:

m_+ = 40 amu,

m_- = 40 amu,

n_{+0} = 0.6 x10^{10} particles/cm^3,

T_- = 500 °K, and

T_e = 23,200 °K.

The calculations were performed for various values of α_0.

Figure 2 shows the behavior of Eq. (27) for $E^2(V(x))$ as a function of $-V(x)$ with $\alpha_0=0.3$ and for several different values of V_+. In this case, $V_{+;min}=0.18879$ V, which is the smallest value for which Eq. (32) and the sheath criterion of Eq. (10) hold. As can be seen from Fig. 2, for values of $V_+<V_{+;min}$, there are certain values of $V(x)$ for which the square of the electric potential would be negative. Therefore choosing $V_+<V_{+;min}$ is physically unrealistic. However, for all values of $V_+\geq V_{+;min}$ the square of the

74

electric field is always positive and hence, according to the sheath criterion, the restriction is that V_+ must be chosen such that $V_+ \geq V_{+;min}$. In the following discussion of the sheath characteristics, V_+ will be chosen such that $V_+ = V_{+;min}$.
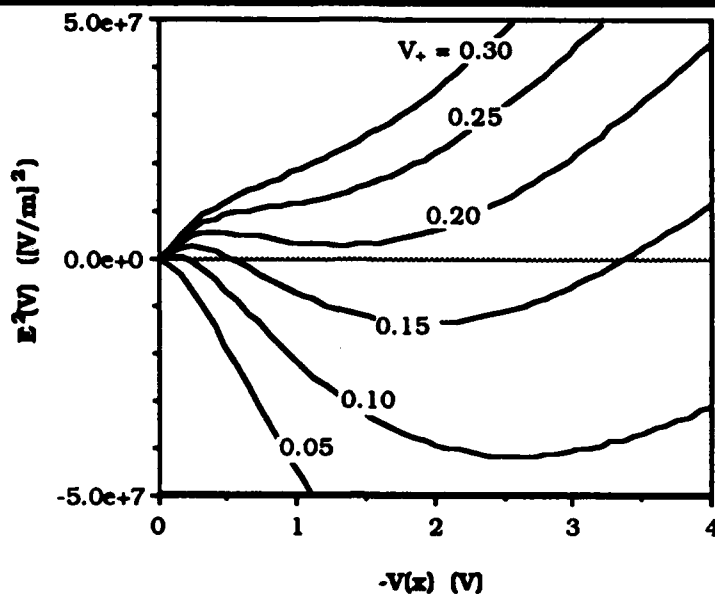

FIG. 2. The behavior of Eq. (27) for $\alpha_0 = 0.3$ and for various values of V_+.

Figure 3 shows the dependence of $V_{+;min}$ on α_0 as determined by the maximum value of the right hand side of Eq. (32). For the case of $\alpha_0 = 0.3$ where $V_{+;min} = 0.18879$ V, this corresponds to an $E^2(V)$ versus $-V(x)$ curve (as in Fig. 2) that has the value zero at $-V(x)=0$ V, reaches a local maximum near $-V(x)=0.5$ V, decreases to zero near $-V(x)=1.25$ V, and then increases as $-V(x)$ increases. Figure 3 also shows the value of the right hand side of Eq. (33) as a function of α_0. This value requires that the slope of the $E^2(V)$ versus $-V(x)$ curve at $-V(x)=0$ be nonnegative. Consider the case for $\alpha_0=0.3$, where the value of the right hand side of Eq. (33) equals 0.06840. For this situation, the $V_+=0.15$ curve in Fig. 2 is positive near $-V(x)=0$ since 0.15 is greater than 0.06840. However, this curve is negative for values of $-V(x)$ between approximately 0.75 and 3.5 V. This clearly shows that while the criterion given in Eq. (33) is necessary for the solution to be physically realistic, it is not always sufficient. From Fig. 3, one can see that the

75

criterion given in Eq. (33) is sufficient for cases in which α_0 is greater than about 0.55 for the assumed discharge parameters. Furthermore, there are values of α_0 near zero for which this criterion is sufficient. However, since the criterion given in Eq. (33) is not sufficient for all α_0, the criterion of Eq. (32), which is both necessary and sufficient for all α_0, must be used.
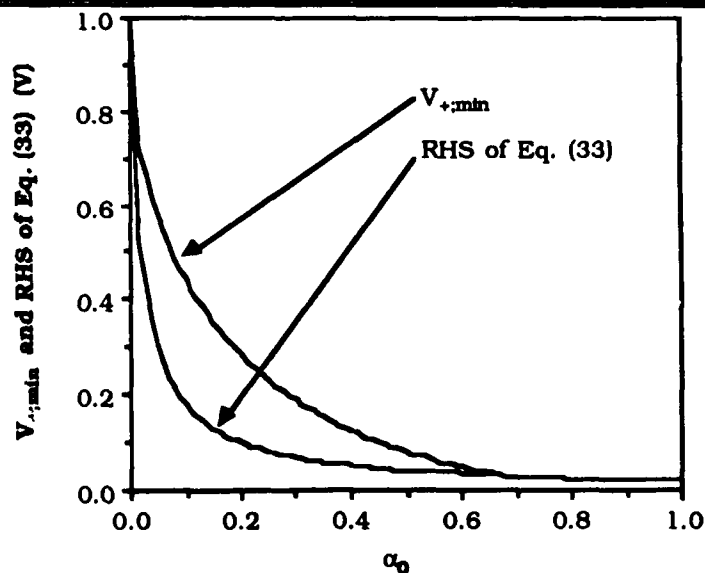

FIG. 3. The dependence of $V_{+;min}$ and the right hand side of Eq. (33) on α_0.

Figures 4a, 4b, and 4c show the dependence of the electric potential, charge density, and electric field respectively for $\alpha_0=0.3$ and $V_+=V_{+;min}$. It should be noted that in order to solve the equations for the electric field and electric potential numerically, it is necessary to start at the surface (i.e., $x=x_s$) where the value of the electric potential is V_s and the value of the electric field is given by Eqs. (27) and (9), and integrate towards the plasma. This procedure is required since, at $V(x)=0$, all derivatives of $V(x)$ with respect to x vanish. Thus, the electric potential, net charge density, and electric field only approach zero asymptotically. This results in the use of $x-x_s$ as the spatial coordinate in Fig. 4a with x_s determined for $V_s=-25$ V.
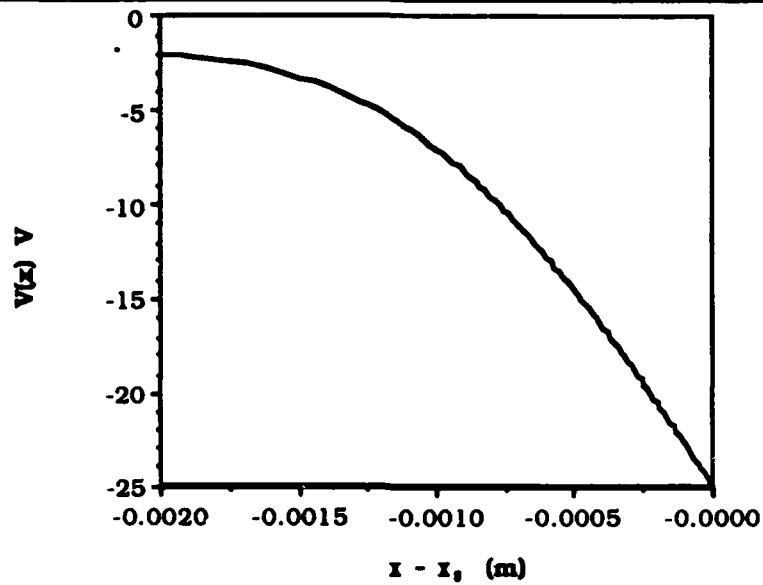
76

FIG. 4a. The spatial distribution of the electric potential in the sheath for $\alpha_0=0.3$, $V_+=V_{+;min}$, and $V_s=-25$ V. In this graph, x_s is the position of the surface.

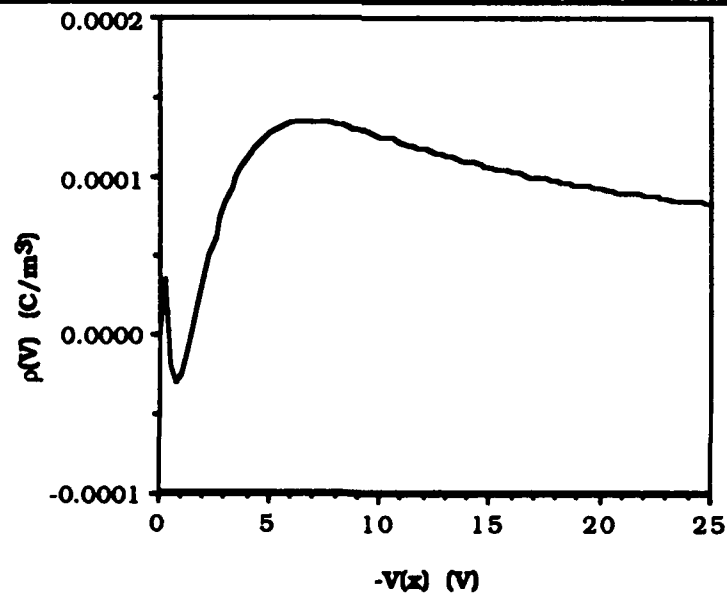

FIG. 4b. The dependence of the charge density on the electric potential in the sheath for $\alpha_0=0.3$ and $V_+=V_{+;min}$.

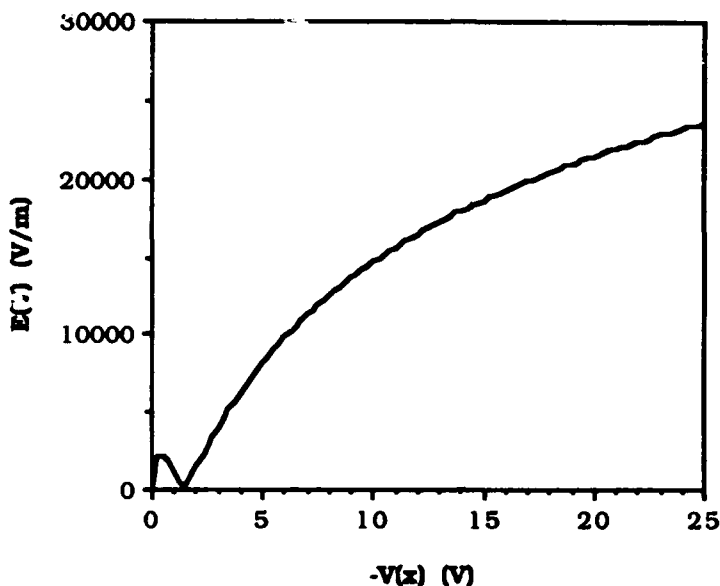FIG. 4c. The dependence of the electric field on the electric potential in the sheath for $\alpha_0 = 0.3$ and $V_+ = V_{+;min}$.

Figure 4a shows that most of the potential in the sheath is dropped across a small region. For this case with a magnitude of 25 V across the sheath, most of the voltage drop is across a region with a dimension of about 1.5 mm. Figure 4b shows the dependence of the charge density on the electric potential in the sheath. In this example, there is a region of negative space charge in the sheath near the plasma sheath boundary (i.e., $V(x) = 0$ V). According to the model, this may be explained by noting that at the plasma sheath boundary, the charge density is zero. After entering the sheath, the negative ions are easily repelled by a small negative electric potential and this results in the first positive space charge region. As a consequence, the positive ion density then decreases until the positive ion density becomes less than the electron density resulting in the negative space charge region. Finally, since the electron density is decreasing exponentially, the electron density eventually becomes less than the positive ion density resulting in a positive space charge region throughout the rest of the sheath. It should be noted however, that this detailed behavior near the plasma sheath boundary involving a negative space charge region may not accurately reflect reality

78

because of assumption (3) used in developing this model, as discussed in Section V.

The current characteristic given by Eq. (37) is shown in Fig. 5a for $V_+=V_{+;min}$ and various values of α_0. An enlargement of the region near where $J_c(V_s)=0$ is shown in Fig. 5b. It can be noted from this figure that a relatively large density of negative ions with respect to the density of electrons (i.e., α_0 near 1) is required before there is a significant effect on the floating potential. Even for $\alpha_0=0.99$, the floating potential is still -4.5 V. However, the introduction of even a small density of negative ions reduces the positive ion saturation current due to the dependence of the positive ion current on $V_{+;min}$, which decreases rapidly with increasing α_0 near $\alpha_0=0$. The capacitance characteristic is shown in Fig. 6. This characteristic is also noticeably effected by changes in the relative density of negative ions near $\alpha_0=0$. It should also be noted that the capacitance is a nonlinear function of the voltage across the sheath.
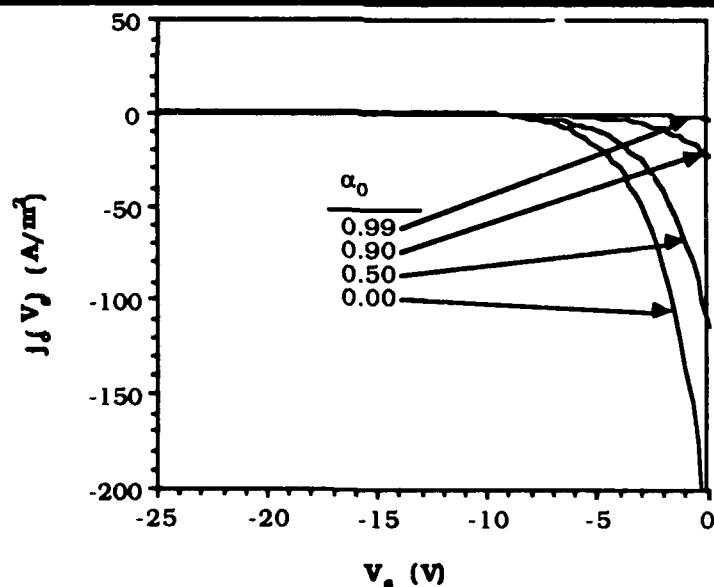

FIG. 5a.The conduction current density collected at the surface as a function of the voltage between the surface and the sheath for $V_+=V_{+;min}$ and for different values of α_0.
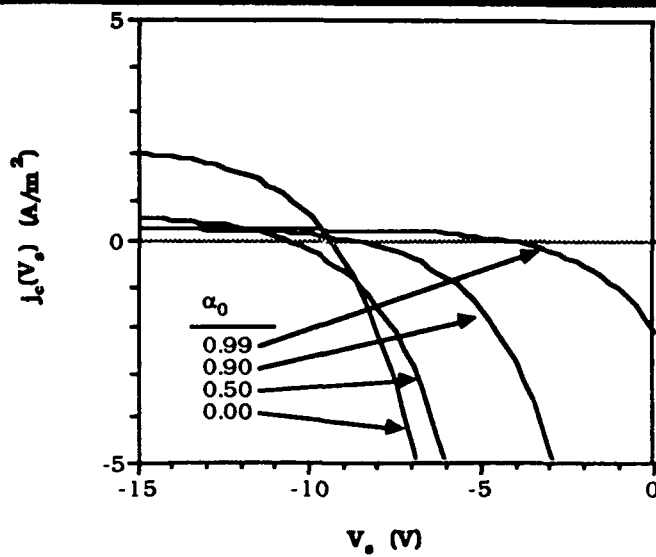
FIG. 5b. Enlargement of Fig. 5a. highlighting the region near where $J_c(V_s)=0$. The voltage V_s for which $J_c(V_s)=0$ is the value of the floating potential, V_f.
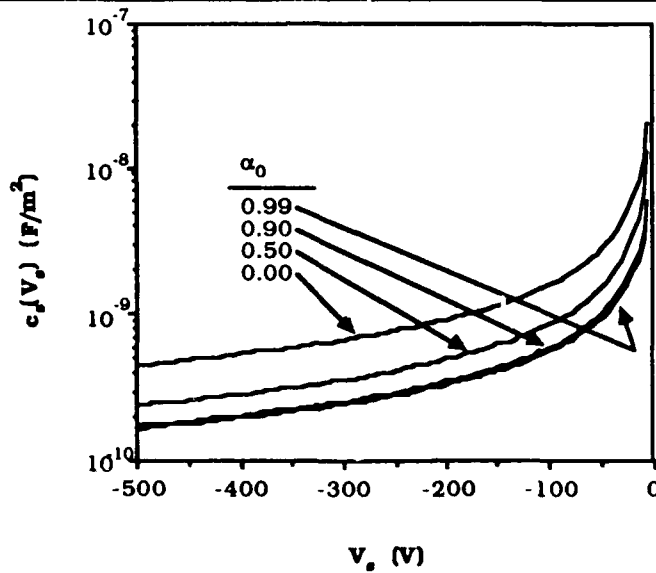

FIG. 6. The capacitance per unit area of the sheath as a function of the voltage between the surface and the sheath for $V_+=V_{+;min}$ and for different values of α_0.

V. APPLICABILITY AND EXTENSIONS OF THE MODEL

The assumptions used in the derivation of this collisionless plasma sheath model have some important consequences with regard to its application and extensions. Though it has not been explicitly shown, it can be noted that it is possible to allow any of the ionic species to be multiply charged by making appropriate changes in the previous derivation. In addition, while this model can not readily be extended to a case involving more than one positive ion species, it can be extended to a situation involving more than one negative ion species. Thus, assumption (1) of the model may be relaxed to include any plasma consisting of neutrals, electrons, single multiply charged positive ion species, and multiple multiply charged negative ion species.

Assumption (2), which allows the problem to be treated as one-dimensional, is valid only if the thickness of the sheath is much smaller than the dimensions of the system. Assumption (4) restricts the applicability of the model to cases where the surface is at a negative potential with respect to the plasma. In addition, in order for assumptions (5) and (6) to be valid, the magnitude of the electric potential at the surface must be significantly larger than the voltage equivalent of either the negative ion or electron temperatures. If this condition is satisfied, the loss of electrons and negative ions from the bulk of the plasma will be small and their velocity distributions should be only slightly displaced from an equilibrium situation. Very near the surface however, there will still be some departure from assumption (6), since the Boltzmann density distribution assumes an equal number of particles moving both toward and away from the surface, while, in reality, near the surface particles move predominantly toward the surface. However, since near a surface at a large negative potential, the electron and negative ion densities are very small with respect to the positive ion density, any deviations in their contributions to the net charge density may be neglected.

Assumption (7) is only satisfied if the sheath region is small with respect to the mean free path of a positive ion. Assumption (9) assumes a perfectly absorbing and nonemitting surface. It should be noted that it is possible to perform a derivation equivalent to the one presented here in which the surface is assumed to have a nonzero reflection or emission coefficient.

Assumptions (3) and (8) are the assumptions which most limit the model. First, in order for the velocity distribution of the positive ions to be considered monoenergetic as in assumption (8), their average drift energy must be much greater than their thermal energy in the bulk of the plasma. This means that V_+ must be much greater than kT_+/e, where T_+ is the thermal temperature of the positive ions. From Fig. 3, it is clear that when V_e is much greater than V_+, this condition is satisfied, except as one approaches the situation where there are no electrons (i.e. $\alpha_0=1$) and T_- is less than or equal to T_+. However in reality, even if the positive ions enter the sheath with an average drift energy which is much larger than the thermal energy of these ions in the bulk of the plasma, the width of the velocity distribution function of these ions may be much broader than is expected from the thermal energy of the ions in the bulk of the plasma. This is result of the fact that the ions are flowing from the point at which they are created to the plasma sheath boundary and any collisions that these ions undergo before they reach the plasma sheath boundary will broaden their energy distribution. However, this assumption will still be valid throughout most of the sheath region, except near the plasma sheath boundary, since in the sheath the ions gain large amounts of energy relative to the kinetic energy with which the ions are injected into the sheath.

The above discussion points out the fact that this model does not address the origin of the drift velocity other than noting that it is due to the fact th·t positive ions are created in the plasma and are lost at the surface. Other authors have attempted to model the origin of the drift velocity through the use of a presheath concept. However, as implied by assumption (3), the use of a presheath has been avoided in this discussion. It should be noted that by using the equation for the electric potential in the plasma sheath resulting from this model under the boundary conditions indicated in Fig. 1, one finds that the solution for the electric potential only asymptotically approaches zero as one proceeds towards the plasma from the surface. Hence, the sheath would be infinite in extent if it is required that the electric field and the net charge density be zero at the plasma sheath boundary, as was assumed in this derivation. However, in reality, the electric field and the net charge density have a small but nonzero value at the plasma sheath edge and the resulting solution of the sheath then has a

finite size. In either case, however, most of the potential in the sheath is dropped over a finite distance.

VI. MODEL IMPLICATIONS FOR DC AND RF DISCHARGES

This model has several important implications for dc and rf discharges in electronegative gases. For dc discharges, the model predicts that in the positive column it is possible to achieve a very large density of negative ions. As previously shown, the floating potential decreases slowly as the ratio of the negative ion density to the positive ion density increases. Hence, the voltage equivalent of the negative ion temperature is much smaller in magnitude than the floating potential, even when the negative ion density is greater than 99% of the total density of negatively charged particles. Therefore, practically no negative ions are able to escape to the walls of the dc discharge. The negative ions are essentially trapped in the plasma by the floating potential at the surface. Hence, in most cases involving negative ions, their density in the bulk of the plasma increases until volume losses equal volume production.

For rf discharges, it can also be shown that the negative ions are trapped within the plasma in a similar manner. By the same argument as given above, practically no negative ions may escape to any side walls of a rf reactor since these walls are at the floating potential. In addition, using a model of a rf plasma that has been developed by Metze, Ernie, and Oskam[9], the loss of negative ions to the electrodes may be predicted. This model shows that the magnitude of the electric potential across the plasma sheath at an electrode is never significantly less than magnitude of the floating potential. This result is a consequence of the current characteristic and capacitance characteristic of the plasma sheath. When the magnitude of the sheath voltage is only slightly less than magnitude of the floating potential, very large electron currents can be collected. However, when the magnitude of the sheath potential is greater than the magnitude of the floating potential, the maximum current that can be collected is the much smaller positive ion saturation current. Since the net current through the sheath during an rf cycle is zero if a blocking capacitor is in series with the

---

[9] A. Metze, D. W. Ernie, and H. J. Oskam, J. Appl. Phys. **60**, 3081 (1986).

electrode, the magnitude of the voltage across the sheath during that portion of the cycle during which a large electron current can flow through the sheath must be only slightly smaller than the magnitude of the floating potential. Again, for this argument, since the magnitude of the electrode potential is always near or greater than the magnitude of the floating potential, practically no negative ions ever escape to the electrodes. Hence, in most rf plasmas, the negative ion density will increase until volume losses equal volume production. Therefore, a very large density of negative ions may be expected for plasmas in electronegative gases.

ACKNOWLEDGMENTS

APPENDIX A

In this Appendix, the coefficient of V_+ on the left hand side of Eq. (30) is shown to be greater than or equal to zero, i.e.,

$$- V(x) - F[V(x)] \geq 0 , \tag{A1}$$

for $V(x) \leq 0$.

It will first be useful to prove that the function $g(z)$ defined by

$$g(z) = z + \exp(- z) - 1 \tag{A2}$$

is non-negative for z non-negative. To prove this statement, first note that

$$g(0) = 0 . \tag{A3}$$

The derivative of the function $g(z)$ with respect to z is

$$\frac{dg(z)}{dz} = 1 - \exp(- z) . \tag{A4}$$

Since z is non-negative, the derivative is also non-negative. Therefore,

$$g(z) \geq 0 \tag{A5}$$

if z is non-negative, as desired.

The substitution of $-V(x)/V_e$ for z in Eqs. (A2) and (A5) is valid since, if $V(x) \leq 0$, then $-V(x)/V_e$ is non-negative. Multiplying both sides of the resulting inequality by V_e yields

$$- V(x) - V_e \left[1 - \exp\left(\frac{V(x)}{V_e}\right) \right] \geq 0 \,. \tag{A6}$$

Similarly, using V_- for the negative ions,

$$- V(x) - V_- \left[1 - \exp\left(\frac{V(x)}{V_-}\right) \right] \geq 0 \,. \tag{A7}$$

Multiplying Eq. (A6) by $(1 - \alpha_0)$, and Eq. (A7) by α_0, and then adding, yields

$$- V(x) - (1 - \alpha_0) V_e \left[1 - \exp\left(\frac{V(x)}{V_e}\right) \right] - \alpha_0 V_- \left[1 - \exp\left(\frac{V(x)}{V_-}\right) \right] \geq 0 \,. \tag{A8}$$

But from the definition of F(x) in Eq. (31), Eq. (A8) is equivalent to Eq. (A1). Thus, Eq. (A1) is shown to hold for all $V(x) \leq 0$.

APPENDIX B

In this Appendix, it will be shown that Eq. (33) is the limit of Eq. (32) as the potential V(x) approaches zero.

When V(x) is equal to zero, Eq. (32) is an indeterminate form which may be evaluated by expan' .ing the numerator and denominator in a Taylor's series about the point V(x) = 0. Expanding F[V(x)] yields

$$F[V(x)] = (1 - \alpha_0) V_e \left[1 - \left(1 + \frac{V(x)}{V_e} + \frac{V^2(x)}{V_e^{\,2}} + \dots \right) \right]$$

$$+ \alpha_0 V_- \left[1 - \left(1 + \frac{V(x)}{V_-} + \frac{V^2(x)}{V_-^{\,2}} + \dots \right) \right] \,. \tag{B1}$$

where the neglected terms are of a higher order in V(x). This expression simplifies to

$$F[V(x)] = -V(x) - (1 - \alpha_0) \frac{V^2(x)}{2 V_e} - \alpha_0 \frac{V^2(x)}{2 V_-} + \dots . \qquad \text{(B2)}$$

Substituting this expression into Eq. (32) yields

$$V_+ \geq \frac{\left[-V(x) - (1 - \alpha_0) \frac{V^2(x)}{2 V_e} - \alpha_0 \frac{V^2(x)}{2 V_-} + \dots \right]^2}{4 \left\{ -V(x) - \left[-V(x) - (1 - \alpha_0) \frac{V^2(x)}{2 V_e} - \alpha_0 \frac{V^2(x)}{2 V_-} + \dots \right] \right\}} . \qquad \text{(B3)}$$

Simplifying this expression yields

$$V_+ \geq \frac{V^2(x) + \dots}{\left[(1 - \alpha_0) \frac{2}{V_e} + \alpha_0 \frac{2}{V_-} \right] V^2(x) + \dots} . \qquad \text{(B4)}$$

In the limit as V(x) approaches zero, the terms of higher order in V(x) in the numerator and denominator may be neglected. Thus, cancelling the $V^2(x)$ term from both the numerator and denominator yields the result given in Eq. (33).

APPENDIX C

In this Appendix, it will be shown that for the case of a only one singly charged positive ion species and electrons, Eq. (33) is a sufficient condition for Eq. (10) to be satisfied for V(x)≤0.

It will be useful to first prove that the function g(z) defined by

$$g(z) = 2 [z + \exp(-z) - 1] - [1 - \exp(-z)]^2 , \qquad \text{(C1)}$$

is non-negative for z non-negative. To prove this statement, first note that

$$g(0) = 0 . \qquad \text{(C2)}$$

The derivative of the function g(z) with respect to z is

$$\frac{dg(z)}{dz} = 2 [1 - \exp(-z)] - 2 [1 - \exp(-z)] \exp(-z) , \qquad \text{(C3)}$$

and it may be rewritten as

$$\frac{dg(z)}{dz} = 2 [1 - \exp(- z)]^2 .$$ (C4)

This derivative is clearly non-negative. Therefore,

$$g(z) \geq 0$$ (C5)

if z is non-negative, as desired.

Using Eq. (C1), Eq. (C5) may be rewritten as

$$2 [z + \exp(- z) - 1] \geq [1 - \exp(- z)]^2 ,$$ (C6)

for z non-negative. The left hand side of Eq. (C6) is positive and the inequality may be rewritten as

$$1 \geq \frac{[1 - \exp(- z)]^2}{2 [z + \exp(- z) - 1]} ,$$ (C7)

where z is non-negative. Caution is needed in performing this division since the numerator and denominator both go to zero as z goes to zero. However, the division is valid in the limit as z goes to zero and the value of the right hand side at z = 0 will be defined to be this limit.

The substitution of $-V(x)/V_e$ for z in Eq. (C7) is valid since if $V(x) \leq 0$ then $-V(x)/V_e$ is non-negative. Multiply both sides of the resulting inequality by $V_e/2$ yields

$$\frac{V_e}{2} \geq \frac{\left\{ V_e \left[1 - \exp\left(\frac{V(x)}{V_e}\right) \right] \right\}^2}{4 \left\{ - V(x) - V_e \left[1 - \exp\left(\frac{V(x)}{V_e}\right) \right] \right\}} .$$ (C8)

The right hand side is clearly the same as the right hand side of Eq. (32) for the case when there are no negative ions, i.e., $\alpha_0 = 0$. This proves that Eq. (33) is a sufficient condition for the sheath criterion given by Eq. (10) to be satisfied for the case when there is only one singly charged positive ion species and electrons (i.e., $\alpha_0 = 0$).

SECTION VI

THE RADIAL DISTRIBUTIONS OF CHARGED PARTICLE DENSITIES AND ELECTRIC FIELD STRENGTH IN THE POSITIVE COLUMN

The Radial Distributions of Charged Particle Densities and Electric Field Strength in the Positive Column

A. Metze,[a] D. W. Ernie, and H. J. Oskam
Department of Electrical Engineering
University of Minnesota
Minneapolis, MN 55455

ABSTRACT

A model is presented for the radial distribution of ion and electron densities and electric field strength in the positive column of a dc discharge for a plasma consisting of a singly charged positive ion species, electrons, and neutrals. The set of equations involved consists of the particle and momentum conservation equations for the ions and electrons and Poisson's equation. Utilizing this single set of equations and appropriate assumptions, this model has been solved, through suitable numerical techniques, for various tube radii, R, and gas pressures, p_0. These calculations show the development of both the ambipolar electric field in the "bulk" of the positive column and the sheath field "near" the discharge wall. The results also demonstrate the existence of a nonzero difference between the ion and electron densities at the discharge axis, with an increase in this difference for decreasing Rp_0.

I. INTRODUCTION

Several authors have reported theories concerning the radial distributions of charged particle densities and the electric field strength in the cylindrical positive column of a direct current discharge. These theories were all confined to plasmas containing a singly charged positive ion species and electrons, with the authors making various assumptions in order to arrive at an analytic solution or, more recently, a numerical analysis. Schottky[1] developed an ambipolar diffusion theory in 1924 in which he assumed

---

a) Present address: Honeywell Systems and Research Center, 3660 Technology Drive, Minneapolis, MN 55418.
[1] W. Schottky, Z. Phys. **25**, 625 (1924).

quasineutrality of the plasma and neglected the effect of charged particle inertia on the radial structure of the positive column. Subsequent authors have also assumed quasineutrality of the plasma, but included the charged particle inertia term in the conservation of momentum equations.[2,3] Several other authors included Poisson's equation for calculating the radial electric field strength inside the plasma.[4-8] However, in order to arrive at a tractable solution, they either omitted the charged particle inertia term[4-6] or the effect of ion density diffusion on the ion current density towards the discharge walls[7,8]. All the authors have assumed a Maxwellian distribution of the random energy of the ions and electrons with constant ion and electron temperatures.

This paper deals with calculations of the radial charged particle density distributions, the radial charged particle current densities, and the radial electric field strength in the cylindrical positive column of a dc discharge. The set of equations involved consists of the particle conservation equations, the momentum conservation equations including the diffusion and inertia terms, and Poisson's equation. The common assumption that the energy distribution of the random energies of the electrons and ions is Maxwellian with temperatures independent of radial position will be made. In the next section the the assumptions used in deriving the model and the resulting set of equations will be given, along with the method of solution used in the numerical calculations. The results obtained for realistic discharge parameters and for various values of the discharge tube radius, R, and gas pressure, p_0, will be presented and discussed in Sec. III. The validity of the assumptions used will be compared with the calculated results in order to determine the self-consistency of the theory presented.

[2]S. A. Self and H. N. Ewald, Phys. Fluids **9**, 2486 (1966).

[3]H. W. Friedman, Phys. Fluids **10**, 2053 (1967).

[4]W. P. Allis and D. J. Rose, Phys. Rev. **93**, 84 (1954).

[5]I. M. Cohen, Phys. Fluids **6**, 1492 (1963).

[6]I. M. Cohen and M. D. Kruskal, Phys. Fluids **8**, 920 (1965).

[7]J. R. Forrest and R. N. Franklin, J. Phys. D **1**, 1357 (1968).

[8]J. H. Ingold, Phys. Fluids **15**, 75 (1972).

II. THEORETICAL MODEL

In the first part of this section, the assumptions used in deriving the model will be discussed. The resulting equations used for the calculations of the radial distributions of the charged particle densities and the electric field strength will then be presented. Finally, the boundary conditions for the model and the method of solution of the set of equations will be given in the last two parts of this section.

A. Assumptions

The model and calculations presented in this paper refer to a positive column of a dc gaseous discharge under cylindrical symmetry. The plasma is assumed to consist of a singly charged positive ion species, electrons, and neutrals. The following assumptions will be made for the present model:

(1) The energy distribution of the random energy of the ions and electrons is Maxwellian with temperatures T_i and T_e, respectively. This is an assumption made by previous authors and is valid, except at locations close to the discharge tube wall. The latter point will be discussed in more detail when presenting the boundary conditions of the model.

(2) All quantities are independent of the axial coordinate z and the azimuthal angle ϕ.

(3) The ion and electron temperatures T_i and T_e are independent of the radial coordinate r. This assumption was also made by all previous authors.

(4) The ionization frequency v_i of the electrons is very small with respect to the collision frequencies for momentum transfer v_{mi} and v_{me} of the ions and electrons, respectively. Therefore, the effect of ionizing collisions on the momentum loss (gain) of the charged particles can be neglected.

(5) The ion and electron production is a linear function of the electron density, while the only charged particle loss from the plasma is by diffusion towards the discharge tube wall. The calculations can be extended to nonlinear production (loss) processes. However, the main features of the results presented would not change significantly.

(6) The friction force between the ions and electrons can be neglected with respect to the friction force between the charged particles and the neutral particles. This is a valid assumption for low degrees of ionization.

(7) The positive column is in steady state with no net current flowing to the discharge tube walls, so that the radial ion and electron current densities are equal.

B. Equations

The assumptions given above result in the following set of equations:

$$\frac{1}{r}\frac{d}{dr}\left[r\,\Gamma_r(r)\right] = \nu_i\,n_e(r) \tag{1}$$

$$\frac{m_i}{r}\frac{d}{dr}\left[\frac{r\,\Gamma_r^2(r)}{n_i(r)}\right] + kT_i\frac{d}{dr}\,n_i(r) - e\,n_i(r)\,E_r(r) = -\,m_i\,\Gamma_r(r)\,\nu_{mi} \tag{2}$$

$$\frac{m_e}{r}\frac{d}{dr}\left[\frac{r\,\Gamma_r^2(r)}{n_e(r)}\right] + kT_e\frac{d}{dr}\,n_e(r) + e\,n_e(r)\,E_r(r) = -\,m_e\,\Gamma_r(r)\,\nu_{me} \tag{3}$$

$$\frac{1}{r}\frac{d}{dr}\left[r\,E_r(r)\right] = \frac{e}{\varepsilon_0}\left[n_i(r) - n_e(r)\right]. \tag{4}$$

Here, $\Gamma_r(r)$ is the radial particle flow density of the ions and electrons; $n_i(r)$ and $n_e(r)$ are the ion and electron particle densities; m_i and m_e are the ion and electron masses; ε_0 is the permittivity of free space; and $E_r(r)$ is the radial component of the electric field strength.

Equation (1) is the continuity equation of the charged particles, while Eqs. (2) and (3) are the conservation of momentum equations (volume force equations) for the ions and electrons, respectively. Equation (4) is Poisson's equation and is needed for a self-consistent calculation of the radial electric field strength. The assumption that the ion and electron temperatures are independent of coordinates eliminates the need to use the conservation of energy equations for the ions and the electrons.

The term on the right hand side of Eqs. (2) and (3) is the volume friction force. Since the radial drift velocity of the neutral particles is very small with respect to the radial drift velocity of the ions and electrons, it is neglected in this term. The terms on the left hand side of Eqs. (2) and (3) are the volume inertia force, the volume diffusion force, and the volume electric field force, respectively. Previous theories of the radial properties of the positive column which incorporated Poisson's equation have used various approximations concerning the effect of the different volume force terms on the radial particle density distributions, etc. Several authors neglected one or both volume inertia force terms,[4-7] while one author neglected the volume diffusion force for the ions[8]. The motivation for these approximations result from the fact that when all three volume force terms related to the ions are included in the theoretical model, an instability occurs in the numerical calculations (for certain numerical techniques) when the radial ion drift energy is equal to one half the kinetic ion pressure, i.e., the radial ion drift velocity v_{di} is equal to the isothermal ion sound speed $v_{ri}=(kT_i/m_i)^{1/2}$. This instability problem in the numerical techniques has been discussed in the literature.[8,9] The method described below for solving the set of Eqs. (1)-(4) circumvents this difficulty.

C. Boundary Conditions

The four functions to be determined from Eqs. (1)-(4) are $n_i(r)$, $n_e(r)$, $\Gamma_r(r)$, and $E_r(r)$. Appropriate boundary conditions are thus required for these functions. Because of symmetry, both $\Gamma_r(r)$ and $E_r(r)$ must be zero at the axis of the positive column, i.e., $\Gamma_r(r=0)=0$ and $E_r(r=0)=0$. The two other required boundary conditions are the values of $n_i(r=0)$ and $n_e(r=0)$. For the model presented here, these values will be different, i.e., $n_i(r)\neq n_e(r)$, since it will not be assumed that the discharge plasma is quasineutral. It should be noted that the values of $n_i(r=0)$ and $n_e(r=0)$ then determine the spatial derivative of $E_r(r)$ at r=0. Moreover, the cylindrical symmetry of the positive column requires that the radial derivatives of $n_i(r)$ and $n_e(r)$ equal zero at r=0.

[9]H. W. Friedman and E. Levi, Phys. Fluids **10**, 1499 (1967).

The boundary condition for the electron density at the wall of the discharge tube has been discussed by several authors. A summary of this discussion is given in Ingold.[8] If it is assumed that the velocity distribution of the electrons at the wall, which is assumed to be a perfect sink for the electrons, is Maxwellian in the forward direction and zero in the backward direction, then the following boundary condition must hold at the wall:

$$n_e(R) = \Gamma_r(R) \left(\frac{2kT_e}{\pi\, m_e} \right)^{\frac{1}{2}}. \tag{5}$$

This condition is also the boundary condition resulting from collisionless space charge theory and is equal or very close to the boundary condition of other theories.

D. Method of Solution

The method of solution used in this paper consists of expanding the functions $n_i(r)$, $n_e(r)$, $\Gamma_r(r)$, and $E_r(r)$ in power series of the radial coordinate r, around r=0. The calculation of the coefficients of the four power series is performed in the following steps:

(1) The boundary conditions $\Gamma_r(r=0)=0$ and $E_r(r=0)=0$ as well as the symmetry conditions (i.e., the radial derivatives of the charged particle densities equal zero at r=0) are used. The values of $n_i(r=0)$, $n_e(r=0)$, and the constants v_i, v_{mi}, v_{me}, T_i, and T_e are chosen and substituted into Eqs. (1)-(3). These values will depend on the parameters of the experimental situation being modeled, such as the electric current density inside the positive column, the type of gas, the gas pressure, the tube radius, etc, and can be appropriately chosen. For example, the collision frequencies and charged particle temperatures may be available from experimental data presented in the literature or can be theoretically calculated.

(2) The coefficients of the power series are determined, either by a standard computer technique or, if possible, by deriving a recurrence relation between the coefficients. During the calculations, non-physical solutions for the unknown functions may occur. As a result one of the parameters, v_i, is changed until a physical solution having sufficient accuracy

is obtained. The accuracy can be determined by extending the power series to higher powers of r and comparing the results.

(3) The radius of the discharge tube walls is determined from Eq. (5). If the calculated tube radius is different from the desired tube radius, the calculations are repeated using a different value for the net charged particle density at the axis $\Delta n(r=0)=n_i(r=0)-n_e(r=0)$. The calculations are repeated until the proper consistency is reached between the tube radius for the experimental conditions being modeled and the theoretical results.

It should be noted that the set of Eqs. (1)-(4) can easily be transformed into a set of dimensionless equations, with the same method of solution being used to obtain the dependence of positive column properties on discharge parameters. Most previous authors have used the dimensionless approach when developing theories concerning the positive column. However, since the present paper attempts to model the properties of positive column discharges for which experimental information is available, the dimensionless approach has been avoided.

III. NUMERICAL CALCULATIONS AND DISCUSSION

Numerical calculations were performed for the model presented in Sec. II, utilizing the method of solution outlined. These calculations were for a discharge in helium with the following assumed parameters:

$m_i = 4$ amu (for He$^+$),

$v_{mi}/p_0 = 3.0 \times 10^7$ s^{-1} (for He$^+$),

$v_{me}/p_0 = 2.3 \times 10^9$ s^{-1},

$T_i = 300$ °K,

$n_i(r=0) = 1.0 \times 10^{16}$ m^{-1},

where the values for v_{mi} and v_{me} are from Ref. 10. Results are presented below for different values of R and p_0. For each selection of R and p_0, the appropriate value for T_e was chosen from the experimental work of Leiby and Rogers[11] and the values of v_i and $n_e(r=0)$ were adjusted, as indicated in

[10]J. H. Ingold and H. J. Oskam, Phys. Fluids **27**, 214 (1984).

[11]C. C. Leiby, Jr. and C. W. Rogers, presented at the 20th Gaseous Electronics Conference, Palo Alto, California,1967 (unpublished).

Sec. II, to give a physical solution consistent with the chosen values of R and p_o.

Figures 1-3 show the results of calculations for a discharge tube radius R=1.0 cm and a gas pressure p_o=5 Torr, leading to the product Rp_o=5.0 cm-Torr. From the results of Leiby and Rogers, these conditions imply an electron temperature T_e=26,000 ^oK. The required net charged particle density on the axis is then $\Delta n(r=0)$=6.8 X 10^{12} m^{-3}, with an ionization collision frequency v_i=1.95 X 10^4 s^{-1}. Figure 1 gives the plots of the ion density $n_i(r)$, the electron density $n_e(r)$, and the net charged particle density $\Delta n(r)$. The curves for $n_i(r)$ and $n_e(r)$ are close to the shape of the zero order Bessel function $J_0(2.4r/R)$ resulting from the ambipolar diffusion theory for the positive column.[12] However, there is a deviation from this shape, especially for $n_i(r)$, near the tube wall. This deviation is indicative of the development of a thin sheath region near the wall, which is not modeled by the ambipolar theory. The development of this sheath region is also indicated in the curve of $\Delta n(r)$, which increases rapidly near the wall. From these results it can be seen that, while this model predicts the development of a sheath region, there is no clear distinction between the sheath region and the bulk plasma, as can be expected. Therefore, the assignment of different regions of the discharge to these two categories is somewhat arbitrary, as discussed previously by Self and Ewald.[2]. Finally, the instability point discussed in Sec. II at which the the radial ion drift velocity v_{di} is equal to the isothermal ion sound speed v_{ri} is also shown in Fig. 1. This point is very near the wall under these discharge conditions.

The radial electric field $E_r(r)$ and the resulting electric potential V(r) are shown in Fig. 2. For comparison, the ambipolar radial electric field $E_a(r)$ calculated from the ambipolar diffusion theory is also plotted in this figure. The value of $E_r(r)$ is relatively small near the axis, but increases to larger values near the wall. This is again indicative of the development of the sheath near the wall. A comparison between $E_r(r)$ and $E_a(r)$, indicates that the two values are equal near the axis, but deviate from each other near the wall. This deviation is due to the fact that the ambipolar theory does not model the sheath region, with $E_a(r) \rightarrow +\infty$ for $r \rightarrow R$. The curve of V(r) also shows the smooth transition from the bulk plasma region near the axis

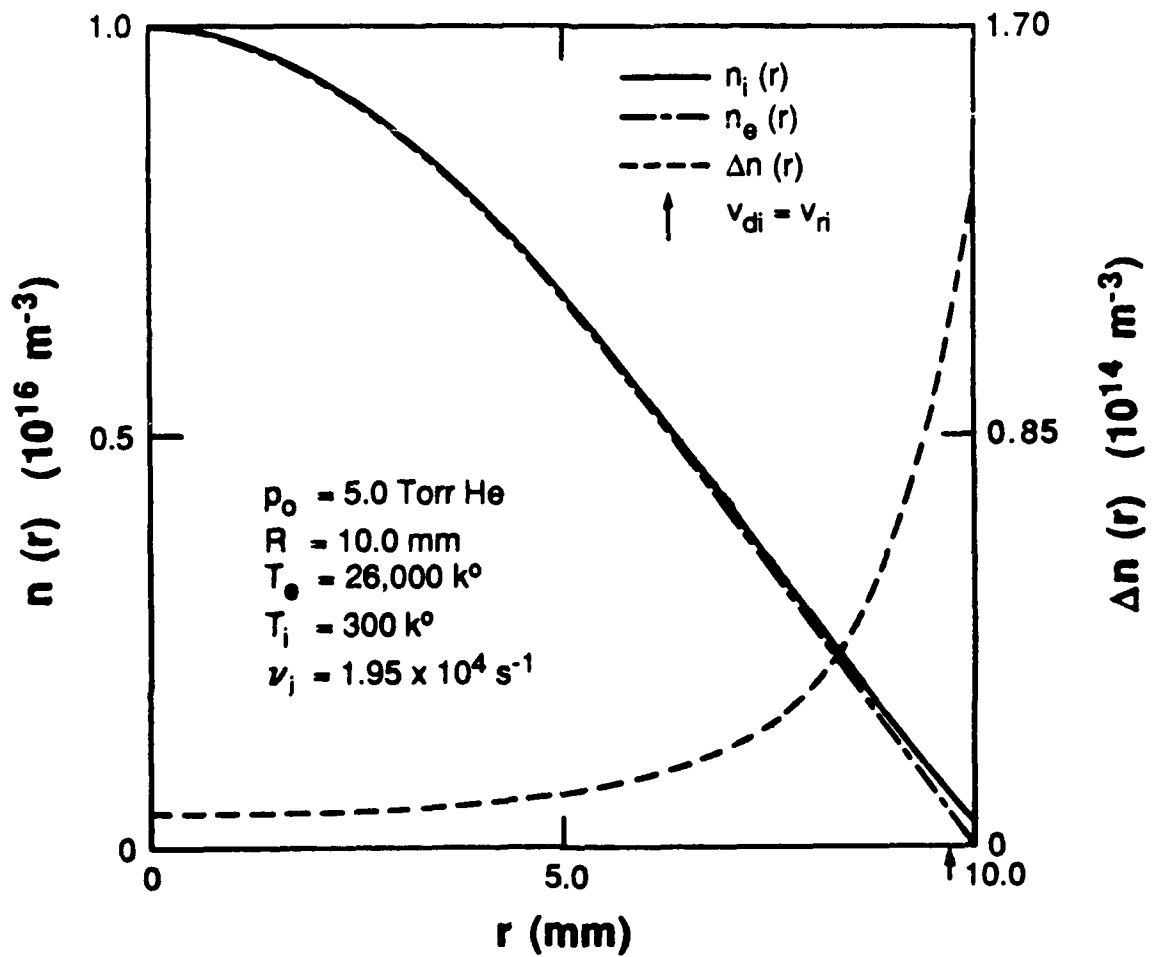---

[12]H. J. Oskam, Phillips Res. Rep. **13**, 335 (1958).

Fig. 1. Numerical calculations of the ion density $n_i(r)$, the electron density $n_e(r)$, and the net charged particle density $\Delta n(r)$ for $Rp_o=5.0$ cm-Torr.
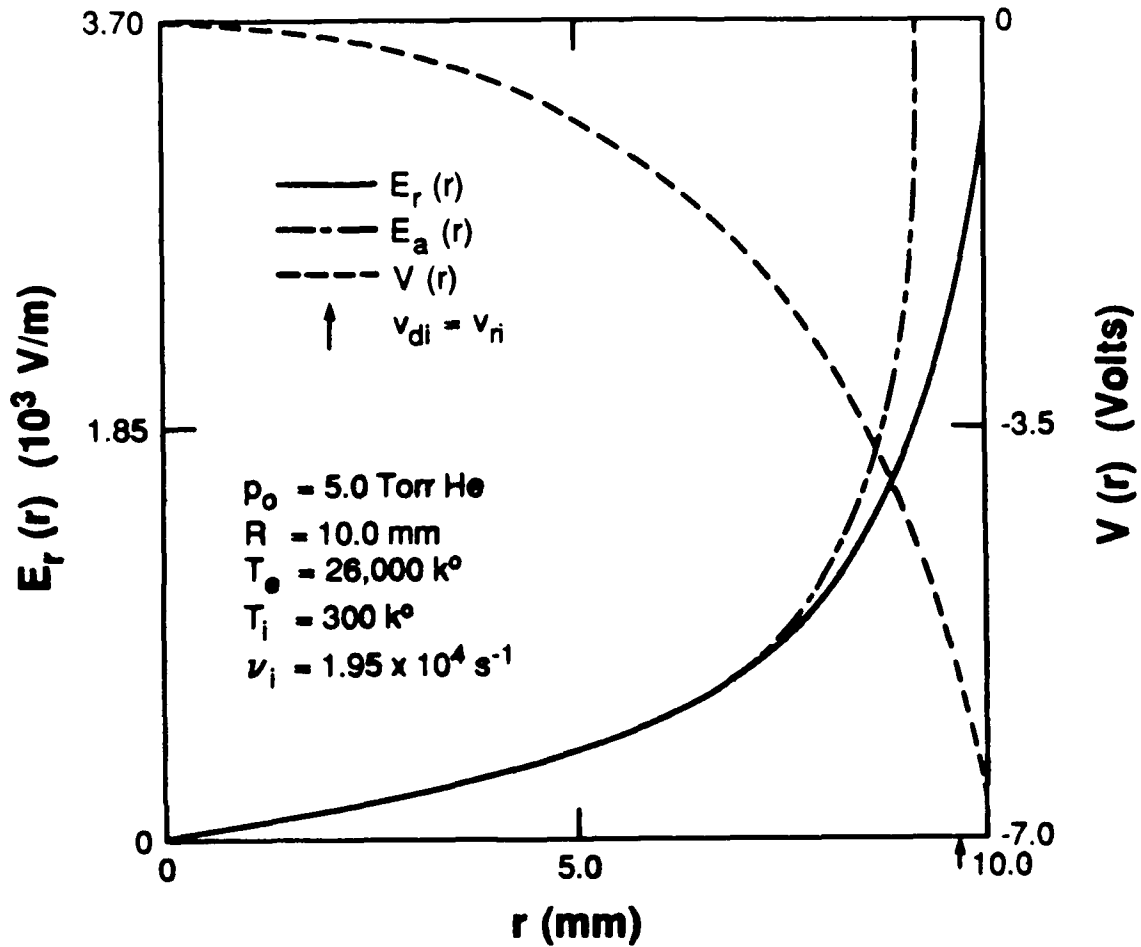
Fig. 2. Numerical calculations of the radial electric field strength $E_r(r)$ and the resulting electric potential $V(r)$ for $Rp_o = 5.0$ cm-Torr. The ambipolar radial electric field $E_a(r)$ is also shown for comparison.
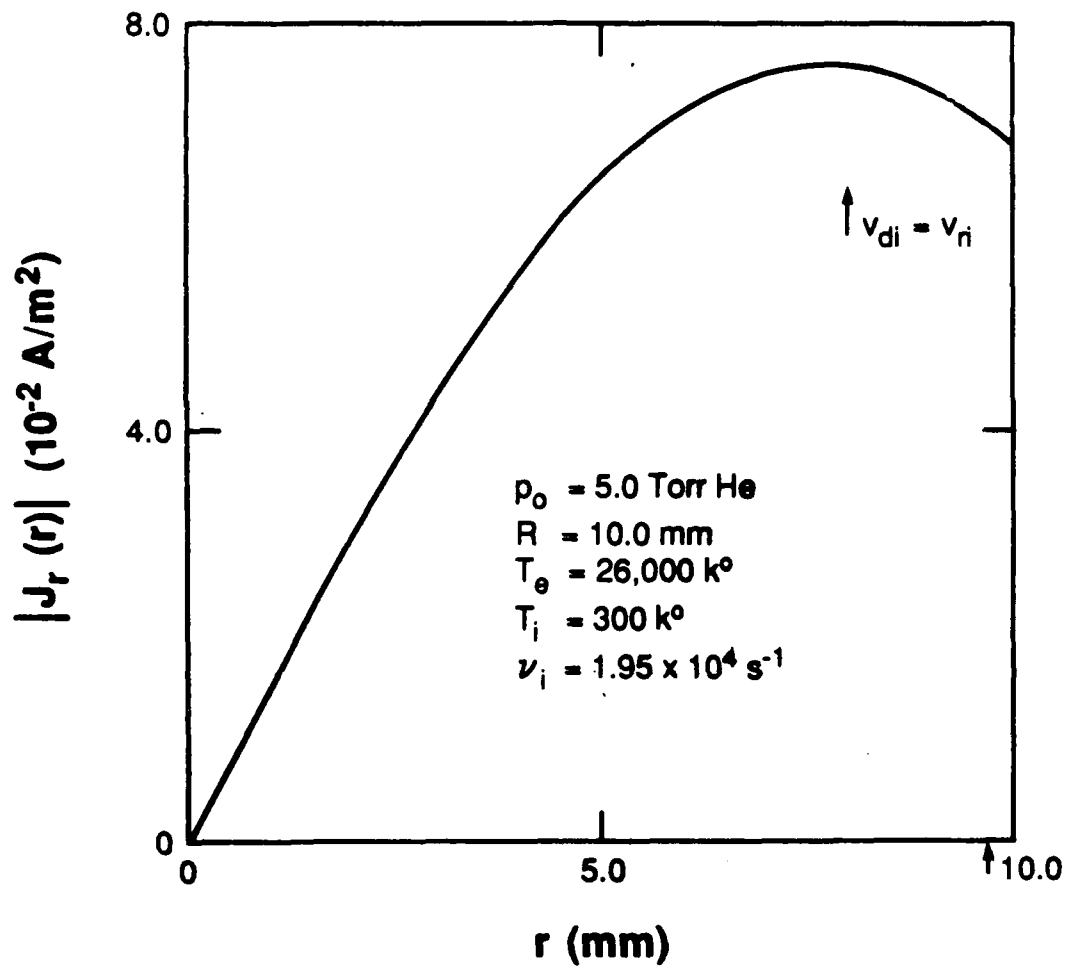
Fig. 3. Numerical calculations of the radial charged particle current density $J_r(r)$ for $Rp_0=5.0$ cm-Torr.

to the sheath region near the wall. The resulting value of the potential at the wall relative to the axis is $V(r=R)=-6.6$ V. This value can be compared with the value, V_a, given by Eq. (22a) in Ref. 13 for the quasineutral inertia limited theory of the positive column. For the discharge parameters discussed here, $V_a=-9.5$ V. The discrepancy between these two values is a result of the assumptions of quasineutrality and inertia limited flow used in deriving the expression for V_a.

Figure 3 is a plot of the radial charged particle current density $J_r(r)=e\Gamma_r(r)$. The maximum in this curve is a consequence of the cylindrical geometry and the fact that the particle production rate $v_i n_e(r)$ decreases with increasing r. However, the total radial charged particle current per unit length at radius r, $2\pi r J_r(r)$, is a monotonically increasing function of r, as required.

For comparison, the results of calculations for R=0.5 cm and $p_o=1.0$ Torr are given in Figs. 4-6. This leads to a value $Rp_o=0.5$ cm-Torr, which is 10 times larger than the value of Rp_o for the previous case. For these conditions, the measurements of Leiby and Rogers imply $T_e=45,000$ °K, leading to a required net charged particle density on the axis of $\Delta n(r=0)=4.9 \times 10^{13}$ m^{-3}. The resulting ionization frequency is $v_i=6.67 \times 10^5$ s^{-1}. Figure 4 shows the plots of $n_i(r)$, $n_e(r)$, and $\Delta n(r)$ for this situation. As in the previous case, the curves for $n_i(r)$ and $n_e(r)$ are close to the shape of the zero order Bessel function $J_0(2.4r/R)$ for the bulk of the plasma, with a significant deviation occurring, especially for $n_i(r)$, only near the tube wall. This deviation is again indicative of the development of a sheath region. as is also shown by the curve for $\Delta n(r)$ A comparison between Fig. 1 and Fig. 4 shows that the resulting sheath region is larger for smaller values of Rp_o. In addition, this comparison also shows that the values for $\Delta n(r)$ increase with decreasing Rp_o, with nearly an order of magnitude difference in $\Delta n(r)$ occurring between these two cases.

Figure 5 presents the results for $E_r(r)$ and $V(r)$ for this second case, along with the curve for $E_a(r)$ from the ambipolar diffusion theory. Again, the curve for $V(r)$ demonstrates the smooth transition from the bulk plasma region near the axis to the sheath region near the wall. For this situation, the resulting wall potential is $V(r=R)=-12.1$ V, as compared to the
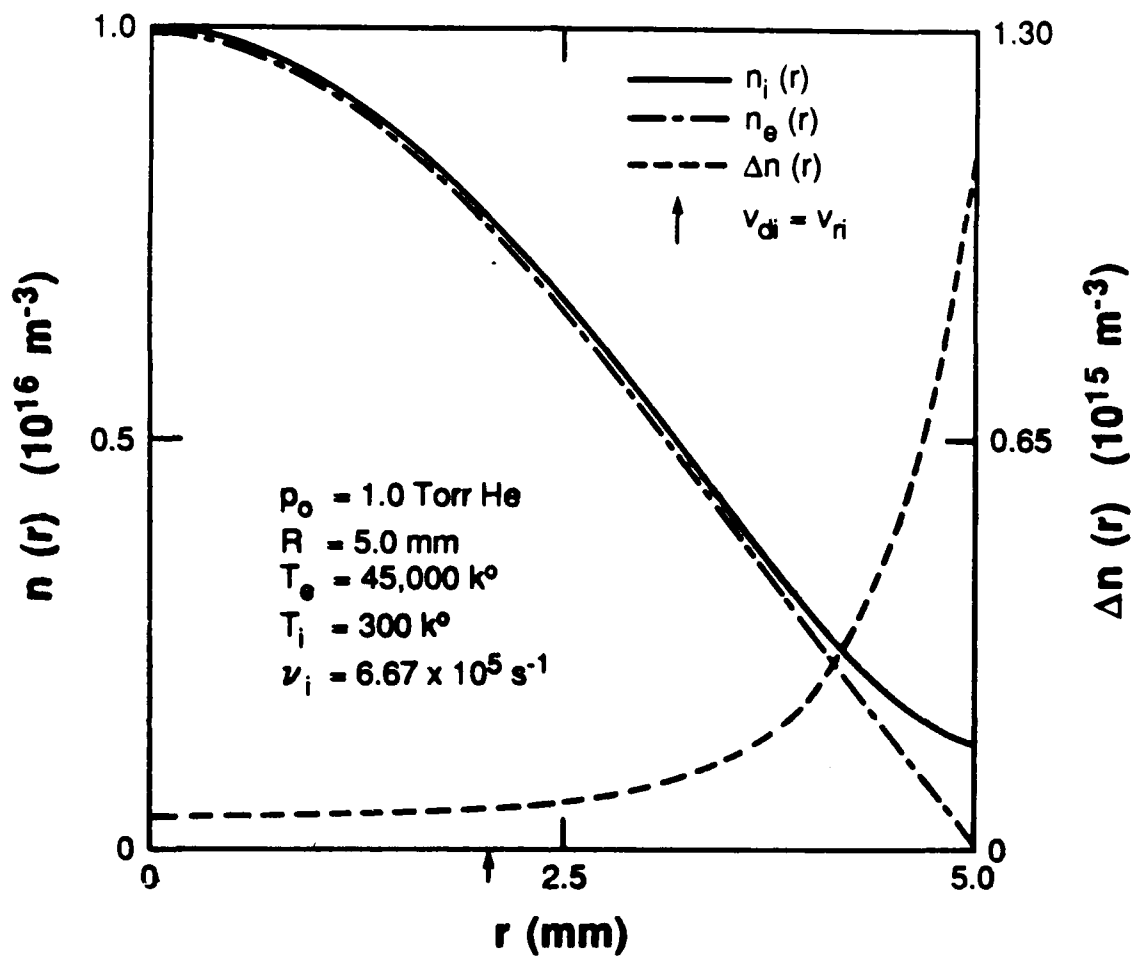
---

[13]S. A. Self, Phys. Fluids **6**, 1762 (1963).

Fig. 4. Numerical calculations of the ion density $n_i(r)$, the electron density $n_e(r)$, and the net charged particle density $\Delta n(r)$ for $Rp_o=0.5$ cm-Torr.
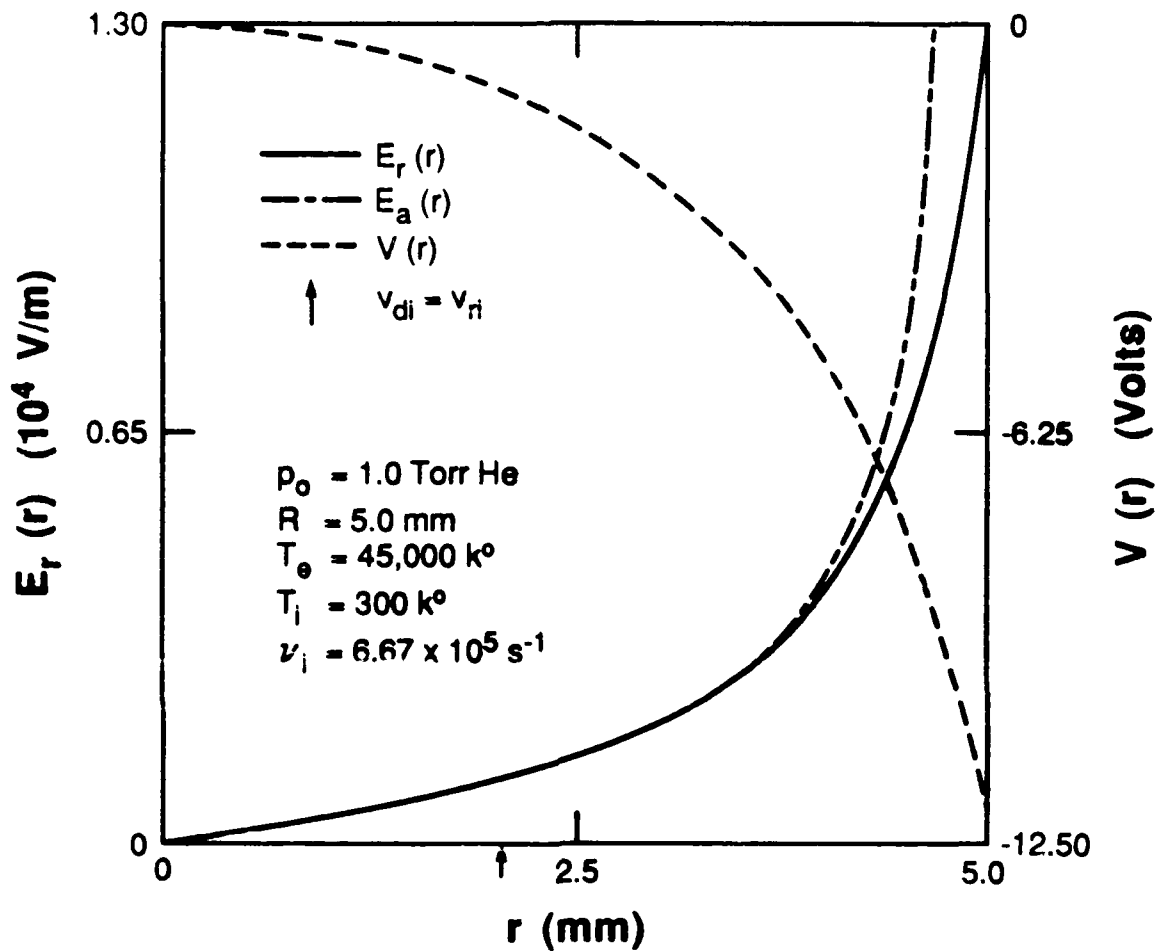
Fig. 5. Numerical calculations of the radial electric field strength $E_r(r)$ and the resulting electric potential $V(r)$ for $Rp_o=0.5$ cm-Torr. The ambipolar radial electric field $E_a(r)$ is also shown for comparison.
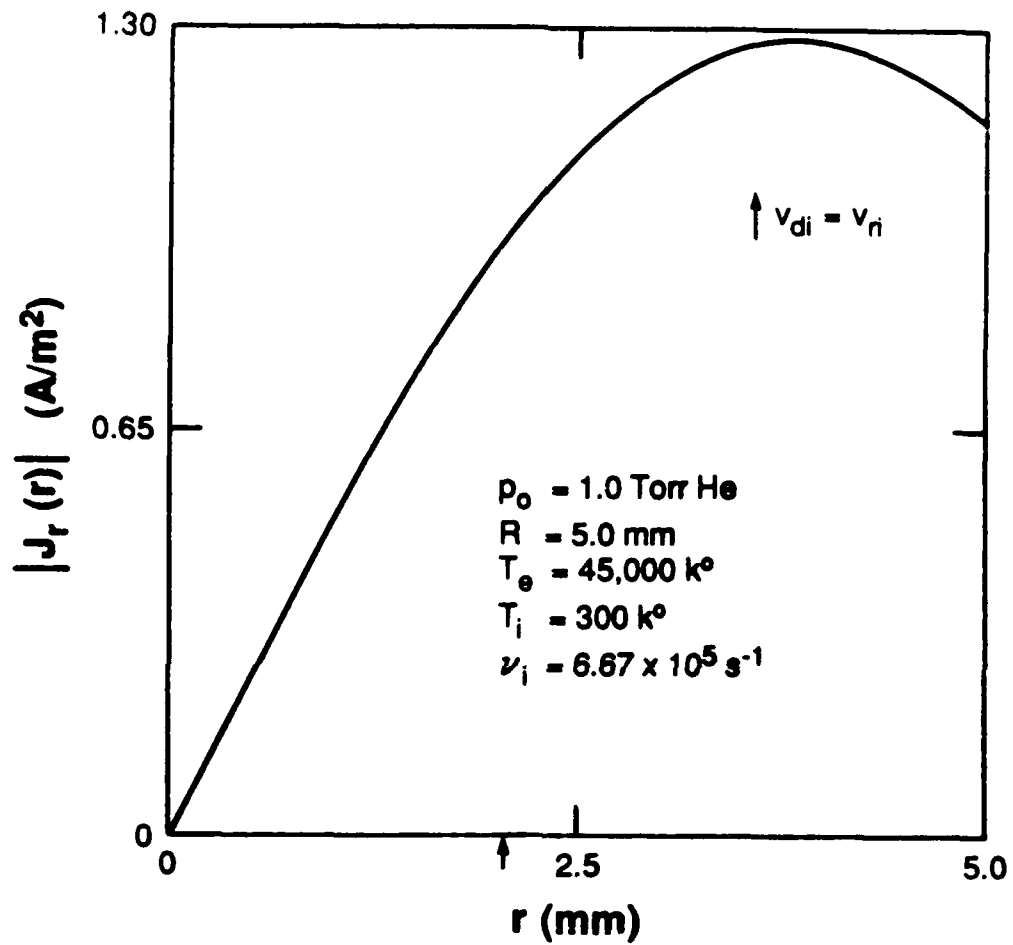
103

Fig. 6. Numerical calculations of the radial charged particle current density $J_r(r)$ for $Rp_o=0.5$ cm-Torr.

quasineutral inertia limited value $V_a=-16.5$ V. The magnitude of the radial electric field shown in this figure is significantly larger than the electric field in Fig. 2. This is a consequence of the higher electron temperature for the situation depicted in Fig. 5, which leads to enhanced electron diffusion to the wall. This results in the generation of a larger space charge induced radial electric field in order to retard the electrons and accelerate the ions toward the wall. As a result, the point $v_{di}=v_{ri}$ is closer to the axis in Fig. 5 than in Fig. 2, since the ion drift velocity at a given relative radial distance from the axis is larger for a larger electric field.

Figure 6 shows $J_r(r)$ for the situation where $Rp_o=0.5$ cm-Torr. The value of $J_r(r)$ for this case is more than an order of magnitude larger than those shown in Fig. 3.

From the above results, it is possible to investigate the applicability of the Bohm criterion, $v_{di} \geq (kT_e/m_i)^{1/2}$, for these discharge conditions.[14] For both discharge conditions discussed above, $v_{di}(r) < (kT_e/m_i)^{1/2}$ for all values of r. Thus, the Bohm criterion is never met, even though the results presented in Figs. 1-6 clearly show the development of a sheath region near the discharge tube wall. The formation of a sheath region even in the absence of the Bohm criterion being fulfilled, has been discussed previously by Ingold.[8]

Finally, the self-consistency of the theory in terms of the assumptions and boundary conditions used can be discussed in view of the calculations presented above. Assumption (4) in Sec. II states that v_i is small with respect to v_{mi} and v_{me}. As can be seen by comparing the calculated values for v_i with the values given for v_{mi} and v_{me}, this assumption is indeed satisfied for the cases presented. The importance of the boundary condition chosen for the electron density at the wall in determining the results of the calculations can be determined by comparing the tube radii used above with the tube radii predicted by other commonly employed boundary conditions for the same discharge parameters. In addition to the boundary condition of Eq. (5) which was used in these calculations, another commonly used boundary condition is $n_e(r=R)=0$. From Figs. 1 and 3 it is clear that this condition is closely approximated at r=R in these figures. Indeed, calculations show that the tube radius is increased by less than 0.2% by the

---

[14]D. Bohm, in *The Characteristics of Electrical Discharges in Magnetic Fields*, edited by Guthrie and R. K. Wakerling (McGraw-Hill, New York, 1949), Chap. 3.

use of this boundary condition. Therefore, the assumption of the boundary condition of Eq. (5) is consistent with the results.

IV. CONCLUSIONS

A model has been presented for the radial distribution of the ion and electron densities and electric field strength in the cylindrical positive column of a dc discharge for a plasma consisting of a singly charged positive ion species, electrons, and neutrals. Under appropriate assumptions, the resulting set of equations involved consists of the particle conservation equation, the momentum conservation equations, and Poisson's equation. A method of solution for this set of equations using a power series expansion has been outlined, which avoids the instability problem encountered by previous authors. This allows for the inclusion of all the volume force terms in the conservation of momentum equations for the ions and electrons.

The results of calculations based on this model shew the development of the bulk plasma region near the discharge tube axis and the sheath region near the tube wall. There is no clear distinction between these two regions, with a smooth transition occurring from the bulk plasma region to the sheath region, as can be expected. While the results near the tube axis are consistent with the ambipolar model, they deviate considerably from this model in the sheath region near the wall. However, even at the axis, there is a net space charge density which increases for decreasing values of Rp_0. The electric potential at the wall relative to the axis is on the order of the value predicted by the quasineutral inertia limited theory, with the wall potential increasing for decreasing values of Rp_0. The results show that the development of a sheath region can occur even for situations in which the Bohm criteria is never met.

The importance of the boundary condition chosen for the electron density at the discharge tube wall was investigated. It was found that the choice of either Eq. (5) or $n_e(r=R)=0$ as the boundary condition has little effect on the solution for the cases studied.

ACKNOWLEDGMENTS